Doctoral Dissertation (Shinshu university)

Study on nanostructure and stimuli responsiveness of hydrogel microspheres

(ハイドロゲル微粒子のナノ構造と刺激応答性に関する研究)

2022 年 3 月

信州大学総合医理工学研究科　総合理工学専攻

Yuichiro Nishizawa

西澤　佑一朗

Table of Contents

1. Introductory remarks

1.1. Background[1]

Hydrogels are soft polymeric materials that consist of cross-linked hydrophilic or amphiphilic polymer chains. As they are swollen by water, they are biocompatible and deformable.[2-5] Hydrogels are ubiquitous in e.g. jellies and separating medical materials. Most living tissue is also composed of hydrogels. Moreover, the stimulus-responsiveness of hydrogels has received great attention since Tanaka et al. discovered volume-phase-transition behavior,[6] and several types of hydrogels that respond to external stimulation such as solvent, temperature, pH, light, or chemical agents have been developed.

Among these, hydrogels, whose size typically ranges from several tens of nanometers to several micrometers, are called hydrogel microspheres (microgels, nanogels) and they combine the features of colloids with those of hydrogels described above. While the first reported gel particles were benzene-swollen polystyrene particles cross-linked with divinylbenzene, which were synthesized by Staudinger in 1935,[7,8] this thesis focuses on water-swollen microgels. Microgels were first prepared by Pelton et al. in 1986,[9] and this field has developed rapidly over the last 20 years.[10-15] As microgels are colloidal in size, they can experience Brownian motion and respond quickly to external stimulation, as described by the Tanaka–Fillmore equation.[16] As microgels, in contrast to rigid colloidal particles such as silica and polystyrene, contain hydrated polymer chains on their surface, microgels exhibit good colloidal stability and can thus be used in densely packed states where microgels are usually deformed and in contact with one another. Due to their advantages, microgels are expected to find numerous applications, e.g. in carriers for drug-delivery systems,[12,17] cell scaffolds,[12,18] sensors,[12,19] molecular separation,[20-22] molecular chaperones,[23] catalysts,[24,25] emulsifiers,[26,27] energy-conversion materials,[28-30] and model systems for glasses,[32,33] crystals,[34-37] and blood cells.[38,39]

In the first published report of microgels, thermoresponsive microgels were prepared via aqueous free-radical precipitation polymerization,[9] which allows synthesizing uniformly sized microgels, and is consequently one of the most frequently used techniques for the synthesis of thermoresponsive microgels. This technique can be employed for the synthesis of many types of microgels, provided that the monomers are soluble in water and the polymers formed via polymerization are water-insoluble.[2-5,40] Inverse miniemulsion polymerization[41] or template techniques[38] can be used to synthesize microgels composed of hydrophilic polymer chains that cannot precipitate in water. Furthermore, seeded emulsion/precipitation polymerization allows designing microgels with more complex architectures, e.g., nanocomposite, hollow, and core–shell structures.[42-48] Given that polymerization techniques strongly affect the microgel nanostructures, it is important to elucidate the structure of the resulting microgels before investigating their physicochemical properties, functions, and applications.

As microgels are water-swollen particles, it is of paramount importance to characterize both their colloidal and network structures. In bulk hydrogels, the network structure is typically evaluated using scattering techniques; these techniques provide additional information in the case of microgels. Dynamic light scattering (DLS) allows characterizing the hydrodynamic diameter of microgels based on the Stoks-Einstein equation and the diffusion coefficient of Brownian motion.[49,50] As microgels, unlike bulk hydrogels, are too small to be observed by the naked eye, DLS measurements are crucial for discussing their swelling properties. Static light scattering and small-angle neutron/X-ray scattering provide structural information on the morphology, radius of gyration, and mesh size of the microgels.[51-54] Electrophoresis, which is a characterization technique specific to colloidal particles, can not only determine the electrophoretic mobility and surface properties, but in combination with DLS also to evaluate their structure.[55,56] Similarly, changes in their physicochemical properties have been analyzed using UV–vis adsorption, IR, and/or NMR spectroscopy to investigate the microgel structure.[28-31,57]

Microscopy, which allows directly visualizing individual colloidal particles, is especially important in determining the size, shape, and distribution of microgels (**Table 1**). In order to understand the averaged data obtained from ensemble techniques, visualization by microscopy should be performed first after the synthesis of microgels. Electron microscopy has been widely used for visualizing microgels under vacuum conditions. In a pioneering study, thermoresponsive microgels were examined using transmission electron microscopy (TEM) to determine the polymer density distribution of the microgels and the uniformity of their size.[9] TEM imaging detects the transmitted electron beam, and therefore, the internal structure of the microgels can be analyzed using TEM images. However, in reality, an evaluation of the polymer density distribution using only TEM images is difficult, because the contrast is too low to detect low-density regions. Instead, TEM is better suited for the visualization of the internal structure of metal composite microgels[25,43,58-62] and microgels stained with metal ions.[44-47,63] Conversely, scanning electron microscopy (SEM), which depicts the secondary/backscattered electrons or X-rays generated when a sample is exposed to an electron beam, is often used to visualize the surface structure of microgels. Nonconductive samples such as microgels have to be sputtered with a conductive layer prior to SEM imaging, which sometimes impedes the precise visualization of microgels that are highly deformed on the substrate. Similar to TEM, SEM has mainly been employed to clarify the size (distribution) of microgels.[48] Moreover, SEM images may provide 3D information on the microgels as the imaging angle can be varied.[64]

Electron microscopy allows imaging with high spatial resolution; however, it has the major limitation of being conducted under vacuum conditions. It is generally difficult to elucidate the nanostructures of microgels via electron microscopy due to the deformation of the dried microgels under vacuum conditions, although Horigome et al. succeeded in observing microgels in the swollen state via SEM using ionic liquids.[65] While Gelissen et al. have visualized the thermoresponsiveness of

a single microgel with metal nanoparticles as markers in water by liquid-cell *in situ* TEM,[66] the low density hydrogel regions could not be visualized. Cryogenic (cryo-) electron microscopy has been used to circumvent this obstacle. In this technique, the microgel structure is immobilized in the dispersed state by rapidly freezing a microgel dispersion. Crassous et al. first reported cryo-TEM imaging for solid core–hydrogel shell particles.[67,68] While evaluating microgels with low polymer density is difficult, this technique is suitable for determining the structures of microgels with large density difference such as hollow, core–shell, and nanocomposite structures.[47,69-72] The deformation structures of microgels at oil/water interfaces have been visualized using cryo-SEM.[73] Geisel et al. have clarified the deformation structure of microgels at oil/water interfaces using freeze–fracture shadow-casting (FreSCa), which is a method to calculate the height of the sample by the shadow formed during sputtering.[74] The structures of deformed microgels at oil/water interfaces have also been analyzed using simulations.[75,76] More recently, cryo-electron tomography (cryo-ET) has been used to quantitatively determine the size and spatial distribution of nanocomposite materials within the microgels via 3D topographic reconstruction at different angles.[77]

Optical microscopy (OM) and fluorescence microscopy (FM) are imaging techniques with a spatial resolution of ~200 nm, which is due to the use of vis/UV light. However, the spatial resolution of OM/FM for microgels is further reduced due to their low polymer density and blurry surface. A great advantage of these techniques is their high temporal resolution, which allows observing dynamic behavior in real time, such as the packing of concentrated microgel suspensions,[34] the pre-melting of colloidal crystals[78] and self-organization processes. For example, OM observations have revealed the adsorption and arrangement behavior of microgels at the air/water interfaces during the drying of microgel dispersions.[79-81] This self-organization is the key to forming thin microgel films that show structural color,[82] in contrast to other colloidal dispersions that produce ring-shaped structures that originate from the coffee-ring effect.[83] Moreover, OM observations have clarified that microgels with anisotropic structures, such as Janus microgels and ellipsoidal microgels, promote one-dimensional self-assembly.[84-86] Recently, the temporal resolution has been further improved by combining FM with a high-speed camera. This approach has revealed the adsorption and deformation kinetics of microgels at air/water interfaces[87] and their flow behavior under blood-flow-like conditions (shear velocity: 10^2–10^3 s^{-1}, i.e., similar to that in arterioles).[88] On the other hand, super-resolution fluorescence microscopy (SRFM) enables a spatial resolution of ~20 nm in water by overcoming the Abbe diffraction limit.[89-91] SRFM has been used to determine the cross-linking distribution of single microgels, and the observed structures have often been compared with the results obtained from scattering techniques.[92,93] SRFM is a suitable technique for the observation of single microgels not only in the dispersed state, but also in densely packed states. The structures of microgels with different volume fractions have been visualized using two types of fluorescence-labelled microgels and dSTORM[94,95] in order to clarify the structural changes with increasing volume fraction. It should be noted here that

SRFM requires fluorescence labeling.

Atomic force microscopy (AFM) is a scanning probe microscopy technique that images by detecting the displacement of a cantilever and delivers information on the height and morphology of a sample, as well as its physical properties such as stiffness, Young's modulus, and adhesion force.[96-98] Traditionally, AFM observations were routinely conducted in air,[47] but since 2007, *in situ* AFM has received increasing attention, as it allows examining water-swollen microgels and their stimulus-responsiveness.[99-105] Wiedemair et al. have used *in-situ* AFM to evaluate thermoresponsive microgels, and successfully observed the changes in their structures and elastic modulus with increasing temperature.[99] The advantage of AFM is its high spatial resolution (~1 nm), albeit that its ability to image only substrate-bound samples with a temporal resolution of tens of seconds to minutes per image is somewhat limiting.

In this context, the author of this thesis has applied high-speed (HS) AFM to directly visualize the nano-dynamics of microgels. This imaging method had been originally improved to directly visualize the dynamics of biomolecules and to obtain exceptionally high spatial–temporal resolution (spatial resolution: ~1 nm,; temporal resolution: 50 ms/frame) in water.[106,107] Matsui et al. first employed HS-AFM to visualize the dynamic processes of artificial polymeric microspheres and revealed that the softness (deformability) of particles strongly affects their adsorption behavior on the substrate.[108] Moreover, HS-AFM can be improved with relative ease compared to other microscopy techniques, i.e., the introduction of a temperature controller into the cantilever holder of the HS-AFM allows visualizing the thermoresponsiveness of microgels.[109]

The present thesis comprises the investigation of three topics associated with the nanostructure and nanodynamics of microgels. In **Chapter I**, the thermoresponsiveness of single microgels is investigated. The results demonstrate that microgels prepared by precipitation polymerization exhibit a non-thermoresponsive nanostructure, and that the nanostructure strongly depends on the polymerization technique. In **Chapter II**, the effect of the chemical composition of the microgels on their nanostructure is investigated. The results show that the nanostructure of the microgels is affected by the monomer reactivity ratios. **Chapter III** focuses on the mechanism of precipitation polymerization. The changes in the nanostructure and thermoresponsiveness of developing microgels during precipitation polymerization are evaluated using light scattering and HS-AFM. Furthermore, direct observation of the precipitation polymerization is conducted to clarify the way in which the polymerization proceeded.

Table 1. Features of each microscopy.

Microscopy	Imaging	Condition	Resolution		Suitable evaluation
			Spatial	Temporal	
TEM	Transmitted electron beam	Vaccume	Several tens nm[a]	-	Size uniformity, internal structure (nanocomposite)
In situ TEM		In water		Real time	Stimulus responsivity
Cryo-TEM		Freezing		Static	Internal structure (nanocomposite)
SEM	Secondary / backscatteried electron	Vaccume	Several tens nm	-	Size uniformity, surface structure (nanocomposite)
Cryo-SEM		Freezing		Static	Surface structure (pickering emulsion)
Cryo-ET	Transmitted electron beam	Freezing	Several tens nm	Static	Internal structure (nanocomposite)
OM (FM)	Visible light	In water (fluoresence labeling)	~ 200 nm	Real time	Dynamic behavior
+high-speed camera				Slow motion	Fast dynamic behavior (adsorption, flow)
SRFM	Visible light	In water, fluoresence labeling	~20 nm	Static	Internal structure
AFM	Atomic force	In air	~ 1 nm	-	Surface stucture, physical properties
In situ AFM		In water		Static	Surface stucture, physical properties, stimulus responsivity
HS-AFM		In water		Real time	Dynamic behavior (e.g. adsorption, thermoresponsivity)

[a] hydrogel cannot be visualized due to the low contrast

1.2 Reference

1. Y. Nishizawa, K. Honda, D. Suzuki, Recent Development in the Visualization of Microgels. *Chem. Lett.* **2021**, *50*, 1226-1235.
2. W. Richtering, B. R. Saunders, Gel architectures and their complexity. *Soft Matter* **2014**, *10*, 3695-3702.
3. F. Ullah, M. B. H. Othman, F. Javed, Z. Ahmad, H. M. Akil, Classification, processing and application of hydrogels: A review. *Mater. Sci. Eng., C* **2015**, *57*, 414-433.
4. H. Ko, A. Javey, Smart Actuators and Adhesives for Reconfigurable Matter. *Acc. Chem. Res.* **2017**, *50*, 691-702.
5. L. Tang, L. Wang, X. Yang, Y. Feng, Y. Li, W. Feng, Poly(*N*-isopropylacrylamide)-based smart hydrogels: Design,properties and applications. *Prog. Mater. Sci.* **2021**, *115*, 100702.
6. T. Tanaka, Collapse of Gels and the Critical Endpoint. *Phys. Rev. Lett.* **1978**, *40*, 820-823.
7. H. Staudinger, E. Husemann, Über hochpolymere Verbindungen, 116. Mitteil.: Über das begrenzt quellbare Poly-styrol. *Ber. Dtsch. Chem. Ges.* **1935**, *68*, 1618-1634.
8. B. R. Saunders, B. Vincent, Microgel particles as model colloids: theory, properties and applications. *Adv. Colloid Interface Sci.* **1999**, *80*, 1-25.
9. R. H. Pelton, P. Chibante, Preparation of Aqueous Latices with *N*-Isopropylacrylamide. *Colloids Surf.* **1986**, *20*, 247-256.
10. R. Pelton, Temperature-sensitive aqueous microgels. *Adv. Colloid Interface Sci.* **2000**, *85*, 1-33.
11. S. Nayak, L. A. Lyon, Soft Nanotechnology with Soft Nanoparticles. *Angew. Chem., Int. Ed.* **2005**, *44*, 7686-7708.
12. S. Saxena, C. E. Hansen, L. A. Lyon, Microgel Mechanics in Biomaterial Design. *Acc. Chem. Res.* **2014**, *47*, 2426-24340.
13. F. A. Plamper, W. Richtering, Functional Microgels and Microgel Systems. *Acc. Chem. Res.* **2017**, *50*, 131.
14. D. Suzuki, K. Horigome, T. Kureha, S. Matsui, T. Watanabe, Polymeric hydrogel microspheres: design, synthesis, characterization, assembly and applications. *Polym. J.* **2017**, *49*, 695-702.
15. M. Karg, A. Pich, T. Hellweg, T. Hoare, L. A. Lyon, J. J. Crassous, D. Suzuki, R. A. Gumerov, S. Schneider, I. I. Potemkin, W. Richtering, Nanogels and Microgels: From Model Colloids to Applications, Recent Developments, and Future Trends. *Langmuir* **2019**, *35*, 6231-6255.
16. T. Tanaka, D. J. Fillmore, Kinetics of swelling of gels. *J. Chem. Phys.* **1979**, *70*, 1214-1218.
17. J. C. Cuggino, E. R. O. Blanco, L. M. Gugliotta, C. I. A. Igarzabal, M. Calderón, Crossing biological barriers with nanogels to improve drug delivery Performance. *J. Controlled Release* **2019**, *307*, 221-246.
18. Y. Xia, X. He, M. Cao, C. Chen, H. Xu, F. Pan, J. R. Lu, Thermoresponsive Microgel Films for Harvesting Cells and CellSheets. *Biomacromolecules* **2013**, *14*, 3615-3625.

19. M. Wei, Y. Gao, X. Li, M. J. Serpe, Stimuli-responsive polymers and their applications. *Polym. Chem.* **2017**, *8*, 127-143.
20. Y. Hoshino, K. Imamura, M. Yue, G. Inoue, Y. Miura, Reversible Absorption of CO2 Triggered by Phase Transition of Amine-Containing Micro- and Nanogel Particles. *J. Am. Chem. Soc.* **2012**, *134*, 18177-18180.
21. T. Kureha, D. Suzuki, Nanocomposite Microgels for the Selective Separation of Halogen Compounds from Aqueous Solution. *Langmuir* **2018**, *34*, 837-846.
22. T. Kureha, Y. Nishizawa, D. Suzuki, Controlled Separation and Release of Organoiodine Compounds Using Poly(2-methoxyethyl acrylate)-Analogue Microspheres. *ACS Omega* **2017**, *2*, 7686-7694.
23. M. Nakamoto, T. Nonaka, K. J. Shea, Y. Miura, Y. Hoshino, Design of Synthetic Polymer Nanoparticles That Facilitate Resolubilization and Refolding of Aggregated Positively Charged Lysozyme. *J. Am. Chem. Soc.* **2016**, *138*, 4282-4285.
24. Y. Lu, M. Ballauff, Thermosensitive core–shell microgels: From colloidal model systems to nanoreactors. *Prog. Polym. Sci.* **2011**, *36*, 767-792.
25. T. Kureha, Y. Nagase, D. Suzuki, High Reusability of Catalytically Active Gold Nanoparticles Immobilized in Core−Shell Hydrogel Microspheres. *ACS Omega* **2018**, *3*, 6158-6165.
26. T. Ngai, S. H. Behrens, H. Auweter, Novel emulsions stabilized by pH and temperature sensitive microgels. *Chem. Commun.* **2005**, 331-333.
27. T. Watanabe, M. Takizawa, H. Jiang, T. Ngai, D. Suzuki, Hydrophobized nanocomposite hydrogel microspheres as particulate stabilizers for water-in-oil emulsions. *Chem. Commun.* **2019**, *55*, 5990-5993.
28. D. Suzuki, T. Sakai, R. Yoshida, Self-Flocculating/Self-Dispersing Oscillation of Microgels. *Angew. Chem., Int. Ed.* **2008**, *47*, 917-920.
29. S. Matsui, K. Inui, Y. Kumai, R. Yoshida, D. Suzuki, Autonomously Oscillating Hydrogel Microspheres with High-Frequency Swelling/Deswelling and Dispersing/Flocculating Oscillations. *ACS Biomater. Sci. Eng.* **2019**, *5*, 5615-5622.
30. K. Inui, T. Watanabe, H. Minato, S. Matsui, K. Ishikawa, R. Yoshida, D. Suzuki, The Belousov−Zhabotinsky Reaction in Thermoresponsive Core−Shell Hydrogel Microspheres with a Tris(2,2′-bipyridyl)ruthenium Catalyst in the Core. *J. Phys. Chem. B* **2020**, *124*, 3828-3835.
31. B. Guo, Y. Hoshino, F. Gao, K. Hayashi, Y. Miura, N. Kimizuka, T. Yamada, Thermocells Driven by Phase Transition of Hydrogel Nanoparticles. *J. Am. Chem. Soc.* **2020**, *142*, 17318-17322.
32. J. Mattsson, H. M. Wyss, A. Fernandez-Nieves, K. Miyazaki, Z. Hu, D. R. Reichman, D. A. Weitz, Soft colloids make strong glasses. *Nature* **2009**, *462*, 83-86.
33. S. Minami, D. Suzuki, K. Urayama, Rheological aspects of colloidal gels in thermoresponsive microgel suspensions: formation, structure, and linear and nonlinear viscoelasticity. *Curr. Opin.*

Colloid Interface Sci. **2019**, *43*, 113-124.

34. T. Hellweg, C. D. Dewhurst, E. Brückner, K. Kratz, W. Eimer, Colloidal crystals made of poly(*N*-isopropylacrylamide) microgel particles. *Colloid Polym. Sci.* **2000**, *278*, 972-978.
35. T. Okubo, D. Suzuki, T. Yamagata, K. Horigome, K. Shibata, A. Tsuchida, Colloidal crystallization of thermosensitive gel spheres of poly(*N*-isopropylacrylamide) with low degree of cross-linking. *Colloid Polym. Sci.* **2011**, *289*, 12731281.
36. D. Suzuki, K. Horigome, T. Yamagata, K. Shibata, A. Tsuchida, T. Okubo, Colloidal crystallization of thermo-sensitive gel spheres of poly (*N*-isopropyl acrylamide). Influence of degree of cross-linking of the gels. *Colloid Polym. Sci.* **2011**, *289*, 1799-1808.
37. D. Suzuki, T. Yamagata, K. Horigome, K. Shibata, A. Tsuchida, T. Okubo, Colloidal crystallization of thermo-sensitive gel spheres of poly (*N*-isopropyl acrylamide). Influence of gel size. *Colloid Polym. Sci.* **2012**, *290*, 107-117.
38. T. J. Merkel, S. W. Jones, K. P. Herlihy, F. R. Kersey, A. R. Shields, M. Napier, J. C. Luft, H. Wu, W. C. Zamboni, A. Z. Wang, J. E. Bear, J. M. DeSimone, Using mechanobiological mimicry of red blood cells to extend circulation times of hydrogel microparticles. *Proc. Natl. Acad. Sci. U.S.A.* **2011**, *108*, 586-591.
39. A. C. Brown, S. E. Stabenfeldt, B. Ahn, R. T. Hannan, K. S. Dhada, E. S. Herman, V. Stefanelli, N. Guzzetta, A. Alexeev, W. A. Lam, L. A. Lyon, T. H. Barker, Ultrasoft microgels displaying emergent, platelet-like, behaviors. *Nat. Mater.* **2014**, *13*, 1108-1114.
40. A. Pich, W. Richtering, Microgels by Precipitation Polymerization: Synthesis, Characterization, and Functionalization. Chemical Design of Responsive Microgels. Springer-Verlag: Berlin, Heidelberg, 2010, 1.
41. I. Capek, On inverse miniemulsion polymerization of conventional water-soluble monomers. *Adv. Colloid Interface Sci.* **2010**, *156*, 35-61.
42. D. Suzuki, R. Yoshida, Self-oscillating core/shell microgels: effect of a crosslinked nanoshell on autonomous oscillation of the core. *Polym. J.* **2010**, *42*, 501-508.
43. A. Rauh, T. Honold, M. Karg, Seeded precipitation polymerization for the synthesis of gold-hydrogel core-shell particles: the role of surface functionalization and seed concentration. *Colloid Polym. Sci.* **2016**, *294*, 37-47.
44. D. Suzuki, T. Yamagata, M. Murai, Multilayered Composite Microgels Synthesized by Surfactant-Free Seeded Polymerization. *Langmuir* **2013**, *29*, 10579-10585.
45. D. Suzuki, C. Kobayashi, Raspberry-Shaped Composite Microgel Synthesis by Seeded Emulsion Polymerization with Hydrogel Particles. *Langmuir* **2014**, *30*, 7085-7092.
46. C. Kobayashi, T. Watanabe, K. Murata, T. Kureha, D. Suzuki, Localization of Polystyrene Particles on the Surface of Poly(*N*-isopropylacrylamide-co-methacrylic acid) Microgels Prepared by Seeded Emulsion Polymerization of Styrene. *Langmuir* **2016**, *32*, 1429-1439.

47. T. Watanabe, C. Kobayashi, C. Song, K. Murata, T. Kureha, D. Suzuki, Impact of Spatial Distribution of Charged Groups in Core Poly(N-isopropylacrylamide)-Based Microgels on the Resultant Composite Structures Prepared by Seeded Emulsion Polymerization of Styrene. *Langmuir* **2016**, *32*, 12760-12773.
48. T. Watanabe, C. Song, K. Murata, T. Kureha, D. Suzuki, Seeded Emulsion Polymerization of Styrene in the Presence of Water-Swollen Hydrogel Microspheres. *Langmuir* **2018**, *34*, 8571-8580.
49. K. Kratz, T. Hellweg, W. Eimer, Structural changes in PNIPAM microgel particles as seen by SANS, DLS, and EM techniques. *Polymer* **2001**, *42*, 6631-6639.
50. S. Takata, M. Shibayama, R. Sasabe, H. Kawaguchi, Preparation and structure characterization of hairy nanoparticles consisting of hydrophobic core and thermosensitive hairs. *Polymer* **2003**, *44*, 495-501.
51. J. Gao, B. J. Frisken, Cross-linker-free N-isopropylacrylamide gel nanospheres. *Langmuir* **2003**, *19*, 5212-5216.
52. M. Stieger, W. Richtering, J. S. Pedersen, P. Lindner, Small-angle neutron scattering study of structural changes in temperature sensitive microgel colloids. *J. Chem. Phys.* **2004**, *120*, 6197-6206.
53. B. R. Saunders, On the structure of poly(N-isopropylacrylamide) microgel particles. *Langmuir* **2004**, *20*, 3925-3932.
54. R. Keidel, A. Ghavami, D. M. Lugo, G. Lotze, O. Virtanen, P. Beumers, J. S. Pedersen, A. Bardow, R, G. Winkler, W. Richtering, Time-resolved structural evolution during the collapse of responsive hydrogels: The microgel-to-particle transition. *Sci. Adv.* **2018**, *4*, eaao7086.
55. E. Daly, B. R. Saunders, Temperature-dependent electrophoretic mobility and hydrodynamic radius measurements of poly(*N*-isopropylacrylamide) microgel particles: structural insights. *Phys. Chem. Chem. Phys.* **2000**, *2*, 3187-3193.
56. T. Hoare, R. Pelton, Electrophoresis of functionalized microgels: morphological insights. *Polymer* **2005**, *46*, 1139-1150.
57. C. H. Hofmann, F. A. Plamper, C. Scherzinger, S. Hietala, W. Richtering, Cononsolvency Revisited: Solvent Entrapment by *N*-Isopropylacrylamide and *N,N*-Diethylacrylamide Microgels in Different Water/Methanol Mixtures. *Macromolecules* **2013**, *46*, 523-532.
58. D. Suzuki, H. Kawaguchi, Modification of gold nanoparticle composite nanostructures using thermosensitive core-shell particles as a template. *Langmuir* **2005**, *21*, 8175-8179.
59. D. Suzuki, H. Kawaguchi, Gold nanoparticle localization at the core surface by using thermosensitive core-shell particles as a template. *Langmuir* **2005**, *21*, 12016-12024.
60. M. Das, H. Zhang, E. Kumacheva, Microgels: Old materials with new applications. *Annu. Rev. Mater. Res.* **2006**, *36*, 117-142.
61. D. Suzuki, H. Kawaguchi, Hybrid microgels with reversibly changeable multiple brilliant

color. *Langmuir* **2006**, *22*, 3818-3822.

62. D. Suzuki, J. G. McGrath, H. Kawaguchi, L. A. Lyon, Colloidal crystals of thermosensitive, core/shell hybrid microgels. *Journal of Physical Chemistry C. J. Phys. Chem. C* 2007, 111, 5667-5672.
63. T. Hoare, R. Pelton, Curr. Characterizing charge and crosslinker distributions in polyelectrolyte microgels. *Opin. Colloid Interface Sci.* **2008**, *13*, 413-428.
64. H. M. Crowther, B. Vincent, Swelling behavior of poly N-isopropylacrylamide microgel particles in alcoholic solutions. *Colloid Polym. Sci.* **1998**, *276*, 46-51.
65. K. Horigome, T. Ueki, D. Suzuki, Direct visualization of swollen microgels by scanning electron microscopy using ionic liquids. *Polym. J.* **2016**, *48*, 273-279.
66. A. P. H. Gelissen, A. Oppermann, T. Caumanns, P. Hebbeker, S. K. Turnhoff, R. Tiwari, S. Eisold, U. Simon, Y. Lu, J. Mayer, W. Richtering, A. Walther, D. Wöll, 3D Structures of Responsive Nanocompartmentalized Microgels. *Nano Lett.* **2016**, *16*, 7295-7301.
67. J. J. Crassous, M. Ballauff, M. Drechsler, J. Schmidt, Y. Talmon, Imaging the volume transition in thermosensitive core-shell particles by cryo-transmission electron microscopy. *Langmuir* **2006**, *22*, 2403-2406.
68. J. J. Crassous, C. N. Rochette, A. Wittemann, M. Schrinner, M. Ballauff, M. Drechsler, Quantitative Analysis of Polymer Colloids by Cryo-Transmission Electron Microscopy. *Langmuir* **2009**, *25*, 7862-7871.
69. R. Contreras-Cáceres, L. Schellkopf, C. Fernández-López, I. Pastoriza-Santos, J. Pérez-Juste, M. Stamm, Effect of the Cross-Linking Density on the Thermoresponsive Behavior of Hollow PNIPAM Microgels. *Langmuir* **2015**, *31*, 1142-1149.
70. M. Karg, Functional Materials Design through Hydrogel Encapsulation of Inorganic Nanoparticles: Recent Developments and Challenges. *Macromol. Chem. Phys.* **2016**, *217*, 242-255.
71. E. R. Osorio-Blanco, J. Bergueiro, B. E. Abali, S. Ehrmann, C. Böttcher, A. J. Müller, J. L. Cuéllar-Camacho, M. Calderón, Effect of Core Nanostructure on the Thermomechanical Properties of Soft Nanoparticles. *Chem. Mater.* **2020**, *32*, 518-528.
72. J. Schmitt, C. Hartwig, J. J. Crassous, A. M. Mihut, P. Schurtenberger, V. Alfredsson, Anisotropic mesoporous silica/microgel core–shell responsive particles. *RSC Adv.* **2020**, *10*, 25393-25401.
73. M. Destribats, V. Lapeyre, M. Wolfs, E. Sellier, F. Leal-Calderon, V. Ravaine, V. Schmitt, Soft microgels as Pickering emulsion stabilisers: role of particle deformability. *Soft Matter* **2011**, *7*, 7689-7698.
74. K. Geisel, L. Isa, W. Richtering, Unraveling the 3D Localization and Deformation of Responsive Microgels at Oil/Water Interfaces: A Step Forward in Understanding Soft Emulsion Stabilizers. *Langmuir* **2012**, *28*, 15770-15776.

75. R. A. Gumerov, A. M. Rumyantsev, A. A. Rudov, A. Pich, W. Richtering, M. Möller, I. I. Potemkin, Mixing of Two Immiscible Liquids within the Polymer Microgel Adsorbed at Their Interface. *ACS Macro Lett.* **2016**, *5*, 612-616.
76. F. Camerin, M. Á. Fernández-Rodríguez, L. Rovigatti, M.-N. Antonopoulou, N. Gnan, A. Ninarello, L. Isa, E. Zaccarelli, Microgels Adsorbed at Liquid-Liquid Interfaces: A Joint Numerical and Experimental Study. *ACS Nano* **2019**, *13*, 4548-4559.
77. T. Watanabe, Y. Nishizawa, H. Minato, C. Song, K. Murata, D. Suzuki, Hydrophobic Monomers Recognize Microenvironments in Hydrogel Microspheres during Free-Radical-Seeded Emulsion Polymerization. *Angew. Chem., Int. Ed.* **2020**, *59*, 8849-8853.
78. A. M. Alsayed, M. F. Islam, J. Zhang, P. J. Collings, A. G. Yodh, Premelting at Defects Within Bulk Colloidal Crystals. *Science* **2005**, *309*, 1207-1210.
79. K. Horigome, D. Suzuki, Drying Mechanism of Poly(N-isopropylacrylamide) Microgel Dispersions. *Langmuir* **2012**, *28*, 12962−12970.
80. M. Takizawa, Y. Sazuka, K. Horigome, Y. Sakurai, S. Matsui, H. Minato, T. Kureha, D. Suzuki, Self-Organization of Soft Hydrogel Microspheres during the Evaporation of Aqueous Droplets. *Langmuir* **2018**, *34*, 4515−4525.
81. H. Minato, M. Takizawa, S. Hiroshige, D. Suzuki, Effect of Charge Groups Immobilized in Hydrogel Microspheres during the Evaporation of Aqueous Sessile Droplets. *Langmuir* **2019**, *35*, 10412-10423.
82. S. Tsuji, H. Kawaguchi, Colored thin films prepared from hydrogel microspheres. *Langmuir* **2005**, *21*, 8439-8442.
83. R. D. Deegan, O. Bakajin, T. F. Dupont, G. Huber, S. R. Nagel, T. A. Witten, Capillary flow as the cause of ring stains from dried liquid drops. *Nature* **1997**, *389*, 827-829.
84. D. Suzuki, S. Tsuji, H. Kawaguchi, Janus microgels prepared by surfactant-free pickering emulsion-based modification and their self-assembly. *J. Am. Chem. Soc.* **2007**, *129*, 8088-8089.
85. D. Suzuki, K. Horigome, Assembly of Oppositely Charged Microgels at the Air/Water Interface. *J. Phys. Chem. B* **2013**, *117*, 9073-9082.
86. K. Honda, Y. Sazuka, K. Iizuka, S. Matsui, T. Uchihashi, T. Kureha, M. Shibayama, T. Watanabe, D. Suzuki, Hydrogel Microellipsoids that Form Robust String-Like Assemblies at the Air/Water Interface. *Angew. Chem., Int. Ed.* **2019**, *58*, 7294-7298.
87. H. Minato, M. Murai, T. Watanabe, S. Matsui, M. Takizawa, T. Kureha, D. Suzuki, The deformation of hydrogel microspheres at the air/water interface. *Chem. Commun.* **2018**, *54*, 932–935.
88. S. Oura, T. Watanabe, H. Minato, D. Suzuki, Impact of Particle Softness on Segregation of Binary Colloidal Suspensions Flowing in a Microchannel. *Kobunshi Ronbunshu* **2019**, *76*, 226-233.
89. T. A. Klar, S. Jakobs, M. Dyba, A. Egner, S. W. Hell, Fluorescence microscopy with diffraction

resolution barrier broken by stimulated emission. *Proc. Natl. Acad. Sci. U.S.A.* **2000**, *97*, 8206-8210.

90. M. J. Rust, M. Bates, X. Zhuang, Sub-diffraction-limit imaging by stochastic optical reconstruction microscopy (STORM). *Nat. Methods* **2006**, *3*, 793-795.
91. F. Scheffold, Pathways and challenges towards a complete characterization of microgels. *Nat. Commun.* **2020**, *11*, 4315.
92. G. M. Conley, S. Nöjd, M. Braibanti, P. Schurtenberger, F. Scheffold, Superresolution microscopy of the volume phase transition of pNIPAM microgels. *Colloids Surf. A* **2016**, *499*, 18-23.
93. A. A. Karanastasis, Y. Zhang, G. S. Kenath, M. D. Lessard, J. Bewersdorf, C. K. Ullal, 3D mapping of nanoscale crosslink heterogeneities in microgels. *Mater. Horiz.* **2018**, *5*, 1130-1136.
94. G. M. Conley, P. Aebischer, S. Nojd, P. Schurtenberger, F. Scheffold, Jamming and overpacking fuzzy microgels: Deformation, interpenetration, and compression. *Sci. Adv.* **2017**, *3*, e1700969.
95. G. M. Conley, C. Zhang, P. Aebischer, J. L. Harden, F. Scheffold, Relationship between rheology and structure of interpenetrating, deforming and compressing microgels. *Nat. Commun.* **2019**, *10*.
96. M. Horecha, V. Senkovskyy, A. Synytska, M. Stamm, A. I. Chervanyov, A. Kiriy, Ordered surface structures from PNIPAM-based loosely packed microgel particles. *Soft Matter* **2010**, *6*, 5980-5992.
97. A. Mourran, Y. Wu, R. A. Gumerov, A. A. Rudov, I. I. Potemkin, A. Pich, M. Möller, When Colloidal Particles Become Polymer Coils. *Langmuir* **2016**, *32*, 723-730.
98. B. Wedel, Y. Hertle, O. Wrede, J. Bookhold, T. Hellweg, Smart Homopolymer Microgels: Influence of the Monomer Structure on the Particle Properties. *Polymers* **2016**, *8*, 162.
99. J. Wiedemair, M. J. Serpe, J. Kim, J.-F. Masson, L. A. Lyon, B. Mizaikoff, C. Kranz, In-situ AFM studies of the phase-transition behavior of single thermoresponsive hydrogel particles. *Langmuir* **2007**, *23*, 130-137.
100. S. Höfl, L. Zitzler, T. Hellweg, S. Herminghaus, F. Mugele, Volume phase transition of "smart" microgels in bulk solution and adsorbed at an interface: A combined AFM, dynamic light, and small angle neutron scattering study. *Polymer* **2007**, *48*, 245-254.
101. O. Tagit, N. Tomczak, G. J. Vancso, Probing the morphology and nanoscale mechanics of single poly(*N*-isopropylacrylamide) microgels across the lower-critical-solution temperature by atomic force microscopy. *Small* **2008**, *4*, 119-126.
102. S. M. Hashmi, E. R. Dufresne, Mechanical properties of individual microgel particles through the deswelling transition. *Soft Matter* **2009**, *5*, 3682-3688.
103. A. Burmistrova, M. Richter, M. Eisele, C. Üzüm, R. Von Klitzing, The Effect of Co-Monomer Content on the Swelling/Shrinking and Mechanical Behavior of Individually Adsorbed PNIPAM Microgel Particles. *Polymers* **2011**, *3*, 1575-1590.
104. S. Backes, P. Krause, W. Tabaka, M. U. Witt, R. von Klitzing, Combined Cononsolvency and Temperature Effects on Adsorbed PNIPAM Microgels. *Langmuir* **2017**, *33*, 14269-14277.

105. S. Backes, R. Von Klitzing, Nanomechanics and Nanorheology of Microgels at Interfaces. *Polymers* **2018**, *10*, 978.
106. T. Ando, N. Kodera, E. Takai, D. Maruyama, K. Saito, A. Toda, A high-speed atomic force microscope for studying biological macromolecules. *Proc. Natl. Acad. Sci. U.S.A.* **2001**, *98*, 12468-14272.
107. T. Ando, T. Uchihashi, T. Fukuma, High-speed atomic force microscopy for nano-visualization of dynamic biomolecular processes. *Prog. Surf. Sci.* **2008**, *83*, 337-437.
108. S. Matsui, T. Kureha, S. Hiroshige, M. Shibata, T. Uchihashi, D. Suzuki, Fast Adsorption of Soft Hydrogel Microspheres on Solid Surfaces in Aqueous Solution. *Agnew.* Chem., Int. Ed. 2**017,** *56*, 12146-12149.
109. S. Matsui, Y. Nishizawa, T. Uchihashi, D. Suzuki, Monitoring Thermoresponsive Morphological Changes in Individual Hydrogel Microspheres. *ACS Omega* **2021**, 3, 10836-10842.

2. Capture I

"Non-Thermoresponsive Decanano-sized Domains in Thermoresponsive Hydrogel Microspheres Revealed by Temperature-Controlled High-Speed Atomic Force Microscopy"

*Part of this work was published in "Yuichiro Nishizawa, Shusuke Matsui, Kenji Urayama, Takuma Kureha, Mitsuhiro Shibayama, Takayuki Uchihashi and Daisuke Suzuki *Angewandte Chemie International Edition*, **2019**, *58*, 8809-8813.
(https://doi.org/10.1002/anie.201903483)

2.1 Introduction

In most cases reported so far, microgels have been synthesized by precipitation polymerization in water using *N*-isopropyl acrylamide (NIPAm) and *N*,*N*′-methylenebis(acrylamide) (BIS) as a cross-linker because this polymerization technique allows preparation of large amounts of microgels with uniform size, and stimuli-responsive properties can be extended by selecting appropriate co-monomers or by incorporating supramolecular cross-linkers.[1-4] The pNIPAm microgels are one of the most widely used microgels, given that they have a volume-phase-transition temperature (VPTT) around 32 °C.[1] As the physicochemical properties, that is, the degree of swelling, the softness, and the optical properties, of the microgels are governed by their structures, the understanding of the structures of microgels is crucial to developing advanced stimulus-responsive soft materials based on microgels.

So far, there have been many attempts to determine the accurate structure of pNIPAm-based microgels. The structure of microgels has been mainly studied by scattering techniques,[5-10] and imaging techniques including electron microscopy,[11,12] fluorescence microscopy,[13] atomic force microscopy (AFM),[14-16] and super-resolution microscopy.[17-19] Most of these previous reports have concluded that pNIPAm-based microgels prepared by precipitation polymerization exhibit an inhomogeneous structure of the core-shell, where the polymer density of the core is higher than that of the shell, which originates from the difference in reactivity between NIPAm and BIS, that is, BIS is consumed faster than NIPAm.[20-22] However, a definite conclusion about the accurate nanoscale structure of the microgels has not yet been achieved because of the limitations associated with the spatio-temporal resolution of imaging techniques conducted in aqueous solutions.

In this context, the author discovered that thermoresponsive pNIPAm microgels exhibit not only well-known core–shell structures, but also inhomogeneous decanano-scale spherical domains that are not thermoresponsive. A suitable technique to examine this phenomenon is temperature-controlled, high-speed atomic force microscopy (TC-HS-AFM).[23-26]

2.2 Experimental section

Materials

N-isopropyl acrylamide (NIPAm, purity 98%), *N*,*N*'-methylenebis(acrylamide) (BIS, 97%), potassium peroxodisulfate (KPS, 95%), 2,2'-azobis(2-methylpropion amidine) dihydrochloride (V-50, 97%), sodium dodecyl sulfate (SDS, 95%), sorbitan monooleate (span80), ethanol (99.5%), and hexane (96 %) were purchased from Wako Pure Chemical Industries (Japan) and used as received. Fluorosurf was purchased from Fluoro Technology (Japan). Water for the preparation of microgels was initially distilled and subsequently subjected to ion exchange (EYELA, SA-2100E1).

Preparation of Microgels by Precipitation Polymerization

Typical poly(NIPAm-*co*-BIS) microgels that differ with respect to cross-linking density and size were prepared via aqueous precipitation polymerization using KPS as an initiator. Polymerizations were performed in a three-necked round-bottom flask (200 mL) equipped with a mechanical stirrer, condenser, and nitrogen gas inlet. The initial total monomer concentration was held constant at 150 mM. A mixture of NIPAm, BIS, and SDS in water (95 mL) was prepared as the monomer solution in the round-bottom flask. The individual monomer and SDS concentrations are listed in Table S1. To remove any oxygen, the monomer solution was heated to 70 °C in an oil bath and sparged with nitrogen (30 min) under constant stirring (250 rpm). After stabilizing the solution for 30 min, free-radical polymerizations were initiated by adding KPS (2 mM, 0.054 g) in water (5 mL). The solutions were stirred for 4 h, and after the completion of the polymerizations, the obtained dispersions were cooled to room temperature. Each batch of microspheres was purified via two cycles of centrifugation/re-dispersion in water using a relative centrifugal force (RCF) of 415000 × g, followed by dialysis for a week with daily water changes.

Preparation of Microgels by Inverse Miniemulsion Polymerization

In order to compare the effect of the polymerization method, an inverse miniemulsion polymerization was conducted in glass bottle with a magnetic stirrer at constant stirring (450 rpm) using V-50 as a photo-initiator. The initial total monomer concentration was held constant at 1000 mM. A monomer solution (7.5 mL), in which NIPAm (97 mol%, 0.823 g), BIS (3 mol%, 0.035 g), and V-50 (14 mM, 0.029 g) were dissolved, was added to a mixture of Span 80 (1.4 g) and hexane (43 g). The inverse miniemulsion was prepared by ultrasonication using an ultrasonic homogenizer (VC-75, SONICS). Dissolved oxygen was removed from the inverse miniemulsion by sparging with N_2 for 30 min prior to the polymerization. Then, the polymerization was initiated by exposure to UV irradiation (UVL-400HA (365 nm), Rikoukagakusangyo Co. Ltd.) at room temperature (T < LCST) or at 40 °C (LCST < T) for 15 min under an atmosphere of nitrogen. After stabilizing the solution for more than

4 h, the obtained microgel dispersion was centrifuged and redispersed in ethanol to break the emulsion. Subsequently, the dispersion was centrifuged (296000 g) and redispersed in water in order to exchange ethanol for water, before the microgels were purified via dialysis for a week with daily water changes.

Electron Microscopy

The morphology of the microgels in the dried state was visualized by transmission electron microscopy (TEM, JEOL2010; operated at 200 kV). For the TEM observations, diluted microgel dispersions (0.005 wt%, 2 µL) were dropped on carbon-coated copper grids (Okenshoji Co.,Ltd.), which were dried at room temperature.

Light Scattering Measurements

The temperature-dependence of the hydrodynamic diameter (D_h) of the microgels in pure water was determined by dynamic light scattering (DLS; Malvern Instruments Ltd.; ZetasizerNanoS). The DLS data represent averages of three individual measurements of 15 consecutive runs of the intensity autocorrelation (acquisition time: 30 s). The concentration of the microgels in the DLS experiments was approximately 0.002 wt%. The samples were allowed to thermally equilibrate at 25°C for 10 min prior to each measurement. The time-dependent scattering intensity was detected at a total scattering angle of 173°. The hydrodynamic diameter of the microspheres was calculated from the measured diffusion coefficients using the Stokes–Einstein equation (Zetasizer software v6.12).
To gain information on the internal structure of the water-swollen microgels in the bulk solution, static light scattering (SLS) measurements were conducted with a DLS/SLS-5000 (ALV, Langen) and a He−Ne laser (632.8 nm, 22 mW). The scattering angle was changed in increments from 30° to 90°. The SLS data represent averages of 15 consecutive runs of the intensity autocorrelation (acquisition time: 30 s). The samples were allowed to thermally equilibrate at the target temperature (25 °C and 40 °C) for 10 min prior to each measurement.

To analyze the scattering curves of the microgels, a fuzzy sphere form factor, $P(q)_{\text{fuzzy}}$, (eq. 2.1)[7] was used:

$$P(q)_{\text{fuzzy}} = A\left[\frac{3[\sin(qR)-qR\cos(qR)]}{(qR)^3}\exp\left(-\frac{(\sigma_{\text{surf}}q)^2}{2}\right)\right]^2 \qquad \text{(Eq. 2.1)}$$

where, R denotes the radius of the particle where the scattering length density profile decreased to half the core density. σ_{surf} denotes the width of the smeared particle surface (fuzzy layer). A and q are the scale value to normalize the total scatter volume, and the scattering vector, respectively.

Electrophoresis Analysis

The electrophoretic mobility (EPM) of the microgels in aqueous solution was determined using a Zetasizer NanoZS system (Malvern, Zetasizer software Ver. 7.12). The EPM data represent averages of three individual measurements of 20 consecutive runs. In order to equilibrate the sample temperature, the samples were allowed to stand at 25 °C for 10 min before each measurement. The microgel concentration was 0.001 wt%.

TC-HS-AFM Observation

A laboratory-built HS-AFM was used in this study, and the details are described elsewhere.[25,26] All images and movies shown in this paper were acquired in tapping mode, in which a small cantilever (length: 10 μm; width: 2 μm; thickness: 90 nm; BL-AC10-DS, Olympus, Japan) oscillates near its mechanical resonance frequency. The cantilever oscillation was detected by an optical-beam-deflection detector with a red laser (680 nm). Typical values for the spring constant, resonant frequency, and quality factor in an aqueous solution of this cantilever are ~0.1 N/m, ~600 kHz, and ~2, respectively. An amorphous carbon tip was grown on the original bird-beak tip by electron beam deposition, and the carbon tip was subsequently sharpened (radius: ~4 nm) by plasma etching under an argon atmosphere. For the HS-AFM imaging of the microgels, the cantilever free-oscillation amplitude was set to 5~30 nm, and the set-point amplitude was set to 70-90% (depending on the microsphere size) of the free-oscillation amplitude.

To construct the phase images, a phase delay of the oscillating cantilever relative to the driving signal was detected by a lock-in amplifier (HF2LI: Zurich Instrument, Switzerland). A darker contrast in the phase images corresponds to delayed phases, which corresponds to regions with softer mechanical properties compared to those the other regions.[27]

In order to modify the hydrophobic properties of the mica surfaces, fluorosurf (Fluoro Technology, Japan), which forms a hydrophobic fluororesin film upon drying, was dropped (0.5 μL) onto the substrate surface and dried naturally. Then, pNIPAm microgels were physically adsorbed on the substrate using the following procedure: microgel dispersions (0.05 wt%; 3 μL) were dropped on the substrate, and after 5 min, the mica surface was rinsed with pure water to remove any excess of the microgels.

The thermo-responsive behavior of the microgels was observed using a temperature-control device equipped with HS-AFM.[26] The thermocouple was attached to the cantilever holder and immersed in the HS-AFM fluid cell, which was filled with water (80 μL). Applying a DC current through the indium-tin-oxide glass at the bottom of the cantilever holder, the aqueous solution was heated at a rate of ~1.5 °C / min by a feedback control on the software of the HS-AFM. All HS-AFM imaging was performed under the following conditions: 120 ×120 pixels^2; frame rate = 1 fps.

2.3. Results and discussion

2.3.1. Synthesis and characterization of microgels prepared by precipitation polymerization

Initially, the author synthesized a series of pNIPAm microgels by aqueous free-radical precipitation polymerization with different concentrations of BIS or the anionic surfactant sodium dodecyl sulfate (SDS) to obtain microgels that differ with respect to their degree of cross-linking density and size (**Table 2.1**). Here, N and B refer to NIPAm and BIS, respectively, while the number refers to the degree of cross-linking (mol %).

Table 2.1. Chemical composition and properties of pNIPAm-based microgels that differ with respect to cross-linking density, size, and polymerization technique. Swelling ratio was defined as : Swelling ratio = (R_h at 25 °C)^3 / (R_h at 40 °C)^3.

code	NIPAm	BIS	SDS	TEM		D_h		EPM		swelling ratio
				D_{TEM}	CV	25 °C	40 °C	25 °C	40 °C	
	mol%	mol%	mM	nm	%	nm	nm	10^{-8} $m^2V^{-1}s^{-1}$		
NB1	99	1	0.5	332	7	379	157	-0.62	-2.64	14
NB2	98	2	0.5	254	9	350	166	-1.01	-2.71	9.4
NB3	97	3	0.5	166	4	336	173	-1.92	-3.23	7.3
NB4	96	4	0.5	248	7	323	167	-1.77	-3.31	7.2
NB5	95	5	0.5	235	7	329	171	-1.87	-2.92	7.1
NB6	94	6	0.5	225	7	312	191	-1.83	-2.78	4.5
NB10	90	10	0.5	201	5	296	201	-2.02	-2.65	3.2
NB5S1	95	5	1.0	159	6	230	124	-1.06	-2.74	6.4
ME	97	3	-	400	18	536	229	-1.33	-3.44	13
ME(G)	97	3	-	1110	24			polydisperse		

To confirm that the structures of these microgels are similar to those of previous reports, the microgels were characterized by various conventional techniques. First, the size uniformity of the microgels was confirmed by TEM (**Figure 2.1**). The monodispersed microgels were regularly arranged and separated from each other, indicating the presence of a shell layer with low polymer density that cannot be visualized by TEM, a feature which has already been reported (**Figure 2.1a-h**).[11,12, 28, 29] Subsequently, to gain information on the structure of the microgels in the swollen (25 °C) and collapsed states (40 °C) in aqueous solution, static light scattering (SLS) measurements were carried out, and the scattering curves for the microgels were analyzed (**Figure 2.2, Table 2.2**). All scattering curves of the microgels with different cross-linking densities in the swollen and collapsed states can be well fitted by a fuzzy sphere form factor, $P(q)_{fuzzy}$ [Eq. (S1) **Figure 2.2**],[7] which describes core–shell structures with two zones of different polymer densities.. The core–shell structure of the microgels was also supported by the different temperature dependence of overall hydrodynamic diameter, D_h, and the electrophoretic mobility, EPM (**Figure 2.3**), which indicate that the core deswells at lower temperatures than the shell.[30]

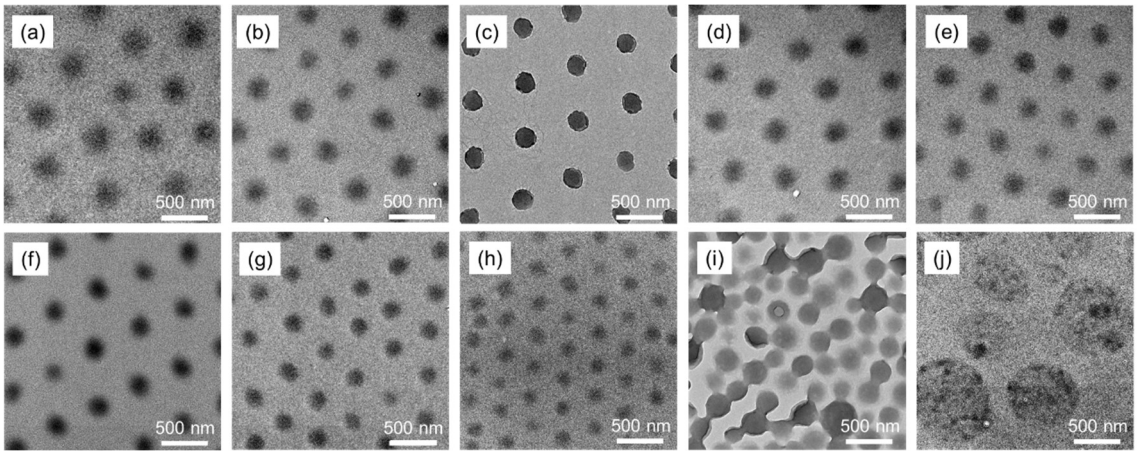

Figure 2.1. TEM images of dried microgels that differ with respect to cross-linking density, SDS concentration during the polymerization, and polymerization technique: (a) NB1, (b) NB2, (c) NB3, (d) NB4, (e) NB5, (f) NB6, (g) NB10, (h) NB5S1, (i) ME, and (j) ME(G).

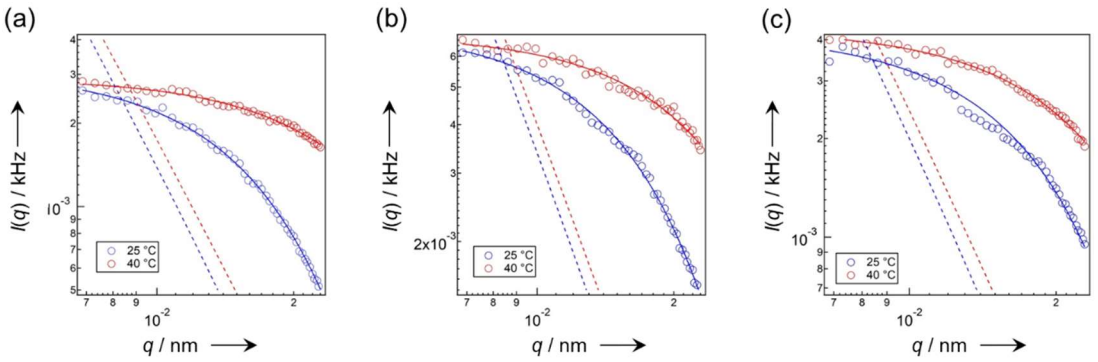

Figure 2.2. SLS intensities of individual microgels and fitting curves obtained from eq. S1 (solid line) at 25 °C (blue) and 40 °C (red): (a) NB3, (b) NB6, and (c) NB10.

Table 2.2. Summary of the results of the SLS measurements. Fitting parameters of eq. S1 and R_g / R_h ratio of the microgels that differ with respect to the cross-linking density (25 °C and 40 °C).

code	25 °C					40 °C				
	σ_{surf}	R	R_g	R_h	R_g/R_h	σ_{surf}	R	R_g	R_h	R_g/R_h
	nm	nm	nm	nm		nm	nm	nm	nm	
NB3	25	102	79	174	0.45	4.8	69	54	81	0.67
NB6	22	97	75	158	0.47	5.5	75	58	83	0.70
NB10	13	107	83	166	0.50	8.1	84	65	88	0.74

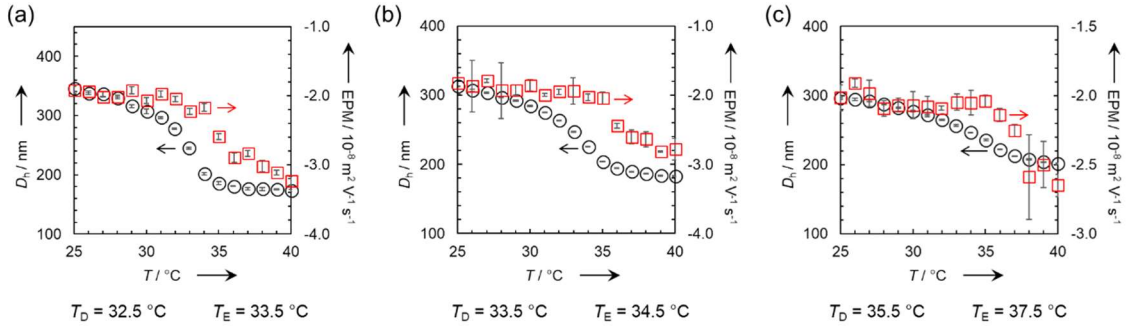

Figure 2.3. Temperature dependence of D_h (left axis, black) and EPM (right axis, red) of microgels with different cross-linking densities. (a) NB3, (b) NB6, and (c) NB10.

2.3.2. Evaluation by TC-HS-AFM

Subsequently, the author visualized the nanoscopic structures of these well-characterized microgels by TC-HS-AFM. **Figures 4a** and **4b** show height images and the corresponding phase images of NB3 microgels attached to a hydrophobized mica substrate in aqueous solution. It should be noted that the phase images, which reflect the difference in physical properties of the sample,[27] corroborate a shell layer surrounding a microgel core (**Figure 2.4a, b**). The diameter of the microgels obtained from the height images is almost identical with the width of the core region obtained from phase images, which suggests that the microgels observed in the height images represent only the core region (**Figure 2.5**). As confirmed by three-dimensional images constructed from these height images, the volume of individual microgels decreases with increasing temperature (**Figure 2.4c**). This observation is consistent with the temperature dependence of microgel volume calculated from the DLS-derived D_h (**Figure 2.6**).

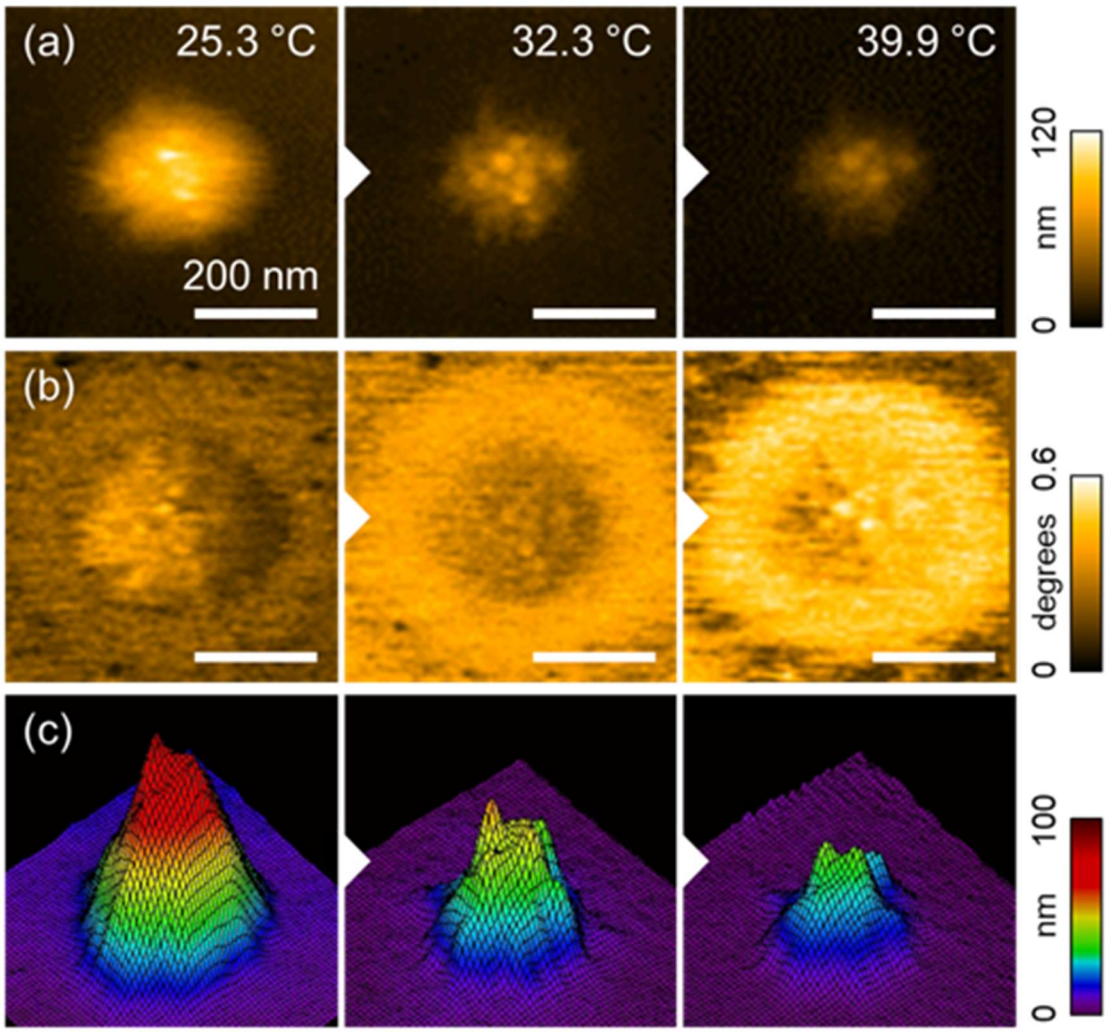

Figure 2.4. TC-HS-AFM analysis of representative pNIPAm microgels (NB3). Temperature dependence of the (a) height images, (b) phase images, (c) 3D images constructed from each height image.

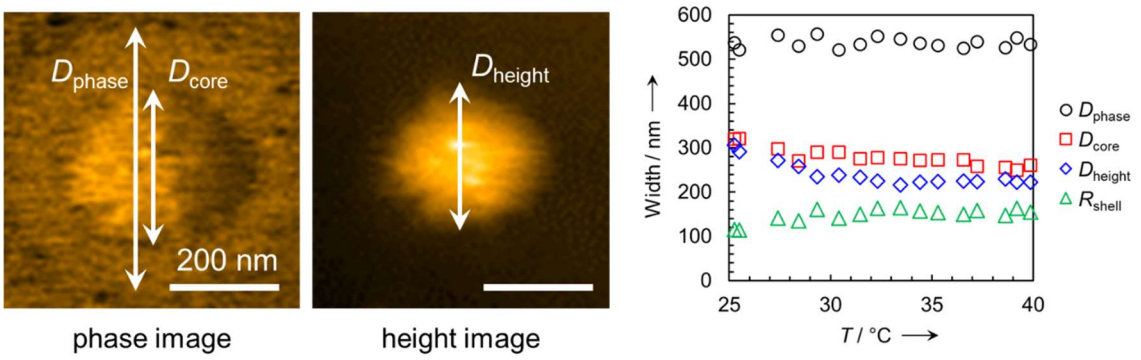

Figure 2.5. Temperature dependence of $D_{phase,}$ $D_{core,}$ and $D_{height.}$ These parameters were measured using phase and height images. R_{shell}, which calculated by R_{shell} = (D_{phase} - D_{core})/2, is also plotted. As the thermoresponsive behavior of D_{core} and D_{height} is almost identical, microgels observed by height images exhibited only the core region. The R_{shell} value is almost consistent with $4\sigma_{surf}$, which corresponds to the length of the shell layer of the microgels as estimated by the SLS measurements.[3]

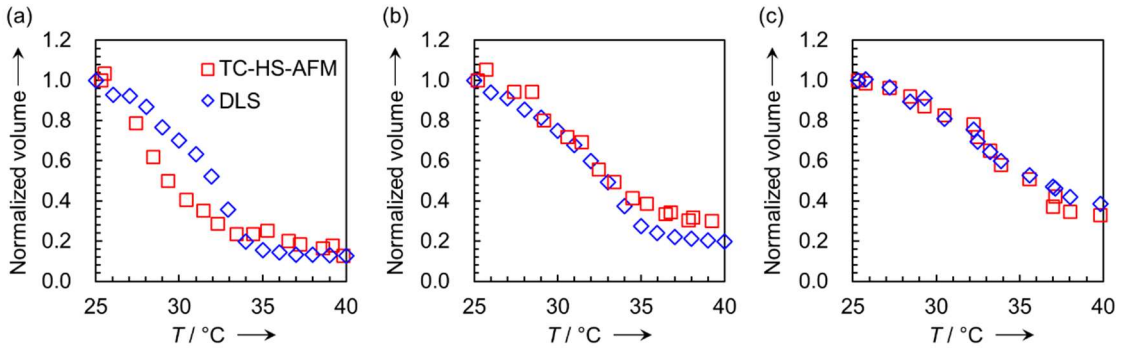

Figure 2.6. Temperature dependence of the normalized volume, calculated from height images or D_h for (a) NB3, (b) NB6, and (c) NB10. The obtained data show good agreement with each other. The deviation of the thermoresponsive behavior might be caused by a restriction of the volume changes due to the adsorption on the solid surface.

Here, as shown in height images, the decanano-sized domains become clearly visible by increasing the temperature. Most interestingly, the domain exists even when the NB3 microgels are in the swollen state at 25.3 °C, and the number and size of the domains remain almost constant while increasing the temperature, indicating that the domains are not thermoresponsive (**Figures 2.7, 2.8**). In addition, when comparing the height and phase images at each temperature, it can be observed that the domains exist in the core region of the microgels. These trends are qualitatively consistent with the other pNIPAm-based microgels with different cross-linking densities (**Figure 2.9-2.14**). Because of non-thermoresponsiveness of the domains, the domains must be BIS-rich aggregates formed in the initial stage of precipitation polymerization.[1] Additionally, it is widely accepted that a cross-linked gel shell suppresses core swelling in core–shell microgels.[31] A similar effect may occur for the decanano-scale domains.

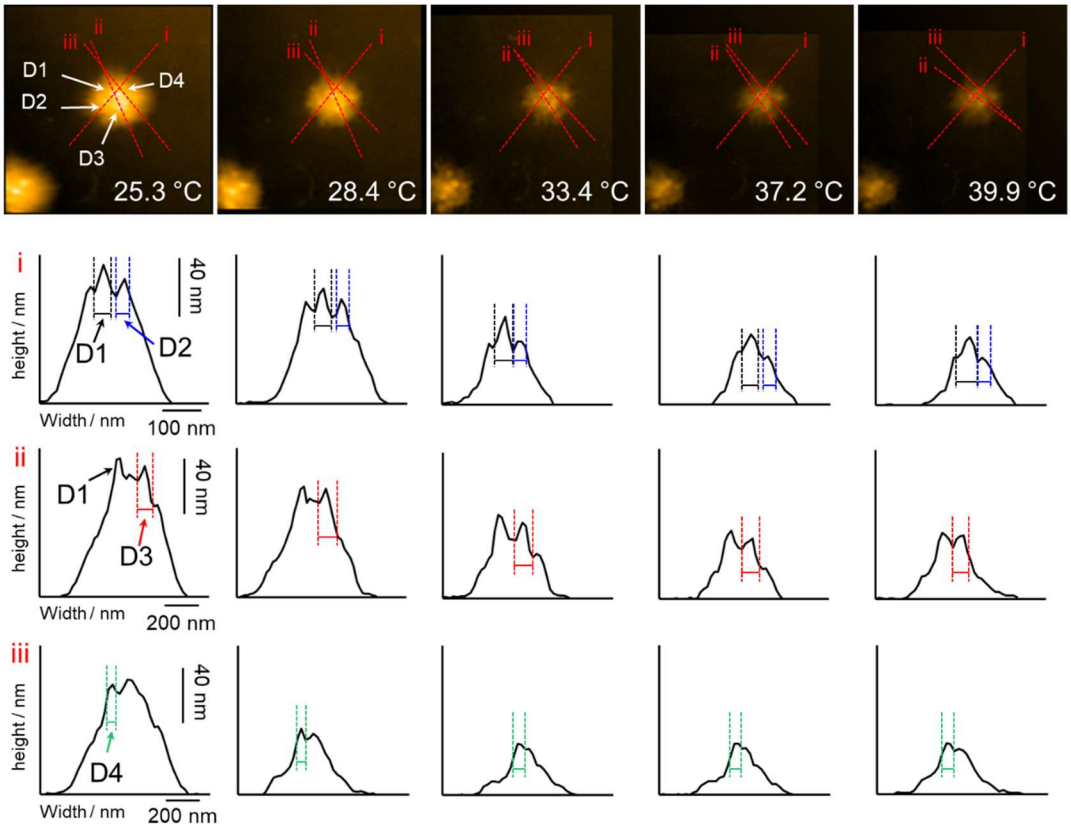

Figure 2.7. Details of the measurement of domain size in the case of NB3. Temperature dependence of height images and cross-section profiles corresponding to each red line. The domain size was evaluated from the cross-section profiles of the domain region observed by TC-HS-AFM. Note that the region, whose height is higher than the surroundings', e.g. in a bump in the cross-section profile, was considered as a domain, and its width was measured.

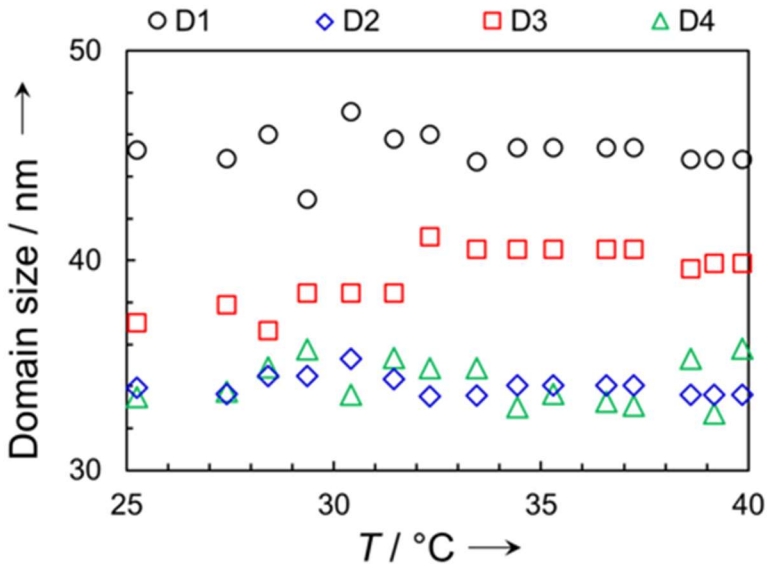

Figure 2.8. Temperature dependence of domain size in Figure 7.

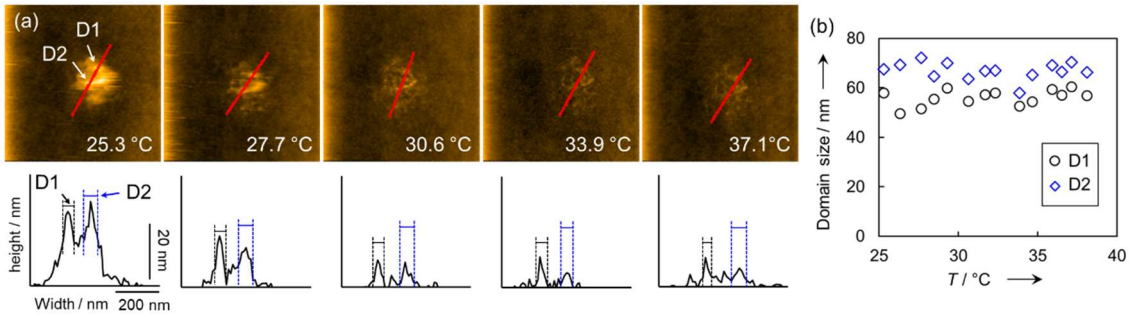

Figure 2.9. (a) Temperature dependence of the height images (above), corresponding cross-section profiles (below), and (b) domain size for NB1 microgels.

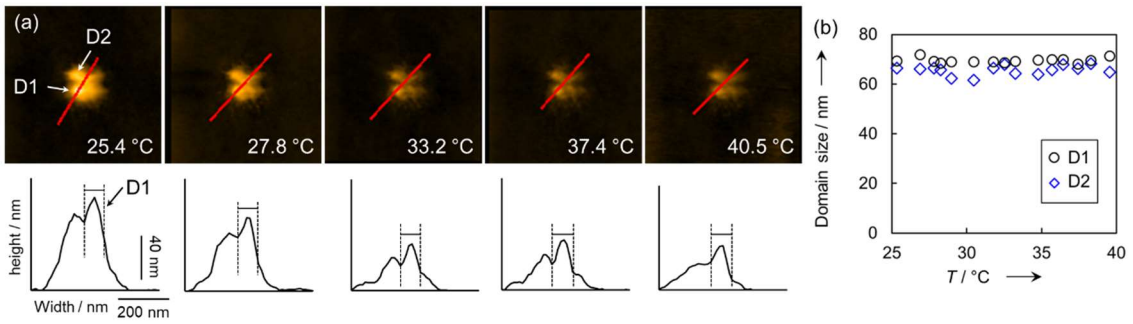

Figure 2.10. (a) Temperature dependence of the height images (above), corresponding cross-section profiles (below) and (b) domain size for NB2 microgels.

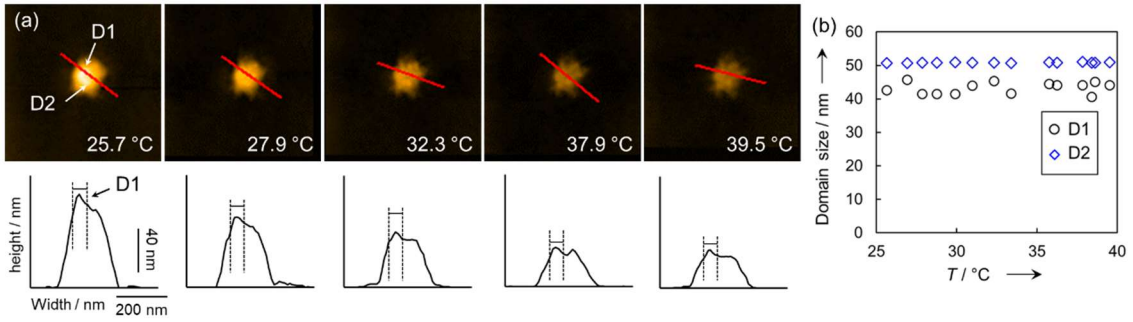

Figure 2.11. (a) Temperature dependence of the height images (above), corresponding cross-section profiles (below) and (b) domain size for NB4 microgels.

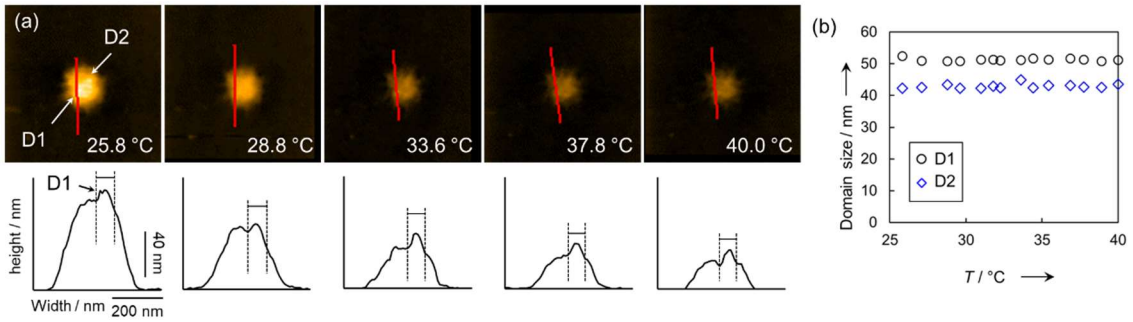

Figure 2.12. (a) Temperature dependence of the height images (above), corresponding cross-section profiles (below) and (b) domain size for NB5 microgels.

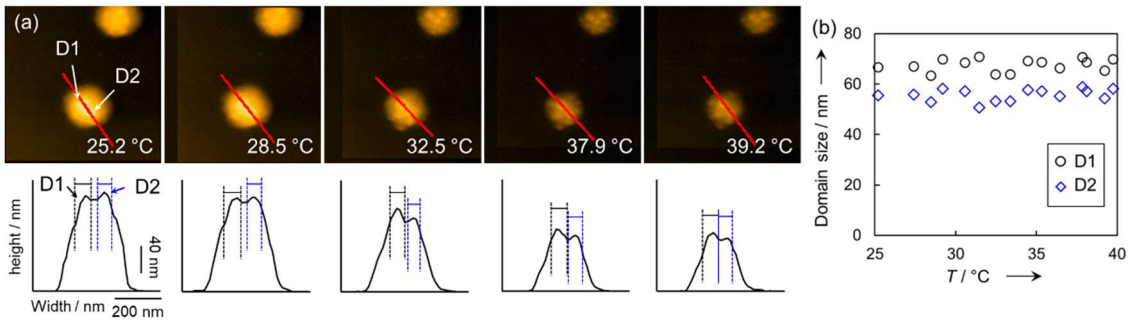

Figure 2.13. (a) Temperature dependence of the height images (above), corresponding cross-section profiles (below) and (b) domain size for NB6 microgels.

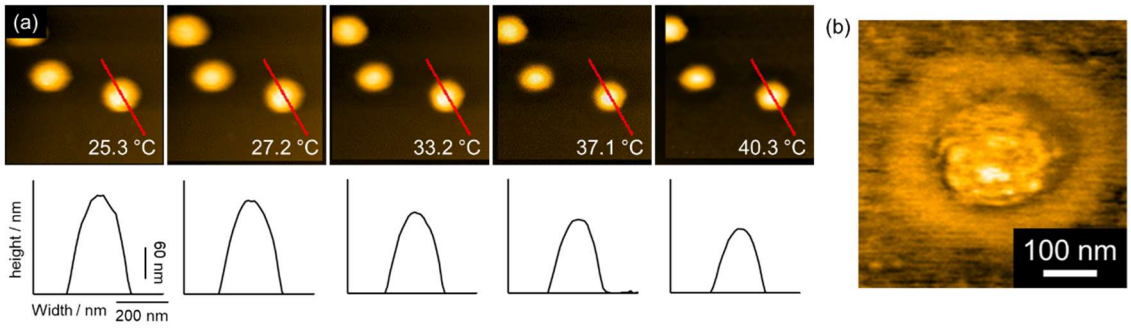

Figure 2.14. (a) Temperature dependence of the height images (above) and corresponding cross-section profiles (below) for NB10 microgels. (b) Phase image of a magnified NB10 microgel at 40.3 °C. Although domains could not be defined using the height images, they were observed in the phase images. Therefore, it seems likely that the domains are embedded in the core region of the highly crosslinked microgels.

So far, several reports have suggested that such nano-sized or decanano-sized inhomogeneous domains exist in thermoresponsive pNIPAm microgels prepared by precipitation polymerization. For example, Saunders has proposed four types of possible microgel structures.[8] Two of the proposed structures are composed of aggregated nanoparticles with or without core–shell structures. In the same paper,[8] a small-angle neutron scattering (SANS) analysis was conducted to elucidate the structure, but conclusive results were unfortunately not obtained. Höfl et al. observed several humps (≈100 nm) on poly(NIPAm-*co*-vinyl acetic acid) microgels (≈1200 nm) only above the VPTT, by means of AFM in an aqueous solution.[32] Thus, it was concluded that the origin of the humps was probably due to the collapsing of dangling chains on the surface of the microgels with an increase in temperature. In contrast to these conclusions, the presence, position, and responsiveness of decanano-sized domains have been clarified, for the first time, herein. Recently, the existence of decanano-sized domains in pNIPAm microgels cross-linked with a fluorophore have been reported by using super-resolution microscopy, although the thermoresponsiveness of the nanostructures was not investigated.[33] This result supports the findings in this study, that is, that the decanano-sized domains are not artifacts of the TC-HS-AFM measurements.

2.3.3. Evaluation of microgels prepared by inverse miniemulsion polymerization

To clarify that the existence of non-thermoresponsive domains in pNIPAm microgels prepared by precipitation polymerization, further experiments were conducted. Initially, the size of the domains in the smaller pNIPAm microgels, which were synthesized with a higher SDS concentration (1 mm), was investigated. The domains were also observed, and their sizes were virtually temperature independent (**Figure 2.15**).

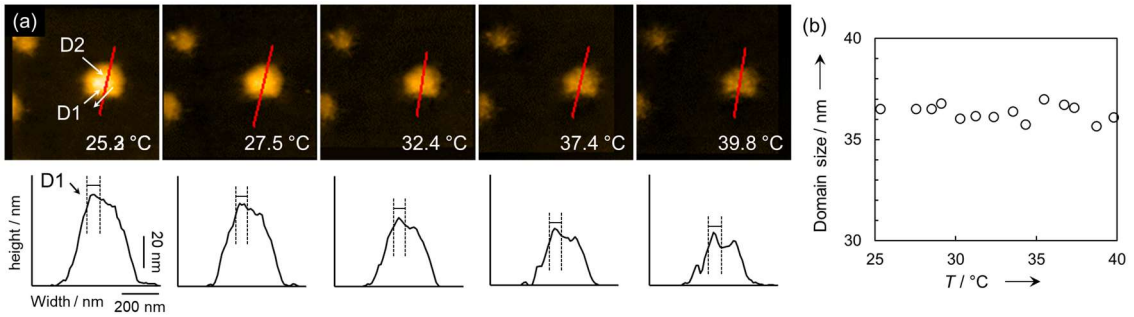

Figure 2.15. (a) Temperature dependence of the height images (above), corresponding cross-section profiles (below) and (b) domain size for NB5S1 microgels.

Then, pNIPAm microgels were prepared by a different polymerization technique, that is, by inverse miniemulsion polymerization,[34,35] where individual aqueous submicron-sized droplets become microgels after the polymerization. In principle, inverse miniemulsion polymerization can be conducted below and above the VPTT. As expected, the decanano-sized domain structure was not observed for microgels synthesized below the VPTT (denoted as ME), neither in the swollen nor collapsed states (**Figure 2.16a,e**). Conversely, for microgels synthesized above the VPTT [denoted as ME(G)], a domain structure distributed over the entire microgel structure was clearly observed, even in the swollen state (25.2 °C; **Figure 2.16b**). The volume of the individual microgels decreased with increasing temperature while maintaining the domain structure (**Figure 2.16d,f,g**), which is analogous to the case of microgels synthesized by precipitation polymerization (**Figure 4**). It is worth noting that the pNIPAm microgels prepared by inverse miniemulsion polymerization (both below and above the VPTT) do not exhibit a core–shell structure, which was confirmed by comparing the height and phase images (**Figure 2.16a,b**).

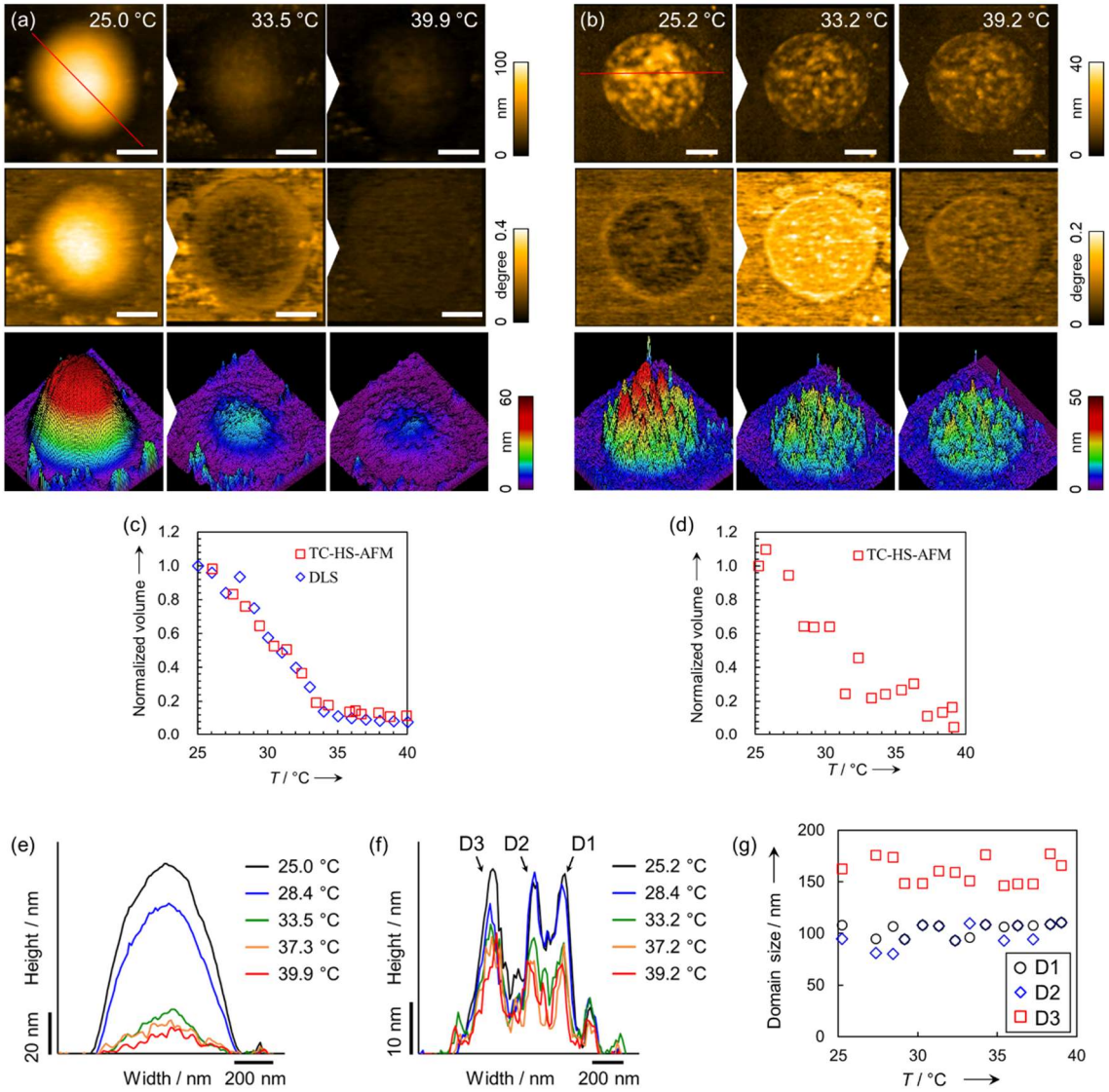

Figure 2.16. Temperature dependence of the height, phase, and 3D images for (a) ME and (b) ME(G). Temperature dependence of the normalized volume for (c) ME and (d) ME(G). (c) Cross-section profiles for ME (e) and ME(G) (f) during heating. (g) Temperature dependence of the domain size in ME(G).

Taking all results and the knowledge from previous reports into consideration, the author proposes plausible structures for the pNIPAm microgels prepared by different polymerization techniques (**Scheme 2.1**): a) inhomogeneous core–shell microgels, with decanano-sized domains in the high-density core, prepared by precipitation polymerization, b) homogeneous microgels prepared by inverse miniemulsion polymerization below the VPTT, and c) inhomogeneous microgels, with many nano-sized to submicron-sized domains in the entire microgel, prepared by inverse miniemulsion polymerization above the VPTT. It should be noted that the homogeneous microgels shown in **Scheme 2.1b** should exhibit inhomogeneities on the molecular scale, which has been discussed predominantly for bulk hydrogels,[36,37] although TC-HS-AFM was unable to distinguish such nanostructures.

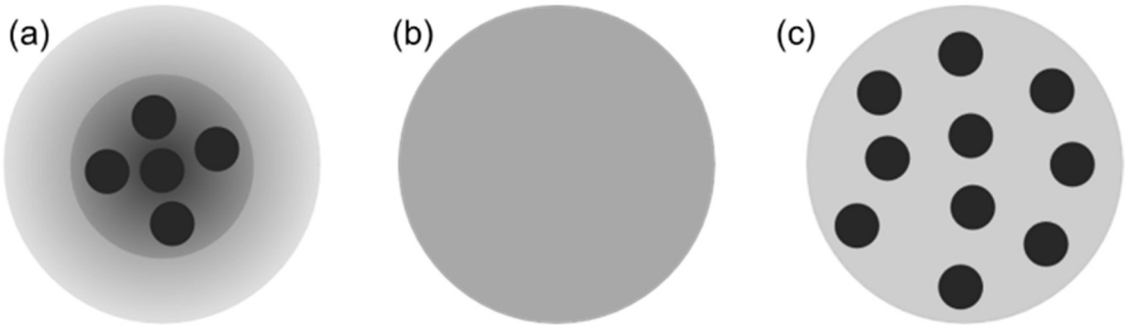

Scheme 2.1. Schematic illustration of the structure of pNIPAm microgels synthesized by different polymerization techniques: a) precipitation polymerization, b) inverse miniemulsion polymerization below the VPTT, and c) inverse miniemulsion polymerization above the VPTT.

2.4. Conclusion

In conclusion, the structure of pNIPAm-based microgels was carefully investigated by TC-HS-AFM, as well as by other conventionally used techniques. By monitoring the thermoresponsive behavior of individual microgels, and comparing it to that of bulk hydrogels, different inhomogeneous structures involving decanano-scale spherical domains, which are not thermoresponsive in thermoresponsive microgels, were discovered. The author also clarified that the structure of the microgels strongly depends on the method used to produce microgels. The approach shown in this study can be expected to be applicable to all thermoresponsive microgels and probably to other stimuli-responsive colloids. Therefore, The author believes that the deeper understanding of stimuli-responsive nanostructures of microgels will help in developing advanced applications, that is, microgel glasses/crystals whose physical properties should be strongly affected by their micro constituents.

2.5. References

1. R. Pelton, Temperature-sensitive aqueous microgels. *Adv. Colloid Interface Sci.* **2000**, *85*, 1–33.
2. S. Nayak, L. A. Lyon, Soft nanotechnology with soft nanoparticles. *Angew. Chem., Int. Ed.* **2005**, *44*, 7686 – 7708.
3. F. A. Plamper, W. Richtering, Functional Microgels and Microgel Systems. *Acc. Chem. Res.* **2017**, *50*, 131–140.
4. T. Kureha, D. Aoki, S. Hiroshige, K. Iijima, D. Aoki, T. Takata, D. Suzuki, Decoupled thermo-and pH-responsive hydrogel microspheres cross-linked by rotaxane networks. *Angew. Chem., Int. Ed.* **2017**, *56*, 15393 –15396.
5. K. Kratz, T. Hellweg, W. Eimer, Structural changes in PNIPAM microgel particles as seen by SANS, DLS, and EM techniques. *Polymer* **2001**, *42*, 6631–6639;
6. S. Takata, M. Shibayama, R. Sasabe, H. Kawaguchi, Preparation and structure characterization of hairy nanoparticles consisting of hydrophobic core and thermosensitive hairs. *Polymer* **2003**, *44*, 495–501.
7. M. Stieger, W. Richtering, J. S. Pedersen, P. Lindner, Small-angle neutron scattering study of structural changes in temperature sensitive microgel colloids. *J. Chem. Phys.* **2004**, *13*, 6197–6206.
8. B. R. Saunders, On the Structure of Poly(*N*-isopropylacrylamide) Microgel Particles. *Langmuir.* **2004**, *20*, 3925–3932.
9. N. Boon, P. Schurtenberger, Swelling of micro-hydrogels with a crosslinker gradient. *Phys. Chem. Chem. Phys.* **2017**, *19*, 23740–23746.
10. R. Keidel, A. Ghavami, D. M. Lugo, G. Lotze, O. Virtanen, P. Beumers, J. S. Pedersen, A. Bardow, R, G. Winkler, W. Richtering, Time-resolved structural evolution during the collapse of responsive hydrogels: The microgel-to-particle transition. *Sci. Adv.* **2018**, *4*, eaao7086.
11. R. H. Pelton, P. Chibante, Preparation of aqueous latices with *N*-isopropylacrylamide. *Colloids Surf.* **1986**, *20*, 247–256.
12. D. Suzuki, H. Kawaguchi, Stimuli-sensitive core/shell template particles for immobilizing inorganic nanoparticles in the core. *Colloid Polym. Sci.* **2006**, *284*, 1443-1451.
13. H. Minato, M. Murai, T. Watanabe, S. Matsui, M. Takizawa, T. Kureha, D. Suzuki, The deformation of hydrogel microspheres at the air/water interface. *Chem. Commun.* **2018**, *54*, 932–935.
14. J. Wiedemair, M. J. Serpe, J. Kim, J. F. Masson, L. A. Lyon, B. Mizaikoff, C. Kranz, In-Situ AFM Studies of the Phase-Transition Behavior of Single Thermoresponsive Hydrogel Particles. *Langmuir* **2007**, *23*, 130–137.

15. A. Mourran, Y. Wu, R. A. Gumerov, A. A. Rudov, I. I. Potemkin, A. Pich, M. Möller, When Colloidal Particles Become Polymer Coils. *Langmuir* **2016**, *32*, 723–730.
16. B. Wedel, Y. Hertle, O. Wrede, J. Bookhold, T. Hellweg, Smart Homopolymer Microgels: Influence of the Monomer Structure on the Particle Properties. *Polymers* **2016**, *8*, 162.
17. G. M. Conley, S. Nöjd, M. Braibanti, P. Schurtenberger, F. Scheffold, Superresolution microscopy of the volume phase transition of pNIPAM microgels. *Colloids Surf. A* **2016**, *499*, 18–23.
18. A. P. H. Gelissen, A. Oppermann, T. Caumanns, P. Hebbeker, S. K. Turnhoff, R. Tiwari, S. Eisold, U. Simon, Y. Lu, J. Mayer, W. Richtering, A. Walther, D. Wöll, 3D Structures of Responsive Nanocompartmentalized Microgels. *Nano Lett.* **2016**, *16*, 7295–7301.
19. S. Bergmann, O. Wrede, T. Huser, T. Hellweg, Super-resolution optical microscopy resolves network morphology of smart colloidal microgels. *Phys. Chem. Chem. Phys.*, **2018**, *20*, 5074–5083.
20. X. Wu, R. H. Pelton, A. E. Hamielec, D. R. Woods, W. McPhee, The kinetics of poly(N-isopropylacrylamide) microgel latex formation. *Colloid Polym. Sci.* **1994**, *272*, 467–477.
21. T. Hoare, D. McLean, Kinetic Prediction of Functional Group Distributions in Thermosensitive Microgels. *J. Phys. Chem. B* **2006**, *110*, 20327–20336.
22. T. Hoare, D. McLean, Multi-Component Kinetic Modeling for Controlling Local Compositions in Thermosensitive Polymers. *Macromolecular Theory and Simulations* **2006**, *15*, 619–632.
23. T. Ando, N. Kodera, E. Takai, D. Maruyama, K. Saito, A. Toda, A high-speed atomic force microscope for studying biological macromolecules. *Proc. Natl. Acad. Sci. U.S.A.* **2001**, *98*, 12468–12472.
24. T. Ando, T. Uchihashi, T. Fukuma, High-speed atomic force microscopy for nano-visualization of dynamic biomolecular processes. *Prog. Surf. Sci.* **2008**, *83*, 337–437;
25. T. Ando, T. Uchihashi, S. Scheuring, Filming Biomolecular Processes by High-Speed Atomic Force Microscopy. *Chem. Rev.* **2014**, *114*, 3120–3188.
26. S. Matsui, Y. Nishizawa, T. Uchihashi, D. Suzuki, Monitoring Thermoresponsive Morphological Changes in Individual Hydrogel Microspheres. *ACS Omega* **2018**, *3*, 10836–10842.
27. S. N. Magonov, V. Elings, M. -H. Whangbo, Phase imaging and stiffness in tapping-mode atomic force microscopy. *Surf. Sci.* **1997**, *375*, 385–391.
28. K. Horigome, D. Suzuki, Drying Mechanism of Poly(N-isopropylacrylamide) Microgel Dispersions. *Langmuir* **2012**, *28*, 12962−12970.
29. M. Takizawa, Y. Sazuka, K. Horigome, Y. Sakurai, S. Matsui, H. Minato, T. Kureha, D. Suzuki, Self-Organization of Soft Hydrogel Microspheres during the Evaporation of Aqueous Droplets. *Langmuir* **2018**, *34*, 4515−4525.

30. E. Daly, B. R. Saunders, Temperature–dependent electrophoretic mobility and hydrodynamic radius measurements of poly(*N*-isopropylacrylamide) microgel particles: structural insights. *Phys. Chem. Chem. Phys.* **2000**, *2*, 3187–3193.
31. C. D. Jones, L. A. Lyon, Shell-Restricted Swelling and Core Compression in Poly(*N*-isopropylacrylamide) Core−Shell Microgels. *Macromolecules* **2003**, *36,* 1988-1993.
32. S. Höfl, L. Zitzler, T. Hellweg, S. Herminghaus, F. Mugele, Volume phase transition of "smart" microgels in bulk solution and adsorbed at an interface: A combined AFM, dynamic light, and small angle neutron scattering study. *Polymer* **2007**, *48*, 245–254.
33. A. A. Karanastasis, Y. Zhang, G. S. Kenath, M. D. Lessard, J. Bewersdorf, C. K. Ullal, 3D mapping of nanoscale crosslink heterogeneities in microgels. *Mater. Horiz.* **2018**, *5*, 1130-1136.
34. Y. S. Leng, F. Candau. Inverse microemulsion polymerization. *J. Phys. Chem.* **1982**, *86*, 2269-2271.
35. I. Capek, On inverse miniemulsion polymerization of conventional water-soluble monomers. *Adv.Colloid Interface Sci.* **2010**, *156*, 35-61.
36. M. Shibayama, Spatial inhomogeneity and dynamic fluctuations of polymer gels. *Macromol. Chem. Phys.* **1998**, *199*, 1–30.
37. M. Shibayama, T. Norisuye, Gel Formation Analyses by Dynamic Light Scattering. *Bull. Chem. Soc. Jpn.* **2002**, *75*, 641–659.

3. Chapter II

"Nanostructure and thermoresponsiveness of poly(*N*-isopropyl methacrylamide)-based hydrogel microspheres prepared via aqueous free radical precipitation polymerization"

*Part of this work was published in "Yuichiro Nishizawa, Haruka Minato, Takumi Inui, Ikuma Saito, Takuma Kureha, Mitsuhiro Shibayama, Takayuki Uchihashi and Daisuke Suzuki, *RSC Advances* **2021**, *11*, 13130-13137."
(https://doi.org/10.1039/D1RA01650D)

3.1. Introduction

As mentioned above capture, (pNIPAm)-based microgels have a volume-phase-transition temperature (VPTT) of ~32 °C and their physicochemical properties change quickly when the temperature increases beyond this point.[1,2] The VPTT of microgels can be controlled by varying the constituent chemical species, such as (meth)acrylamide analogues,[1,3,4] *N*-vinylcaprolactam (VCL),[5,6] and oligo(ethylene glycol) methylester (meth)acrylates.[7-9] This is especially notable in the case of *N*-isopropyl methacrylamide (NIPMAm), which differs from NIPAm only by a single methyl group at the α-position, where the obtained pNIPMAm microgels have a VPTT of ~43 °C.[10–18] The VPTT of microgels can also be tuned *via* the copolymerization of NIPMAm with other chemical species, such as NIPAm or VCL. [19-22]

Thermoresponsive microgels are mainly synthesized *via* aqueous free radical precipitation polymerization in water. In this system, microgels are formed *via* the self-assembly of phase-separated polymer chains.[1,23] In order to control the structure of the microgels, it is therefore important to understand the reactivity ratio between the main monomer and the cross-linker. To date, the structural elucidation of p(NIPAm-*co*-BIS) microgels has mainly been attempted using scattering techniques[24-26] and microscopy, [27,28] and it has been concluded that these microgels show heterogeneous core–shell structures as the BIS cross-linker is consumed faster than the NIPAm.[29] Recently, using TC-HS-AFM, it has be revealed that cross-linked pNIPAm microgels exhibit a non-thermoresponsive nano-structure in the core region.[30-34]

In general, the chemical structure of the monomer determines the reactivity ratio and thus, different reactivity ratios (*i.e.*, monomers) might cause structural changes in the microgels. For instance, the calculated reactivity ratio in the presence of BIS is lower for acrylamide than for methacrylamide (*e.g.*, acrylamide: $r_1 = 0.48$; BIS: $r_2 = 2.0$; methacrylamide: $r_1 = 0.85$; BIS: $r_2 = 0.84$),[35,36] suggesting that the structure of the microgels composed of acrylamide or methacrylamide derivatives is different.

To clarify the internal structure of microgels composed of pNIPMAm, methacrylamide

derivatives, the author investigated the detailed nanostructure and thermoresponsiveness of pNIPMAm-based microgels, prepared by precipitation polymerization, using a combination of electron microscopy, static/dynamic light scattering techniques, and TC-HS-AFM.

3.2. Experimental section

3.2.1. materials

N-Isopropyl methacrylamide (NIPMAm, purity 97%) was purchased from Sigma-Aldrich and used as received. *N*,*N*′-Methylenebis(acrylamide) (BIS, 97%), sodium dodecyl sulfate (SDS, 95%), and potassium peroxodisulfate (KPS, 95%) were purchased from FUJIFILM Wako Pure Chemical Corporation (Japan) and used as received. Fluorosurf® was purchased from Fluoro Technology (Japan). Distilled ion-exchanged water used in the preparation of the microgels was obtained from EYELA, SA-2100E1.

3.2.2. Preparation of microgels by precipitation polymerization

Poly(NIPMAm-*co*-BIS) microgels were synthesized by aqueous free radical precipitation polymerizations, which were conducted in three-necked round bottom flasks (300 mL). The flasks were charged with NIPMAm (1.72 g), BIS (0.232 g), and water (90 mL), before a mechanical stirrer and condenser were installed. Then, the monomer solution was heated to 70 °C and sparged with nitrogen (30 min). Subsequently, an aqueous solution (5 mL) of SDS (0.0578 g) and an initiator solution (5 mL water and 0.0543 g KPS) were added in this order. After 4 h, the thus obtained microgel dispersions were cooled to room temperature to terminate the polymerization. Microgels were purified by two cycles of centrifugation (415 000 × *g*)/redispersion in pure water and dialysis for a week (daily water changes).

3.2.3. Field emission scanning electron microscopy

The size uniformity of the microgels was evaluated by field emission scanning electron microscopy (FE-SEM, Hitachi Ltd., S-5000). For that purpose, microgel dispersions (2 μL; 0.002 wt%) were dried on a polystyrene substrate at room temperature. Prior to the measurements, Pt/Pd was sputtered onto the sample substrates (15 mA, 6 Pa, 80 s).

3.2.4. Light-scattering measurements

To evaluate the thermoresponsiveness of the hydrodynamic diameter (D_h) of the pNIPMAm microgels, dynamic light scattering (DLS) measurements were conducted (Malvern Instruments Ltd.; Zetasizer Nano S). The concentration of the microgel dispersions was approximately 0.002 wt%, and three individual measurements of 15 consecutive runs with 30 s of acquisition time were averaged. Prior to the measurements at each temperature, the samples were allowed to thermally equilibrate (10

min). The D_h of the microgels was derived from the obtained diffusion coefficients using the Stokes–Einstein equation (Zetasizer software v6.12).

The internal structure of the microgels in the dispersed state was evaluated by static light scattering (SLS) measurements using a DLS/SLS-5000 (ALV, Langen) and a He–Ne laser (632.8 nm, 22 mW). The scattering angle was changed from 30° to 90° and 15 individual measurements with 30 s of acquisition time were averaged. The concentration of the microgel dispersions was approximately 0.002 wt% and the samples were allowed to thermally equilibrate (10 min) prior to each measurement (25 °C and 50 °C). The scattering curves obtained from the SLS measurements were fitted by a fuzzy sphere form factor, $P(q)_{\text{fuzzy}}$:

$$P(q)_{\text{fuzzy}} = A\left[\frac{3[\sin(qR) - qR\,\mathrm{c}\quad(qR)]}{(qR)^3}\exp\left(-\frac{(\sigma_{\text{surf}}q)^2}{2}\right)\right]^2 \quad (3.1)$$

where, A, q, R, and σ_{surf} denote the scale values used to normalize the total scattering volume, the scattering vector, the radius of the particle where the scattering-length-density profile decreases to half the core density, and the width of the smeared particle surface (fuzzy layer), respectively.[24]

3.2.5. Electrophoresis analysis

The electrophoretic mobility (EPM) of the pNIPMAm microgels in the swollen and deswollen state dispersed in an aqueous NaCl solution (1 mM) was evaluated using a Zetasizer Nano ZS system (Malvern, Zetasizer software Ver. 7.12). Three individual measurements of 20 consecutive runs with 120 mV were averaged. The concentration of the microgel dispersions was approximately 0.01 wt% and the samples were allowed to thermally equilibrate (10 min) prior to the measurements at 25 °C and 50 °C.

3.2.6. TC-HS-AFM observations

A laboratory-built HS-AFM operated in tapping mode was used in this study.[32] As a AFM cantilever, a miniaturized cantilever (BL-AC10-DS, Olympus, Japan) was used (spring constant: ~0.1 N m^{-1}, quality factor: ~2, resonant frequency: ~600 kHz in water). The cantilever was vibrated at near the resonance frequency and its oscillation amplitude was detected by a fast amplitude detector through an optical-beam-deflection detector with a red laser (680 nm). To gain a sharp AFM probe, a carbon pillar was deposited by electron-beam deposition and that was subsequently sharpened by plasma etching under argon environment, resulting in an end radius of ~4 nm. For the HS-AFM observation of the microgels and microgel sheets, the free-oscillation amplitude of the cantilever far from the sample surface was set to 5–30 nm, and the set-point amplitude was set to 70–90% of the

free-oscillation amplitude, depending on the size and concentration of the microgels.

In addition to the topographic imaging, phase shifts of the cantilever oscillation detected by a lock-in amplifier (HF2LI, Zurich Instruments AG, Switzerland) were imaged simultaneously. The excitation signal was used as the reference of the lock-in detection and the time constant was 20 μs.

In order to adsorb the pNIPMAm microgels on the substrates, a hydrophobized mica substrate was used. For that purpose, Fluorosurf® (0.5 μL) was dropped on freshly cleaved mica and dried at room temperature to produce a hydrophobic fluororesin thin film. Subsequently, pNIPMAm microgel dispersions or pastes of different concentrations were dropped on the hydrophobized mica substrates. After 5 min, excess microgels were thoroughly removed by washing with pure water.

The thermoresponsiveness of the microgels with different adsorption concentrations was visualized using TC-HS-AFM.[30]

The solution temperature was increased by passing a DC current through the conductive indium tin oxide (ITO) glass at the bottom of the solution pool of the cantilever holder. The solution temperature, measured using thermocouples installed near the cantilever, can be increased by 2.0 °C min^{-1}*via* software feedback control.

3.3 Results and discussion

3.3.1. Microgel preparation and characterization in the dispersed state

Initially, the pNIPMAm microgels were prepared by aqueous free radical precipitation polymerization using BIS as the cross-linker. A field emission scanning electron microscopy (FE-SEM) analysis showed that uniformly sized pNIPMAm-based microgels with a size of 224 nm in the dried state were obtained (**Figure 3.1a**). Subsequently, the thermoresponsive behavior of the microgels was evaluated by dynamic light scattering (DLS). As the temperature was increased above 31 °C, the hydrodynamic diameter (D_h) of the microgels (322 nm) gradually decreased to an almost equilibrium size (209 nm) at 50 °C (**Figure 3.1b**). The volume transition temperature, defined as the temperature where the rate of change in volume reaches its maximum, was determined to be 45.5 °C. To examine the structure of the microgels in their swollen and deswollen states in aqueous solution, static light scattering (SLS) measurements were conducted (**Figure 3.1c**). The scattering profiles at 25 °C and 50 °C are described well by a fuzzy-sphere form factor (eqn (3.1)).[24] The thickness of the fuzzy layer(σ_{surf}) and the radius of the particle where the scattering-length-density profile decreased to half the core density (R) of the swollen microgels was 18 nm and 115 nm, whereas those of the deswollen microgels were 4.4 nm and 90 nm, respectively. This result suggests that the pNIPMAm microgels have, as previously reported,[4,37] a heterogeneous core–shell type structure in the swollen state. The electrophoretic mobility (EPM), which reflects the surface properties of a microgel, was -1.65×10^{-8} m^2 V^{-1} s^{-1} at 25 °C and -3.12×10^{-8} m^2 V^{-1} s^{-1} at 50 °C. In the case of pNIPAm microgels with the same BIS composition (D_h: 296 nm), σ_{surf}, R, and the EPM were 13 nm, 107 nm, and $-2.02 \times$

10^{-8} m^2 V^{-1} s^{-1} (swollen state) meanwhile 8.1 nm, 83 nm, and -2.65×10^{-8} m^2 V^{-1} s^{-1} (deswollen state).[32] Wedel *et al.* have reported similar results and concluded that pNIPMAm microgels possess more homogeneous network structures than pNIPAm microgels.[3] The larger EPM of the pNIPMAm microgels in the swollen state at 25 °C suggests that the cross-linking density of the surface of pNIPMAm microgels is lower than that of pNIPAm microgels, which is probably due to self-crosslinking in the latter.[13]

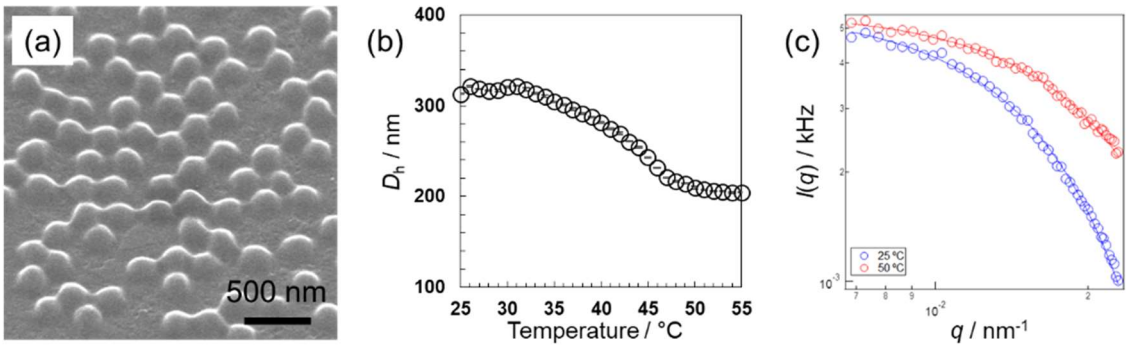

Figure 3.1. (a) FE-SEM images of pNIPMAm-based microgels. (b) Temperature dependence of the hydrodynamic diameter. (c) Scattering curves at 25 °C and 50 °C obtained from SLS measurements. The solid line shows the calculated value derived from eqn (3.1).

3.3.2. TC-HS-AFM observation of a single microgel

Next, the thermoresponsive behavior and nanostructure of a single pNIPMAm microgel were directly visualized using TC-HS-AFM, which allows low-invasiveness, real-time observation of the nanodynamics with controlling the solution temperature over a range from ~ 25 °C to 50 °C.[32,38] Here, the temperature was increased by 2 °C min^{-1}, while height and phase images, which show differences in the physical properties, and 3D images constructed from the height images were obtained at a rate of 1 s per frame (**Figure 3.2**). Due to the evaporation of the sample solution, the thermoresponsive behavior of the microgels was observed separately over a temperature range of ~ 25 °C to ~40 °C (**Figure 3.2a**) and ~40 °C to ~50 °C (**Figure 3.2b**). The phase images show a low-density shell layer with a width of 20 nm, which could not be observed in the height images. The height (D_{height}) and width of the microgel were obtained from the height images (**Figure 3.3a**). In agreement with the results of the DLS measurements, the microgel height decreased above 31 °C, but in contrast to D_h, the magnitude of change in the height is lower (**Figure 3.3b**). Thus, the microgel height did not match D_h at each temperature (*e.g.*, the height, width, and D_h at 25 °C were 233 nm, 347 nm, and 313 nm, respectively). The differences between the DLS and TC-HS-AFM measurements can be attributed to the effect of adsorption and deformation: the amphiphilic microgels were adsorbed on a hydrophobized mica substrate with deformation to minimize the contact area between water and

the substrate.[39] The width of the microgels, including the low-density shell layer, measured from the phase images (D_{phase}) remained almost constant with increasing temperature although the width of the core region in the phase images (D_{core}), along with D_{height}, also decreased (**Figure 3.3c,d**). This result indicates that the shell layer was strongly adsorbed onto the substrate. Thus, the changes in height of the core regions were not matched by the changes in D_h, which reflects the whole spherical microgel dispersed in aqueous solution. The ratio of the highly cross-linked core region of the pNIPMAm microgels (D_{core}/D_{phase}) was 0.78 ($N = 3$), whereas that of the pNIPAm microgels was 0.69 ($N = 3$).[32] This result indicates that the cross-linking distribution of the pNIPMAm microgels is more homogeneous as well as the result of SLS measurement and previous study.[3] The more homogeneous network structure may be caused by the comparable reactivity ratios of methacrylamide derivatives and BIS.[35,36] Moreover, non-thermoresponsive spherical domains with a width of 50–70 nm, similar to those of pNIPAm microgels,[32] were observed in the phase images (**Figure 3.3e,f**). This nanoarchitecture indicates that BIS-rich polymer chains, formed in the early stages of the precipitation polymerization process, aggregated in multiple steps during the nucleation process and formed highly cross-linked spherical domains.[32] Therefore, the authot concluded that the heterogeneous core–shell and non-thermoresponsive domains are formed in the microgels *via* precipitation polymerization even when the reactivity of the chemical species is different.

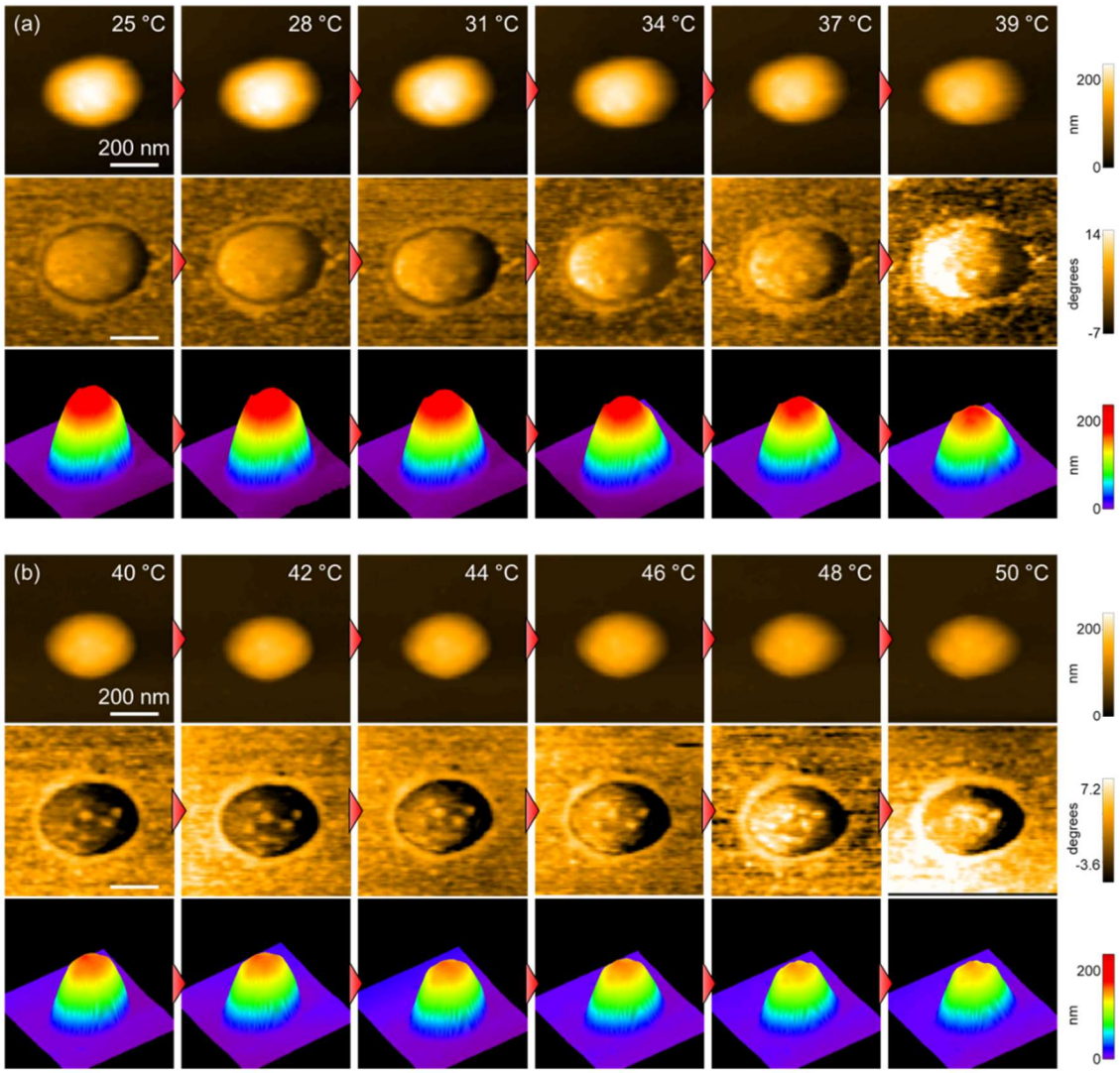

Figure 3.2. TC-HS-AFM images showing how the height (top), phase (middle), and constructed 3D images (bottom) of the pNIPMAm microgels vary with temperature. (a) 25–40 °C, (b) 40–50 °C.

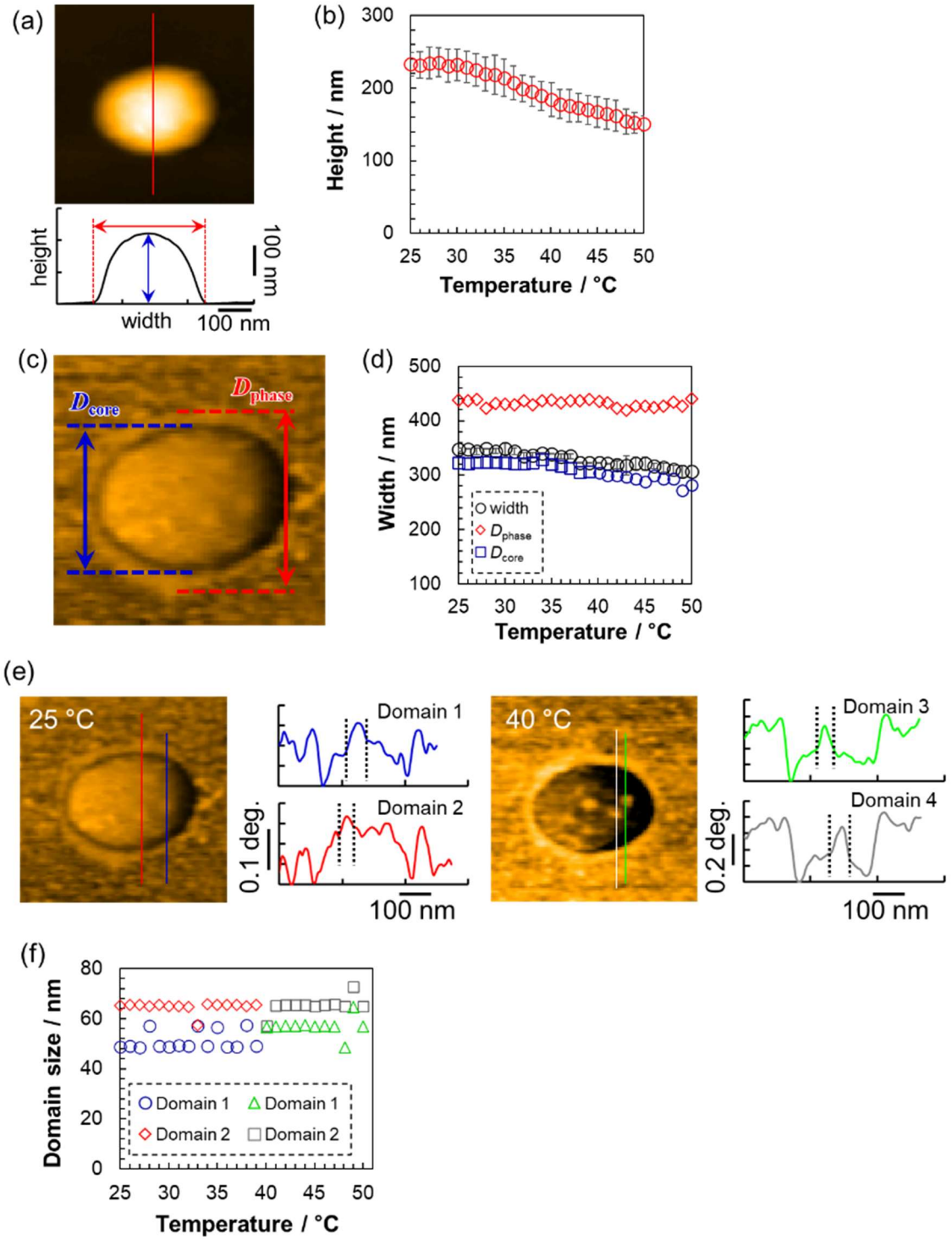

Figure 3.3. (a) Method to evaluate the height and width of the pNIPMAm-based microgels and (b) the change in microgel height with increasing temperature. (c) Definition of D_{phase} and D_{core} in the phase images. (d) Temperature dependence of the width, D_{phase}, and D_{core}. (e) Method to calculate the size of the domains that exist in the core region of the microgels and (f) temperature dependence of each domain size.

3.3.3. Thermoresponsiveness of microgels with different adsorption concentrations

To clarify the effect that the adsorption density has on the thermoresponsive behavior of the pNIPMAm microgels, TC-HS-AFM observations of samples with different concentrations of adsorbed microgels were performed; for that purpose, a loosely arranged state with a concentration of 5.3 particles per μm^2 (**Figure 3.4a**) and a densely packed state (18.8 particles per μm^2) were examined (**Figure 3.4b**). In the case of the loosely arranged state, where the sample was prepared on the substrate by adsorption of a 1.0 wt% microgel dispersion (isolated state: 0.05 wt%, **Figure 3.2**), the thermoresponsive behavior in relation to the height of each microgel was similar to that of the isolated state (**Figure 3.4c**). The decrease in width (347 nm in the isolated state; 271 nm in the loosely arranged state at 25 °C) suggests that the deformation of the microgels on the substrate is suppressed by neighboring microgels.

The densely packed microgels were generated by coating the substrate with a microgel paste prepared by ultracentrifugation of microgel dispersions. In contrast to the loosely arranged sample, the hexagonal shape of the microgels was deformed: the edge-to-edge and vertex-to-vertex distances of a single microgel were 226 nm and 281 nm, respectively at 25 °C (corresponding to the red and blue dotted lines in **Figure 3.4b**). The heights were 89 nm and 119 nm at 25 °C between the edges and the vertices of a single microgel, respectively. When the temperature was increased, the height between the sides increased from 89 nm at 25 °C to 110 nm at 32 °C, decreased to 75 nm at 37 °C, and finally increased again to 133 nm at 50 °C. Conversely, the height at the vertices finally reached 180 nm (**Figure 3.4d**). Notably, the microgels always maintain a hexagonal structure with increasing temperature. These results suggest that the neighboring microgels are almost in contact at their sides during heating and that the probe could not image the substrate. However, the probe was able to approach the substrate closer near the vertices where the microgels had little contact with each other. Previously the structures of three-dimensional densely packed microgels have been investigated using super-resolution microscopy.[40,41] Conley *et al.* have reported on the structural changes of microgels when the volume fraction of the microgels is increased. Initially, the particle radius decreases while maintaining its shape, indicating that the low-density fuzzy layer of the microgels, which could not be observed by super-resolution microscopy, is compressed and interpenetrated.[41] With increasing volume fraction of the microgels, a deformation of the microgels to a hexagonal-like structure was observed, and finally further reduction of particle radius occurs.[41] Thus, the hexagonally deformed pNIPMAm microgels prepared here by precipitation polymerization should be compressed and interpenetrated when the microgels are packed at high density. In addition, the results in this study revealed that their hexagonal shape was maintained during heating, suggesting that compression and interpenetration of the neighboring microgels suppress the thermoresponsiveness in the *x*, *y* direction. The thermoresponsive behavior of isolated and densely packed microgels is illustrated in **Scheme 3.1**. These results show that the thermoresponsiveness of microgels can be controlled by varying not only

the constituent chemical species, but also by controlling the adsorption state. These findings can be expected to be of use in the design of temperature-responsive 2D assemblies such as cell scaffolds.

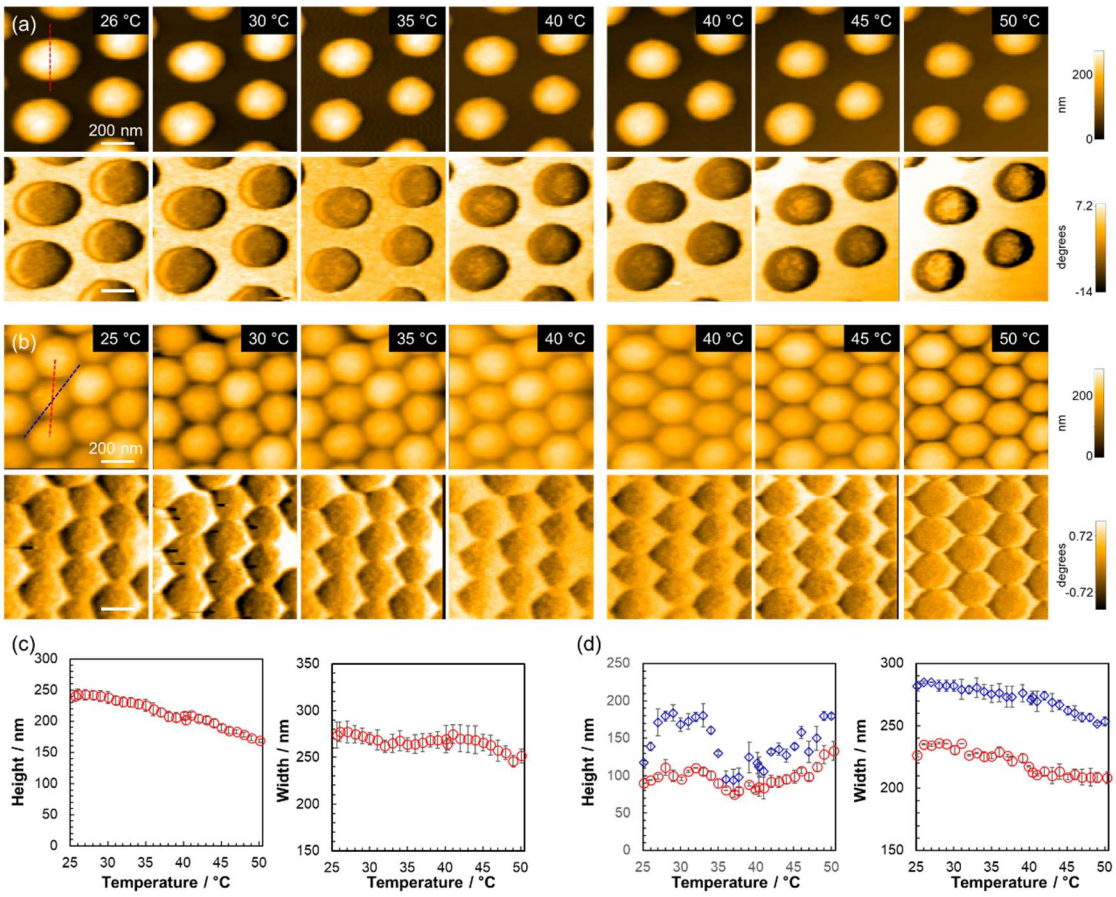

Figure 3.4. Temperature dependence of the microgels at different adsorption concentrations. Height images (top) and phase images (bottom) of (a) the loosely arranged state (5.3 particles per μm^2) and (b) the densely packed state (18.8 particles per μm^2). (c) Temperature dependence of the height and width of the microgels corresponding to the red dotted line in (a). (d) Temperature dependence of the height and width between the edge-to-edge (red circles) and vertex-to-vertex (blue diamonds) of a single microgel. The red and blue plots correspond to the red and blue dotted lines in (b), respectively.

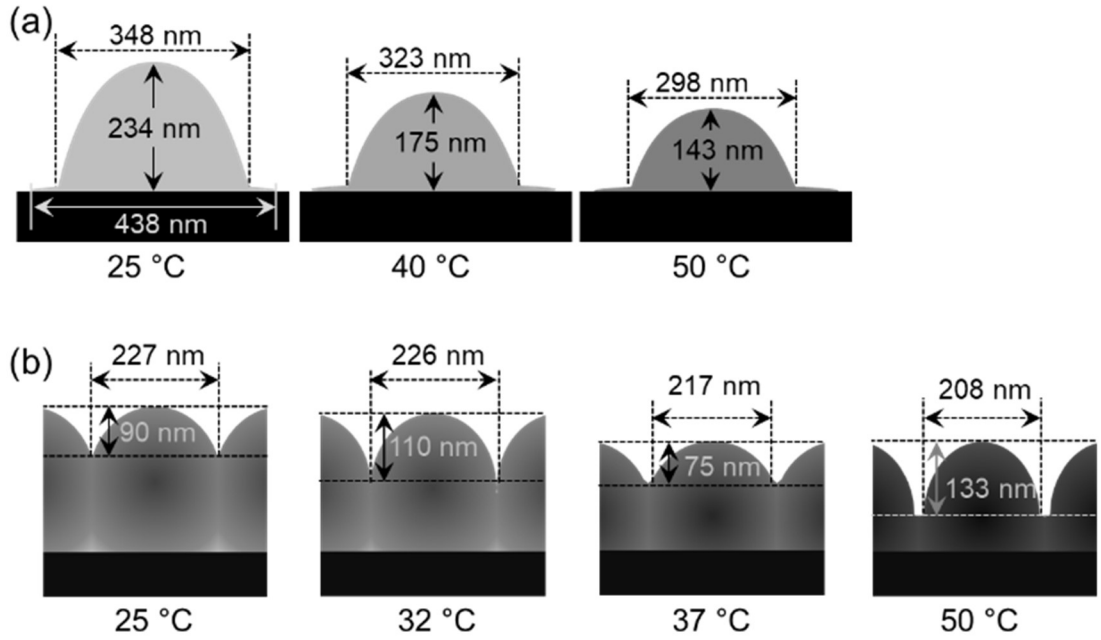

Scheme 3.1. Schematic illustration of the thermoresponsive behavior of the microgels on the substrate in (a) the isolated state and (b) the densely packed state.

3.4. Conclusion

In this study, the nanostructure and thermoresponsiveness of poly(NIPMAm-*co*-BIS) microgels, synthesized by precipitation polymerization, were evaluated using light scattering techniques and temperature-controllable high-speed atomic force microscopy (TC-HS-AFM) observations. These evaluations demonstrated that such pNIPMAm microgels have heterogeneous core–shell and non-thermoresponsive nanostructures in the core region, which is due to the mechanism of the precipitation polymerization. Static light scattering (SLS) and TC-HS-AFM measurements revealed a homogeneous cross-linking structure for the pNIPMAm microgels compared the pNIPAm microgels, and demonstrated that the structure of the microgels is affected by the monomer reactivity ratios. Furthermore, the thermoresponsiveness of microgels with different adsorption concentrations was investigated and the results showed that the thermoresponsiveness of densely packed microgels is suppressed by the compression and interpenetration of neighboring microgels. These findings can be expected to be useful in the design of stimuli-responsive coatings, such as those used as cell scaffolds.

3.5. References

1. R. Pelton, Temperature-sensitive aqueous microgels. *Adv. Colloid Interface Sci.* **2000**, *85*, 1–33.
2. R. H. Pelton, P. Chibante, Preparation of aqueous latices with *N*-isopropylacrylamide. *Colloids Surf.* **1986**, *20*, 247–256.
3. B. Wedel, Y. Hertle, O. Wrede, J. Bookhold, T. Hellweg, Smart Homopolymer Microgels: Influence of the Monomer Structure on the Particle Properties. *Polymers* **2016**, *8*, 162.
4. O. Wrede, S. Bergmann, Y. Hannappel, T. Hellweg, T. Huser, Smart microgels investigated by super-resolution fluorescence microscopy: influence of the monomer structure on the particle morphology. *Soft Matter* **2020**, *16*, 8078-8084.
5. J. Maldonado-Valderrama, T. del Castillo-Santaella, I. Adroher-Benitez, A. Moncho-Jorda, A. Martin-Molina, Thermoresponsive microgels at the air–water interface: the impact of the swelling state on interfacial conformation. *Soft Matter* **2017**, *13*, 230-238.
6. T. Kureha, Y. Nishizawa, D. Suzuki, Controlled Separation and Release of Organoiodine Compounds Using Poly(2-methoxyethyl acrylate)-Analogue Microspheres. *ACS Omega* **2017**, *2*, 7686-7694.
7. T. Kureha, D. Suzuki, Nanocomposite Microgels for the Selective Separation of Halogen Compounds from Aqueous Solution. *Langmuir* **2018**, *34*, 837-846.
8. F. A. L. Janssen, M. Kather, A. Ksiazkiewicz, A. Pich, A. Mitsos, Synthesis of Poly(*N*-vinylcaprolactam)-Based Microgels by Precipitation Polymerization: Pseudo-Bulk Model for Particle Growth and Size Distribution. *ACS Omega* **2019**, *4*, 13795-13807.
9. T. Cai, M. Marquez, Z. Hu, Monodisperse Thermoresponsive Microgels of Poly(ethylene glycol) Analogue-Based Biopolymers. *Langmuir* **2007**, *23*, 8663-8666.
10. D. Duracher, A. Elaissari, C. Pichot, Characterization of cross-linked poly(*N*-isopropylmethacrylamide) microgel latexes. *Colloid Poly. Sci.* **1999**, *277*, 905-913.
11. I. Berndt, J. S. Pedersen, P. Lindner, W. Richtering, Influence of Shell Thickness and Cross-Link Density on the Structure of Temperature-Sensitive Poly-*N*-Isopropylacrylamide−Poly-*N*-Isopropylmethacrylamide Core−Shell Microgels Investigated by Small-Angle Neutron Scattering. *Langmuir* **2006**, *22*, 459-468.
12. D. Suzuki, R. Yoshida, Self-oscillating core/shell microgels: effect of a crosslinked nanoshell on autonomous oscillation of the core. *Polym. J.* **2010**, *42*, 501-508.
13. M. H. Smith, E. S. Herman, L. A. Lyon, Network Deconstruction Reveals Network Structure in Responsive Microgels. *J. Phys. Chem. B* **2011**, *115*, 3761-3764.
14. K. von Nessen, M. Karg, T. Hellweg, Thermoresponsive poly-(*N*-isopropylmethacrylamide) microgels: Tailoring particle size by interfacial tension control. *Polymer* **2013**, *54*, 5499-5510.

15. D. Suzuki, K. Horigome, Assembly of Oppositely Charged Microgels at the Air/Water Interface. *J. Phys. Chem. B* **2013**, *117*, 9073-9082.
16. K. Urayama, T. Saeki, S. Cong, S. Uratani, T. Takigawa, M. Murai, D. Suzuki, A simple feature of yielding behavior of highly dense suspensions of soft micro-hydrogel particles. *Soft Matter* **2014**, *10*, 9486-9495.
17. T. Kureha, D. Aoki, S. Hiroshige, K. Iijima, D. Aoki, T. Takata, D. Suzuki, Decoupled thermo-and pH-responsive hydrogel microspheres cross-linked by rotaxane networks. *Angew. Chem., Int. Ed.* **2017**, *56*, 15393 –15396.
18. M. Takizawa, Y. Sazuka, K. Horigome, Y. Sakurai, S. Matsui, H. Minato, T. Kureha, D. Suzuki, Self-Organization of Soft Hydrogel Microspheres during the Evaporation of Aqueous Droplets. *Langmuir* **2018**, *34*, 4515−4525.
19. M. Keerl, J. S. Pedersen, W. Richtering, Temperature Sensitive Copolymer Microgels with Nanophase Separated Structure. *J. Am. Chem. Soc.* **2009**, *131*, 3093-3097.
20. A. Balaceanu, V. Mayorga, W. Lin, M.-P. Schuerings, D. E. Demco, A. Boeker, M. A. Winnik, A. Pich, Copolymer microgels by precipitation polymerisation of *N*-vinylcaprolactam and *N*-isopropylacrylamides in aqueous medium. *Colloid Polym.Sci.* **2013**, *291*, 21-31.
21. K. C. Clarke, L. A. Lyon, Modulation of the Deswelling Temperature of Thermoresponsive Microgel Films. *Langmuir* **2013**, *29*, 12852-12857.
22. Y. Wu, S. Wiese, A. Balaceanu, W. Richtering, A. Pich, Behavior of Temperature-Responsive Copolymer Microgels at the Oil/Water Interface. *Langmuir* **2014**, *30*, 7660-7669.
23. S. Nayak, L. A. Lyon, Soft nanotechnology with soft nanoparticles. *Angew. Chem., Int. Ed.* **2005**, *44*, 7686 – 7708.
24. M. Stieger, W. Richtering, J. S. Pedersen, P. Lindner, Small-angle neutron scattering study of structural changes in temperature sensitive microgel colloids. *J. Chem. Phys.* **2004**, *13*, 6197–6206.
25. B. R. Saunders, On the Structure of Poly(*N*-isopropylacrylamide) Microgel Particles. *Langmuir.* **2004**, *20*, 3925–3932.
26. R. Keidel, A. Ghavami, D. M. Lugo, G. Lotze, O. Virtanen, P. Beumers, J. S. Pedersen, A. Bardow, R, G. Winkler, W. Richtering, Time-resolved structural evolution during the collapse of responsive hydrogels: The microgel-to-particle transition. *Sci. Adv.* **2018**, *4*, eaao7086.
27. A. Mourran, Y. Wu, R. A. Gumerov, A. A. Rudov, I. I. Potemkin, A. Pich, M. Möller, When Colloidal Particles Become Polymer Coils. *Langmuir* **2016**, *32*, 723–730.
28. G. M. Conley, S. Nöjd, M. Braibanti, P. Schurtenberger, F. Scheffold, Superresolution microscopy of the volume phase transition of pNIPAM microgels. *Colloids Surf. A* **2016**, *499*, 18–23.

29. X. Wu, R. H. Pelton, A. E. Hamielec, D. R. Woods, W. McPhee, The kinetics of poly(*N*-isopropylacrylamide) microgel latex formation. *Colloid Polym. Sci.* **1994**, *272*, 467–477.
30. S. Matsui, Y. Nishizawa, T. Uchihashi, D. Suzuki, Monitoring Thermoresponsive Morphological Changes in Individual Hydrogel Microspheres. *ACS Omega* **2018**, *3*, 10836–10842.
31. K. Honda, Y. Sazuka, K. Iizuka, S. Matsui, T. Uchihashi, T. Kureha, M. Shibayama, T. Watanabe, D. Suzuki, Hydrogel Microellipsoids that Form Robust String-Like Assemblies at the Air/Water Interface. *Angew. Chem., Int. Ed.* **2019**, *58*, 7294-7298.
32. Y. Nishizawa, S. Matsui, K. Urayama, T. Kureha, M. Shibayama, T. Uchihashi, D. Suzuki, Non-Thermoresponsive Decanano-sized Domains in Thermoresponsive Hydrogel Microspheres Revealed by Temperature-Controlled High-Speed Atomic Force Microscopy. *Angew. Chem. Int. Ed.* **2019**, *58*, 8809–8813.
33. H. Minato, Y. Nishizawa, T. Uchihashi and D. Suzuki, Thermo-responsive structural changes of single poly(*N*-isopropyl acrylamide) hydrogel microspheres under densely packed conditions on a solid substrate. *Polym. J.* **2020**, *52*, 1137-1141.
34. Y. Nishizawa, K. Honda and D. Suzuki, Recent Development in the Visualization of Microgels. *Chem. Lett.* **2021**, *50*, 1226-1235.
35. J. Brandup, E. H. Immergut, E. A. Grulke, A. Abe and D. R. Bloch, Polymer Handbook, 4th ed. Wiley: New York, 1999.
36. J. Baselga, M. A. Llorente, J. L. Nieto, I. Hernánndez-Fuentes and I. F. Piérola, Polyacrylamide networks. sequence distribution of crosslinker. *Eur. Polym. J.* **1988**, *24*, 161-165.
37. M. Cors, L. Wiehemeier, Y. Hertle, A. Feoktystov, F. Cousin, T. Hellweg, J. Oberdisse, Determination of Internal Density Profiles of Smart Acrylamide-Based Microgels by Small-Angle Neutron Scattering: A Multishell Reverse Monte Carlo Approach. *Langmuir* **2018**, *34*, 15403-15415.
38. T. Ando, T. Uchihashi, S. Scheuring, Filming Biomolecular Processes by High-Speed Atomic Force Microscopy. *Chem. Rev.* **2014**, *114*, 3120–3188
39. Alvarez, L. H.; Eisold, S.; Gumerov, R. A.; Strauch, M.; Rudov, A. A.; Lenssen P.; Merhof, D.; Potemkin, I. I.; Simon, U,; Wöll D. Deformation of Microgels at Solid−Liquid Interfaces Visualized in Three-Dimension. *Nano Lett.* **2019**, *19*, 8862–8867.
40. G. M. Conley, P. Aebischer, S. Nojd, P. Schurtenberger, F. Scheffold, Jamming and overpacking fuzzy microgels: Deformation, interpenetration, and compression. *Sci. Adv.* **2017**, *3*, e1700969.
41. G. M. Conley, C. Zhang, P. Aebischer, J. L. Harden, F. Scheffold, Relationship between rheology and structure of interpenetrating, deforming and compressing microgels. *Nat. Commun.* **2019**, *10*.

4. Chapter III

"Nanostructures, Thermoresponsiveness, and Assembly Mechanism of Hydrogel Microspheres during Aqueous Free-Radical Precipitation Polymerization"

*Part of this work was published in "Yuichiro Nishizawa, Haruka Minato, Takumi Inui, Takayuki Uchihashi and Daisuke Suzuki, *Langmuir* **2021**, *37*, 151-159."
(https://doi.org/10.1021/acs.langmuir.0c02654)

4.1 Introduction

The development of microgels for a variety of applications has been achieved as the result of the discovery of a preparation method capable of producing uniformly sized microgels in a flask, i.e., aqueous free-radical precipitation polymerization.[1-5] In contrast to other polymerization techniques such as the template technique[6] and inverse miniemulsion polymerization, [6] precipitation polymerization allows the preparation of large amounts of various types of microgels in uniform size. This polymerization technique can be used to produce microgels from many types of chemical species, provided that the constituents (monomers) are water-soluble and the growing polymers are insoluble in water. By taking advantage of the phase separation behavior of thermoresponsive polymers in aqueous solution, various types of thermoresponsive microgels, including poly(meth)acrylamide analogues,[1,7] poly(oligo ethylene glycol methyl ester (meth)acrylates),[8,9] and poly(*N*-vinylcaprolactom),[10,11] can also be prepared in uniform size by aqueous free-radical precipitation polymerization as above mentioned. Thus, this method is practical for a wide range of applications, e.g., biomedical applications.

To control the (nano)structure and physicochemical properties of microgels for the abovementioned applications, an understanding of the mechanism of precipitation polymerization is important. The monomer reactivity ratio between the main monomer and the cross-linker or co-monomer is widely accepted to be a crucial factor in determining the nanostructure of the microgels; [12-14] it is believed that the more rapidly consumed chemical species (i.e., the cross-linker BIS or methacrylic acid) is selectively incorporated into the center of pNIPAm-based microgels, resulting in core/shell structures. [15-20] It should be noted here that Saunders has pointed out that the nodular inhomogeneous core–shell structure composed of aggregated nanoparticles, such as the nanostructures of microgels, has not yet been clarified using scattering techniques.[17,21] However, recently, the detailed nanostructures have been reported by imaging techniques with high spatial resolution.[22,23] Therefore, the polymerization process for the production of thermoresponsive microgels is significantly different from that of typical bulk hydrogels, which is generally conducted below the lower critical solution temperature of the constituent polymers and in which the polymer networks are constructed when

individual polymer chains are in a coiled state. Several attempts to clarify the mechanism by which the microgels grow as the precipitation polymerization proceeds have been made by chromatography,[12] light scattering,[24-26] small-angle neutron scattering,[27] and in silico systems.[28,29] However, there is still no definitive evidence for the mechanism by which microgels are produced via this simple method at the nanoscale.

In this study, the author evaluated the changes in the nanostructure and thermoresponsiveness of the developing microgels during precipitation polymerization by light scattering technique and TC-HS-AFM[30,31] to clarify the mechanism of particle formation. The precipitation polymerization process was directly visualized by temperature-controlled (TC) HS-AFM to obtain evidence of particle formation.

4.2. Experimental Section

4.2.1 Materials

N-isopropyl acrylamide (NIPAm; purity, 98%), *N*,*N*′-methylenebis(acrylamide) (BIS, 97%), potassium peroxodisulfate (KPS, 95%), 2,2′-azobis(2-methylpropionamidine) dihydrochloride (V-50, 97%), ammonium peroxodisulfate (APS, 95%), sodium dodecyl sulfate (SDS, 95%), hydroquinone (99%), sorbitan monooleate (Span 80), ethanol (99.5%), and hexane (96%) were purchased from FUJIFILM Wako Pure Chemical Corporation (Japan) and used as received. *N*,*N*,*N*′,*N*′-tetramethyl ethylenediamine (TEMED, 99%) was purchased from Sigma-Aldrich and used as received. Fluorosurf was purchased from Fluoro Technology (Japan). Water for the preparation of microgels was first distilled and subsequently subjected to ion exchange (EYELA, SA-2100E1).

4.2.2. Preparation of microgels by precipitation polymerization

PolyNIPAm microgels with 10 mol % BIS were prepared via aqueous precipitation polymerization as reported in the previous paper.[23] The initial monomer concentration was held constant at 150 mM. A mixture of NIPAm (1.53 g), the cross-linker BIS (0.232 g), and SDS (0.0144 g) in water (95 mL) was prepared as the monomer solution in a three-neck round-bottom flask (200 mL) equipped with a mechanical stirrer, condenser, and nitrogen gas inlet. To remove any oxygen, the monomer solution was heated to 70 °C in an oil bath and sparged with nitrogen gas (30 min) under constant stirring (250 rpm). Free-radical polymerization was then initiated by adding KPS (0.054 g) in water (5 mL). To investigate the polymerization kinetics, the reaction solution (~500 μL) was taken from the batch reactor and polymerization was terminated by mixing the solution with an excess amount of hydroquinone and cooling it to room temperature. The resultant microgels are denoted as **N(PP)-*t***, where *t* is the sampling time.

4.2.3. Preparation of microgels by feeding precipitation polymerization

Polymerization was performed in a three-neck round-bottom flask (200 mL) equipped with a mechanical stirrer, condenser, and nitrogen gas inlet. An aqueous solution of SDS (72. 8 mL) was prepared in a round-bottom flask and heated to 70 °C in an oil bath. A mixture of NIPAm (2.06 g) and BIS (0.212 g) in water (30 mL) was prepared as the monomer solution. After removing any oxygen in the SDS solution and monomer solution as described above, KPS (2 mM) in water (5 mL) was added to the SDS solution, and the monomer solution was then continuously added (feeding rate: 200 μL/min, 111 min) under constant stirring (250 rpm). To investigate the polymerization kinetics, the reaction solution (~500 μL) was taken from the batch reactor, and the polymerization was terminated by mixing the solution with an excess amount of hydroquinone and cooling it to room temperature.

4.2.4. Preparation of microgels by inverse miniemulsion polymerization

Polymerization was conducted as reported in previous paper.[23] The initial monomer concentration was held constant at 1000 mM. A mixture of NIPAm (0.806 g), the cross-linker BIS (0.0581 g), and the initiator V-50 in water (7.5 mL) was prepared as the monomer solution. The monomer solution was added to a mixture of Span 80 (1.4 g) and hexane (43 g), and the inverse miniemulsion was prepared by ultrasonication using an ultrasonic homogenizer (VC-75, SONICS). To remove any oxygen, the solution was sparged with nitrogen gas (30 min). The polymerization was initiated by applying UV irradiation (UVL-400HA (365 nm), Rikoukagakusangyo Co., Ltd.) at room temperature for 15 min under a nitrogen atmosphere. After polymerization for more than 4 h, the obtained microgel dispersion was centrifuged (5000*g*) and redispersed in ethanol to break the emulsion. Subsequently, the dispersion was centrifuged (296,000*g*) and redispersed in water to exchange ethanol for water. The residual ethanol was completely removed by dialysis for a week with daily water changes.

4.2.5. DLS measurement

The hydrodynamic diameters (D_h) of the microgels in the reaction solutions taken from the batch reactor at each polymerization time and of the final microgels were determined by dynamic light scattering (DLS; Malvern Instruments Ltd.; ZetasizerNanoS). The DLS data represent averages of three individual measurements (acquisition time: 30 s). At least 5 μL of each microgel suspension taken from the batch reactor was added to 1000 μL of water. The samples were allowed to thermally equilibrate at 25 °C for 10 min prior to each measurement. The D_h of the microspheres was calculated from the measured diffusion coefficients using the Stokes–Einstein equation (Zetasizer software v6.12).

4.2.6. HS-AFM observation

The method to observe the thermoresponsive behavior of microgels by HS-AFM was conducted as reported in a previous paper.[23] The author used a laboratory-built HS-AFM in which the tapping mode is employed as an imaging mode.[30,31] For the tapping-mode imaging, the author used a miniaturized cantilever (BL-AC10-DS, Olympus, Japan) with a spring constant of ~0.1 N/m, a resonant frequency of ~600 kHz, and a quality factor of ~2. While the cantilever was oscillated at around the resonant frequency, the oscillation amplitude was detected using a fast lock-in amplifier through an optical-beam-deflection detector with a red laser (680 nm). Because the cantilever has only a blunt tip end with bird-beak-like structure, the author deposited an amorphous carbon pillar on the original tip by electron beam deposition under a scanning electron microscope. Then, the carbon pillar was etched to have a sharp end (radius: ~4 nm) using a plasma etcher under an argon gas. For the HS-AFM imaging of the microgels, the free-oscillation amplitude of the cantilever far from the sample surface was set to 5–30 nm, and the set-point amplitude was set to 70–90% of the free-oscillation amplitude depending on the microsphere size.

As a substrate on which hydrogel particles are suspended, the author used a mica surface covered by a hydrophobic film as the microgels strongly adsorb onto hydrophobic substrates in aqueous solution in order to minimize the hydrophobic surface/water contacts, which leads to high levels of deformation.[23,32] First, the author placed a 0.5 μL droplet of hydrophobic agent (fluorosurf, Fluoro Technology, Japan) on a freshly cleaved mica surface followed by naturally drying the droplet, producing a fluororesin film on the mica. Then, a 3 μL droplet of pNIPAm microgel dispersions was dropped on the substrate. After a 5 min incubation, the surface was thoroughly washed with pure water to remove the excess microgels.

The thermoresponsive behavior of the microgels was observed using a temperature-control device equipped with the HS-AFM.[31] Briefly, the temperature of the observation solution (water) was raised by DC current flowing into the conductive ITO glass at the bottom of the solution pool of the cantilever holder. The solution temperature is measured by thermocouples installed near the cantilever and can be raised at 1.5 °C/min via a software feedback control. Particle volume was calculated by summing the volume occupied by each pixel.

The direct visualization of the precipitation polymerization was conducted as followed: A monomer solution (100 μL) in which NIPAm (2.1 mg) and BIS (0.9 mg) were dissolved with a monomer concentration of 20 mM was injected into the cantilever holder and heated to 40 °C. Polymerization was then initiated by the sequential addition of an aqueous solution of TEMED (80 mM, 4 μL) and an aqueous solution of APS (40 mM, 4 μL). All HS-AFM imaging was performed under the conditions of 120 × 120 pixels^2 and a frame rate of 1 fps.

4.3. Results and discussion

4.3.1. Evaluation of precipitation polymerization

As mentioned above, p(NIPAm-*co*-BIS) microgels prepared by precipitation polymerization have been reported to exhibit highly cross-linked cores and loosely cross-linked shells because of the different reactivity ratios between NIPAm and BIS. Thus, it was anticipated that the microgels formed in the early stages of precipitation polymerization would show lower swelling properties than the final products. To obtain evidence for this hypothesis, the particle volume derived from the hydrodynamic diameter (V_h) and the swelling ratio, which is defined as $V_{h(25°C)}/V_{h(70°C)}$, were calculated from the DLS data of the **N(PP)-*t*** microgels, i.e., the partially formed microgels taken from the reaction solution *t* minutes after the beginning of the polymerization. After the initiation of the precipitation polymerization, the suspension became turbid for ~1 min due to the visible light scattering associated with particle formation. Although it was expected that some polymers or particles were produced during the first minute of reaction, the size of the **N(PP)-0.5** and **N(PP)-1** microgels could not be evaluated by DLS because the scattering intensity was too low. Therefore, **Figure 4.1** shows the data for the **N(PP)** microgels starting 1.5 min after the initiation of polymerization. The V_h of the deswollen **N(PP)** increased from 2.5 × 10^{-4} μm^3 to 31 × 10^{-4} μm^3 in only 10 min and ultimately reached 37 × 10^{-4} μm^3 (**Figure 4.1a**). The swelling ratio also increased from 2.1 (**N(PP)-1.5**) to 3.8 (**N(PP)-10**) and remained almost constant thereafter, as expected. The evolution of the volume of the deswollen **N(PP)** microgel particles was described well by a single-exponential equation (eq 4.1) (**Figure 4.1b**); this result is similar to that in the previous report.[27]

$$V(t) = A\left[1 - \exp\left(\frac{t - B}{\tau}\right)\right] \qquad \text{(Eq. 4.1)}$$

where, A, B, and τ are a constant related to the volume of the microgels, a correction term for the initiation time, and the time constant of the reaction, respectively. This result suggests that the precipitation polymerization follows pseudo-first-order kinetics. In other words, these results indicate that the polymerization rate depends predominantly on the monomer concentration given that the half-life time (10 h for KPS at 70 °C) of the initiator is much longer than the polymerization times.[28]

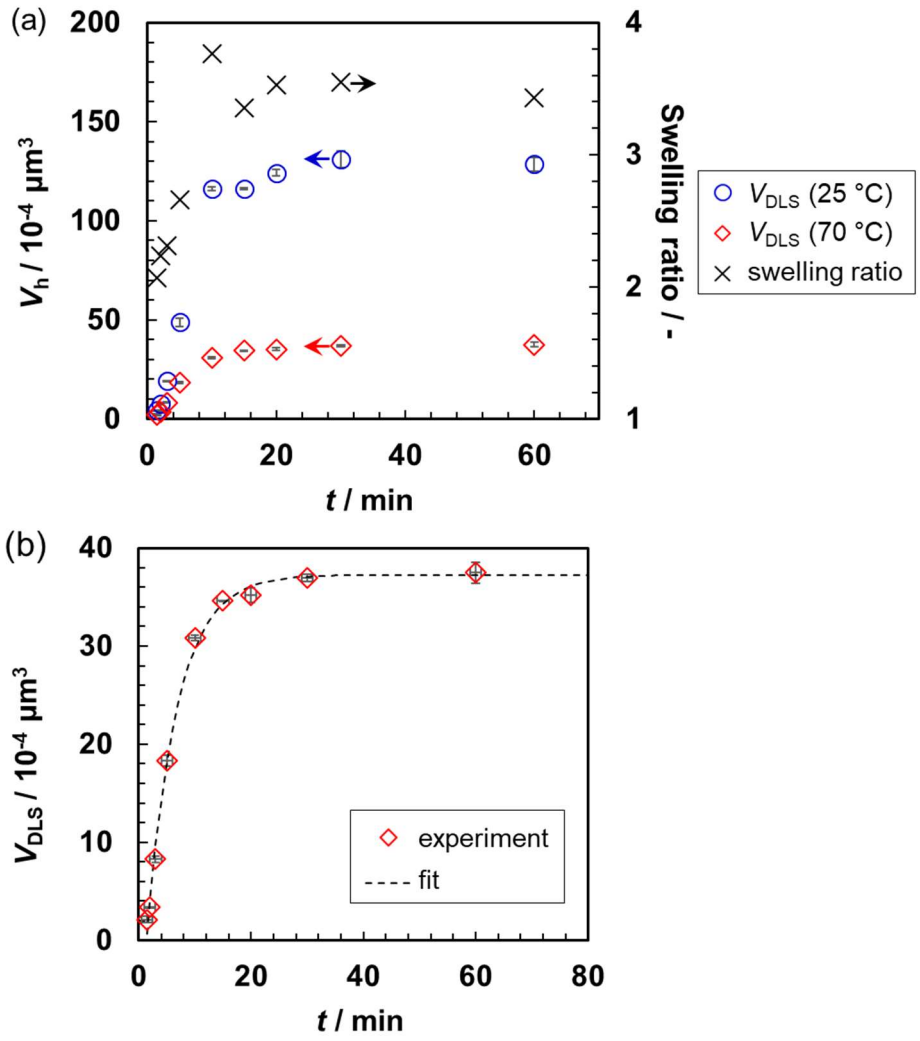

Figure 4.1. (a) Time dependence of V_h in the swollen and deswollen states and the swelling ratio. (b) Change in the volume of the deswollen microgels as polymerization proceeded. The dotted line was fitted according to Eq. 4.1.

Subsequently, the nanostructures and thermoresponsiveness of the **N(PP)-*t*** microgels were evaluated via TC-HS-AFM using samples taken 1.5 min after the initiation of the polymerization. It should be noted here that no particles were observed in either the **N(PP)-0.5** or **N(PP)-1** samples. The **N(PP)-1.5** microgels were nonspherical with a width of ~100 nm, and deca-nanosized spherical domains existed inside them (**Figure 4.2a-c**). The volume of the **N(PP)-1.5** particles decreased from 0.76×10^{-4} µm^3 to 0.61×10^{-4} µm^3 with increasing temperature (**Figure 4.2d**), whereas the width of the spherical domains was almost constant (**Figure 4.2e**). The formation of non-thermoresponsive domains in the microgels was attributed to hydrophobic-interaction-induced aggregation of the phase-separated polymer chains, which had high contents of the cross-linker BIS.[23] Subsequently, the aggregated BIS-rich precursor particles are highly cross-linked, resulting in a decrease in their

swelling ratio. A similar trend was seen in the case of **N(PP)-2** (**Figure 4.3**); however, after 3 min, the surface of the microgels became smooth (**Figure 4.4**), indicating that the spherical domains of the precursor microgels were buried inside the grown microgels through the adsorption of the continuously generated precipitated globular polymers. In addition, it can be expected that the monomers diffuse to the growing microgels and polymerize on the particle surface.[3,4] The time and temperature dependences of the swelling ratio of **N(PP)** derived from the height images did not show the same tendency as those obtained from the DLS measurements because they were affected by the adsorption of the particles onto the substrate (**Figure 4.5**). Nevertheless, the swelling ratio of **N(PP)-1.5** was clearly lower than that of the final product (**N(PP)-60**); the swelling ratios of **N(PP)-1.5** and **N(PP)-60** were 1.3 and 1.9, respectively.

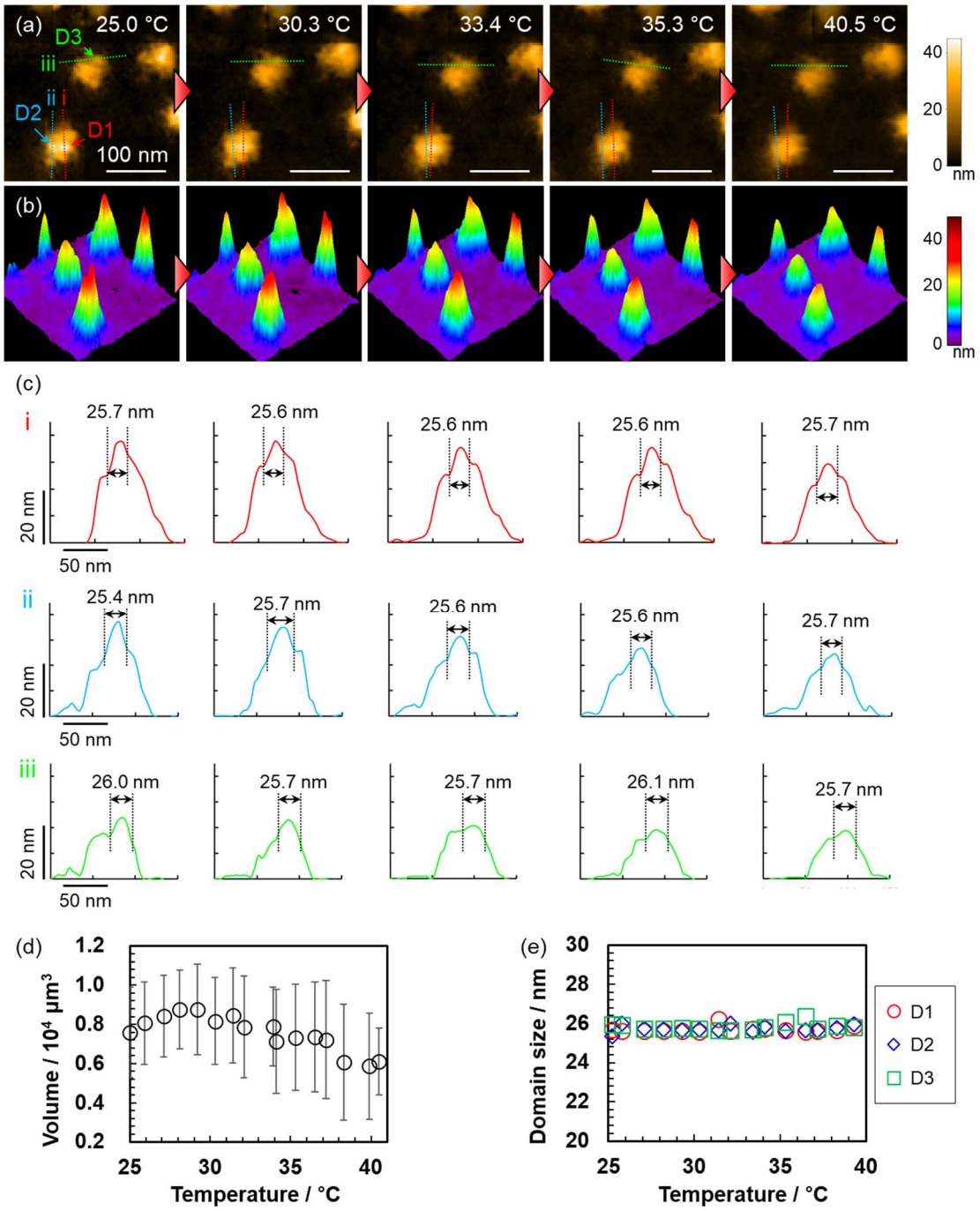

Figure 4.2. HS-AFM analysis of N(PP)-1.5. Temperature dependence of the (a) height images, (b) 3D images and (c) the cross-sectional profiles corresponding to the respective dotted lines. The bump in the cross-section profile was considered to correspond to a domain, the domain size was determined from the width of the bump.[1] (d) Particle volume and (e) domain size in the microgels.

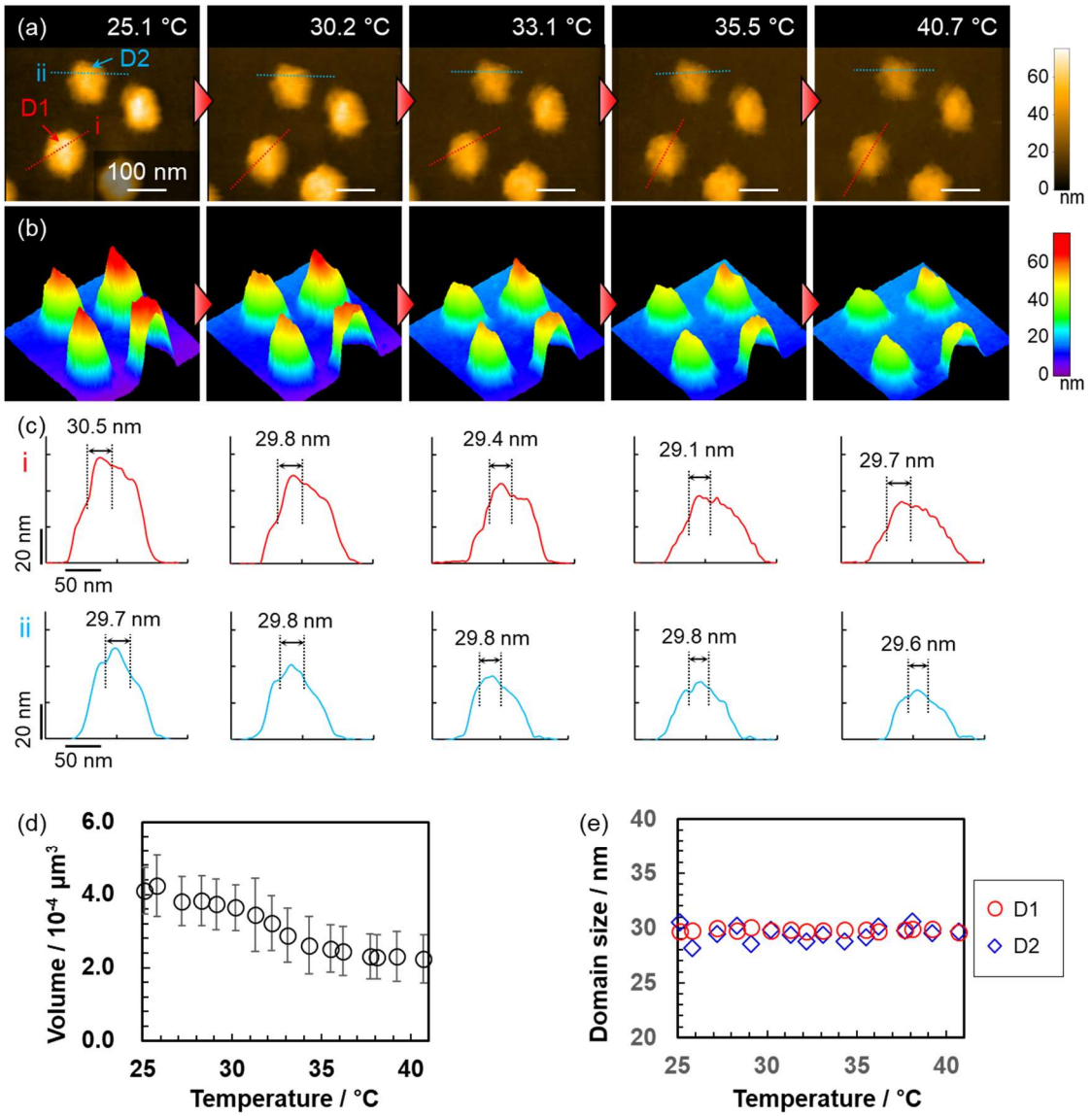

Figure 4.3. TC-HS-AFM analysis of N(PP)-2. Temperature dependence of the (a) height images, (b) 3D images, (c) cross-section profiles corresponding to the respective dotted lines in the height images, (d) particle volume, and (e) domain size in the microgels.

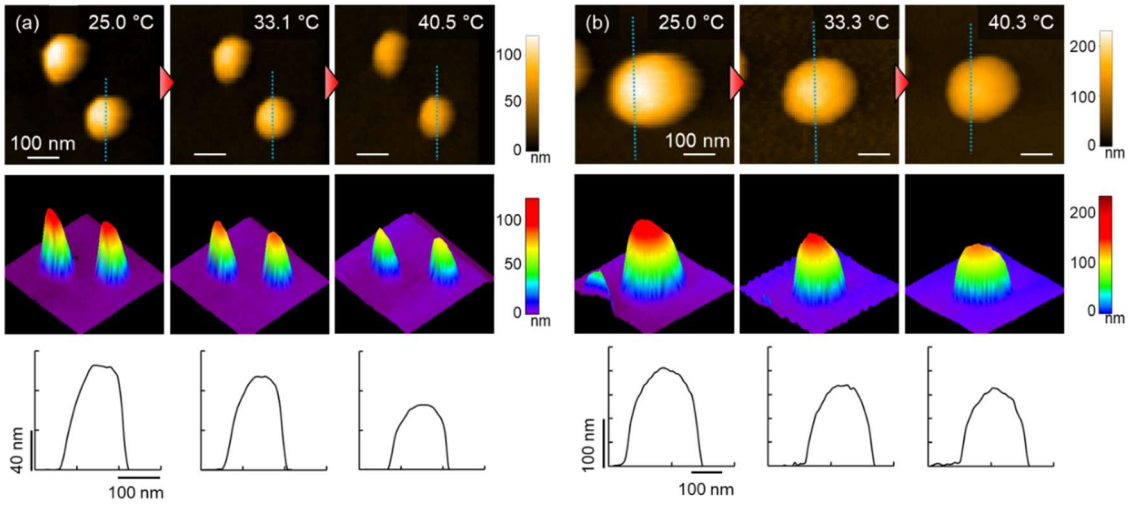

Figure 4.4. TC-HS-AFM analysis of (a) N(PP)-3 and (b) N(PP)-60. Temperature dependence of the height images (top), 3D images (middle), and cross-sectional profile corresponding to the dotted lines in the respective height images (bottom).

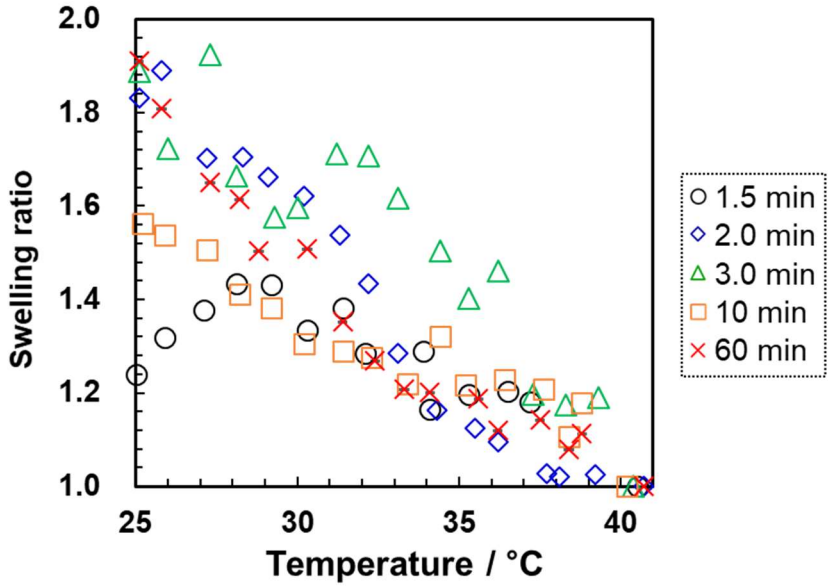

Figure 5. Swelling ratio of the microgels at different polymerization times as a function of temperature. The swelling ratio was defined as $V(T)$ / $V_{40\ °C}$, where $V(T)$ is the volume derived from HS-AFM measurements at temperature T and $V_{40\ °C}$ is the volume at 40 °C.

4.3.2. Evaluation of feeding precipitation polymerization

The inhomogeneous nanostructure, i.e., non-thermoresponsive deca-nanosized domains, in the microgels prepared by precipitation polymerization may lead to some reduction in the swelling properties, thermoresponsiveness, and mechanical strength of the microgels. Non-uniform internal structures have been found to decrease the mechanical properties of bulk polymeric materials;[33,34] however, it should be noted that colloidal microgels were not discussed. As it has been demonstrated by Acciaro et al., the formation of such inhomogeneous structures in microgels can be suppressed by feeding precipitation polymerization (FPP).[35] Using a modified procedure, which is also expected to improve particle homogeneity by hindering the depletion of the cross-linker in the reaction mixture, **N(FPP)-*t*** microgels were prepared and evaluated in a similar manner to the **N(PP)-*t*** microgels. In this case, the suspension remained transparent until 20 min after the initiation of the polymerization due to the low monomer concentration throughout the polymerization. The samples of the suspension could not be evaluated by DLS until 28 min after initiation, indicating that the microgels might be unstable due to insufficient cross-linking. After 28 min, in contrast to **N(PP)** microgels, the **N(FPP)** microgels exhibited a high swelling ratio (**N(FPP)-28**: 11; **N(FPP)-30**: 15); the swelling ratio further decreased to ~4.5 as the polymerization proceeded (**Figure 4.6a**). This indicates that the precipitated polymer chains adsorbed onto the nuclei and formed an outer hydrogel layer, which suppressed the swelling of the internal network.[36] In addition, the D_h values of **N(FPP)** particles with different polymerization times exhibited almost the same thermoresponsiveness, in contrast to the **N(PP)** particles (**Figure 4.7**). The evolution of the particle volume of the deswollen **N(FPP)** microgels was also described well by eq 4.1 (**Figure 4.6b**), suggesting that the feeding precipitation polymerization could be explained by pseudo-first-order kinetics and that the particle volume at any polymerization time could be predicted. The time constants (τ) for FPP and PP were 88 and 5 min, respectively. The increase in τ for FPP suggests that the continuous feeding of the monomer solution causes the decrease in precursor particles during the polymerization, resulting in decelerated polymerization processes.

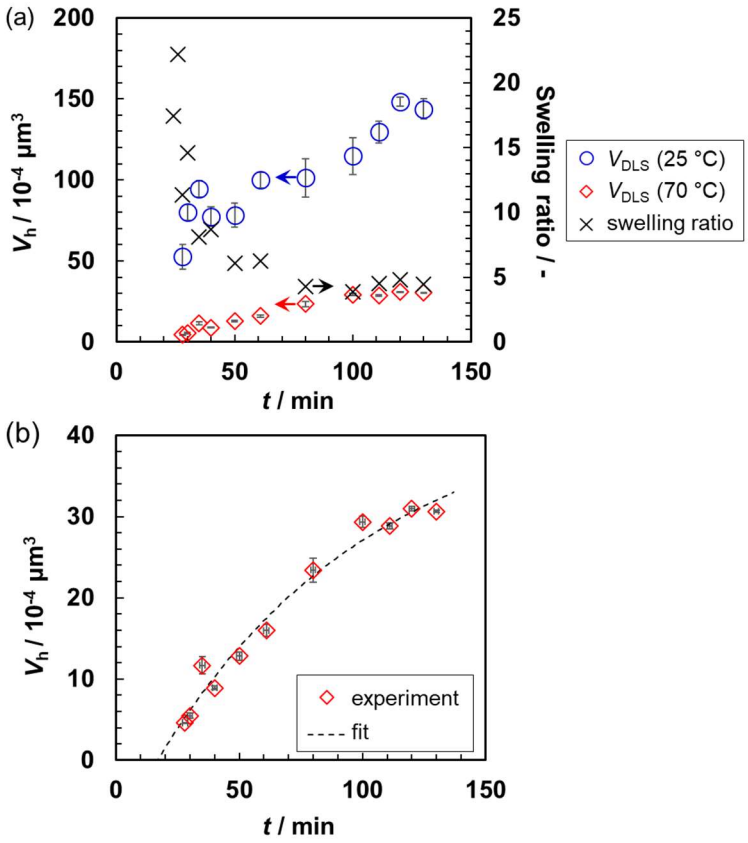

Figure 4.6. (a) Time dependence of V_h in the swollen and deswollen state, and the swelling ratio of N(FPP). (b) Change in the volume of the deswollen microgels as polymerization proceeded. The dotted line was fitted according to Eq. 4.1.

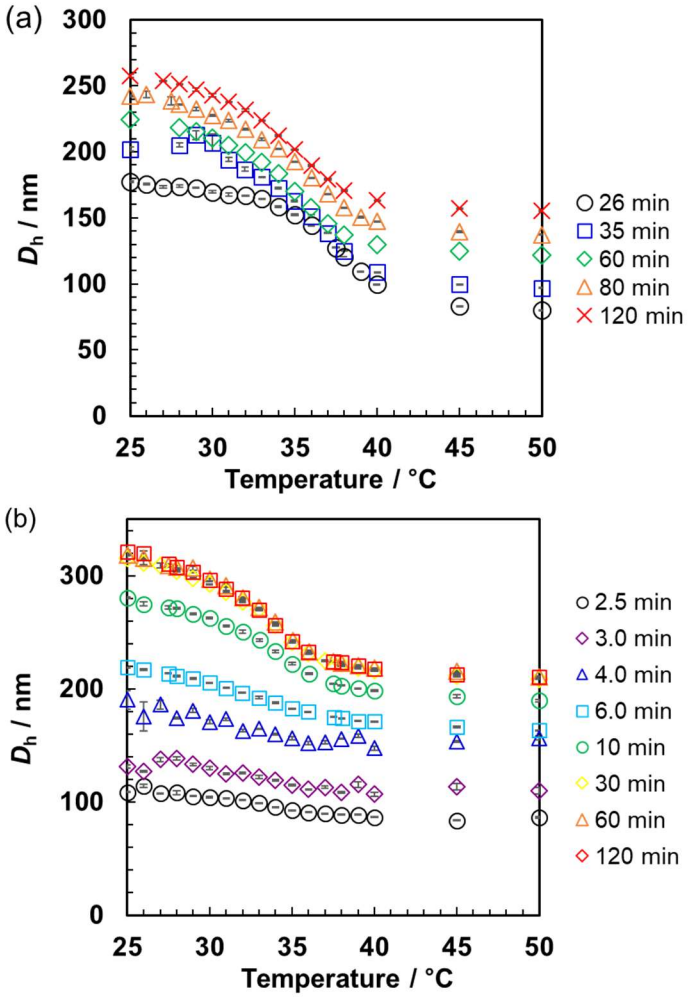

Figure 4.7. Temperature dependence of the D_h in the microgels with different polymerization times: (a) **N(FPP)** and (b) **N(PP)**. Note that the microgels taken from the batch reaction mixtures were colloidally unstable; thus, microgels used in this experiment were re-prepared. The D_h values of the **N(FPP)** microgels exhibited almost the same thermoresponsiveness of regardless of the polymerization time. On the contrary, the **N(PP)** microgels formed in the early stages of the polymerization did not exhibit remarkable thermoresponsive changes in size ($t \leqq 6.0$ min), whereas the microgels polymerized for more than 10 minutes exhibited the maximum change at ~34.5 °C.

Figure 4.8 shows the HS-AFM analysis of the **N(FPP)-30** microgels. The **N(FPP)-30** particles showed a very low-density morphology (**Figure 4.8a,b**).0 Their good swelling properties are shown in **Figure 4.8d**; the particle volume decreased from 3.0×10^{-4} μm^3 to 1.0×10^{-4} μm^3 with increasing temperature. Unfortunately, the swollen **N(FPP)** microgels polymerized for 40 min or longer could not be visualized clearly by TC-HS-AFM because of the low polymer densities of these microgels (**Figure 4.9**). From these results, the author concluded that the inhomogeneous structure of the **N(PP)** particles was largely avoided by changing the polymerization conditions, such as the precipitation speed of the monomers, by tuning the monomer concentration. However, the non-thermoresponsive domains were not completely eliminated; domains with widths of approximately 40–60 nm were present in **N(FPP)-30** (**Figure 4.8a,c,e**). Since non-thermoresponsive inhomogeneous nanoarchitectures were formed in the initial stages of the precipitation polymerization regardless of whether batch or feeding polymerization was employed, the inhomogeneous structures in microgels must originate during the nucleation process via the precipitation/aggregation of the polymer chains. Indeed, such domains did not form in the microgels synthesized via inverse miniemulsion polymerization (**Figure 4.10**), the mechanism of which is similar to that of bulk hydrogel formation, in which polymer chains in coiled states are cross-linked. It should be noted here that only the final products can be evaluated and that inhomogeneous structures that exist in bulk hydrogels, such as spatial and topological inhomogeneities,[37] cannot be visualized by HS-AFM.

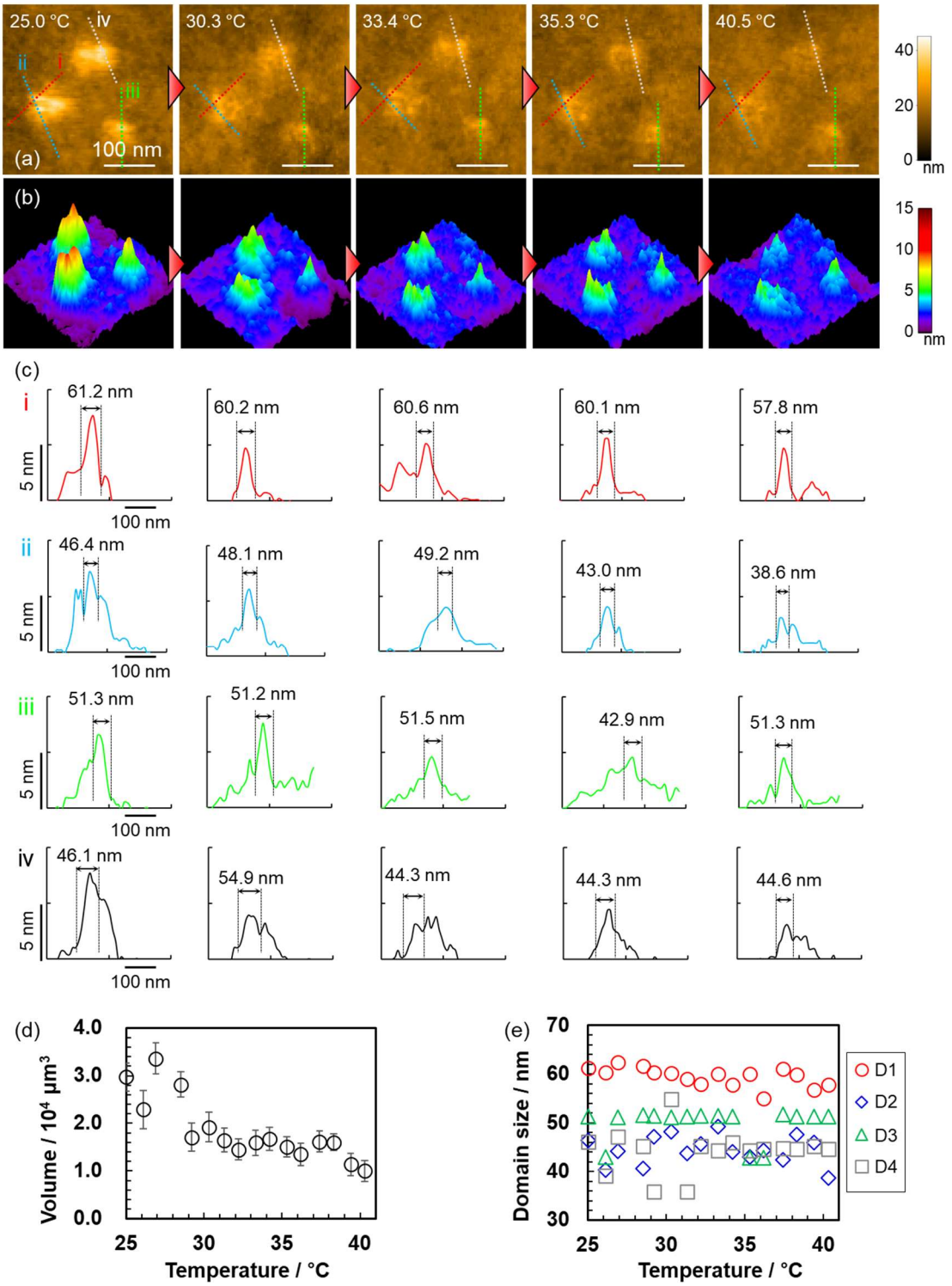

Figure 4.8. HS-AFM analysis of N(FPP)-30. Temperature dependence of the (a) height images, (b) 3D images, (c) the cross-sectional profiles corresponding to the respective dotted lines, (d) particle volume, and (e) domain size in the microgels.

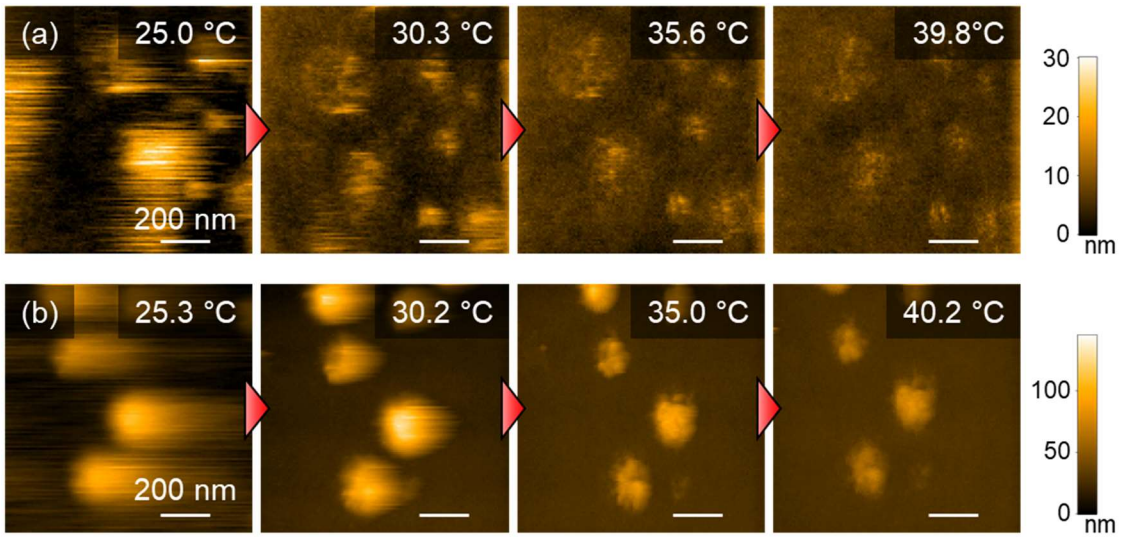

Figure 4.9. Temperature dependence of the height images of (a) N(FPP)-40 and (b) N(FPP)-60. The swollen N(FPP) microgels polymerized for more than 40 minutes could not be observed clearly via HS-AFM, possibly because their polymer densities were too low.

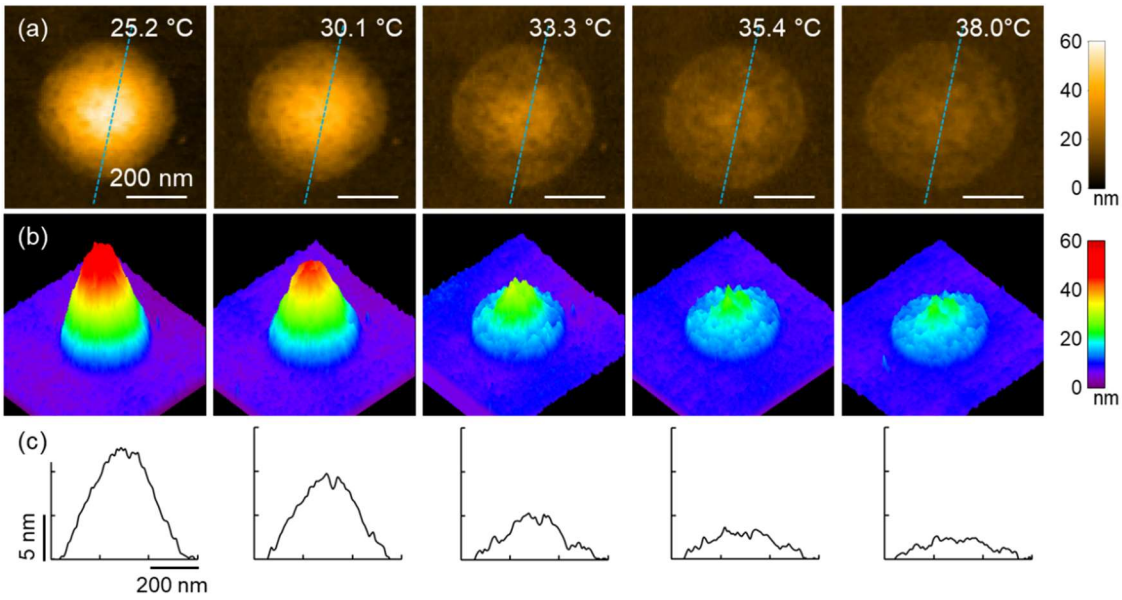

Figure 4.10. HS-AFM analysis of the microgels prepared by inverse miniemulsion polymerization. Temperature dependence of the (a) height images, (b) 3D images, and (c) cross-sectional profiles corresponding to each of the dotted lines in the height images.

Thus far, the author has discussed the characterization and control of the nanostructures of microgels via the precipitation polymerization method, which is expected to enhance the properties of microgels for use in various applications. The polymerization was expected to proceed via the following mechanism:[3,4] The precursor particles formed by phase separation of the polymer chains grow via one of the three different processes: aggregation with other precursor particles (multistep aggregation), adsorption onto extant larger particles, or capture of oligoradicals and monomers. Nuclei are then formed when the aggregates of precursor particles are electrostatically stabilized by charges originating from initiator fragments and then gradually grow via the adsorption of precursor particles. Recently, Rudyak et al. investigated the mechanism of microgel nucleation and particle growth via precipitation polymerization using an in silico system and reported that a single nucleus was formed at 15% conversion of the introduced monomers.[29] On the other hand, in this study, I clarified that some non-thermoresponsive spherical domains with high concentrations of the cross-linker BIS were formed in the microgels just after formation. Based on the polymerization mechanism described above, these spherical domains in the precursor microgels should be formed via multistep aggregation.

4.3.3. Direct visualization of precipitation polymerization

Finally, to clarify the evolution of the particle morphology, the author attempted to directly visualize the particle formation process during precipitation polymerization. The polymerization was conducted in the observation solution of HS-AFM, and continuous imaging was carried out during polymerization (**Figure 4.11**). It should be noted that the polymerization conditions, such as the solution volume, monomer and initiator conditions, and polymerization temperature, were different from those used in the batch precipitation polymerization in a flask, and the polymerization proceeding in the bulk **N(PP)** solution could not be evaluated via HS-AFM. In the first 5 min after initiation, the number of particles in the range of 1 μm^2 increased as the polymerization proceeded via the adsorption of the phase-separated polymer chains that were formed in the bulk solution. These particles moved on the substrate, probably due to Brownian motion and particle–particle interactions, which indicates that these particles are weakly adsorbed on the substrate given that these particles cannot deform in the collapsed state. After 5 min, the number of particles decreased; during this stage, the aggregation or adsorption of the precipitated polymer chains was the rate-determining step (**Figure 4.11b** and **Figure 4.12**). Changes in particle height distribution over time suggest particle growth by the aggregation and/or adsorption process (**Figure 4.11c**). Moreover, the author successfully visualized the initial aggregation process of phase-separated polymer chains. The direct visualization proved that nucleation proceeded via multistep aggregation (**Figure 4.11d**) and the adsorption of precursor particles onto large particles (**Figure 4.11e**). The spherical morphology of the obtained microgels was maintained in the swollen state (25 °C), indicating that cross-linkers were introduced into the microgels (**Figure 4.13**). Moreover, multistep aggregation of the aggregates was observed until ~5

min, and after a short time, aggregation between particles did not occur even when two particles came into contact (**Figure 4.11f**). In DLVO theory, colloidal stability is determined by the sum of electrostatic repulsion and van der Waals attraction.[38] In the initial stages of polymerization (~5 min), the charge density, which originates from the initiator fragments, of the precursor particles and their aggregates is small. The van der Waals attraction might be larger than the electrostatic repulsion, which could result in multistep aggregation. As the polymerization proceeds, the surface charge density of each particle might increase via the aggregation/adsorption process such that the electrostatic repulsion becomes greater than the van der Waals force, thus suppressing the aggregation of the two particles. Although the complete polymerization mechanism, including, e.g., the monomer diffusion to the growing microgels and subsequent polymerization, has not been revealed in this study, the author believes that the progress reported in this work will further the understanding of the formation mechanism of uniformly sized microgels. In the future, if the precipitation polymerization process is understood in greater detail and the controllability of the microgel structures is improved, not only could the swelling properties of the microgels be enhanced but also their mechanical strength could be improved via uniform cross-linking with a functional cross-linker, e.g., rotaxane cross-linkers,[39] similar to that in bulk hydrogels. This would further increase interest in precipitation polymerization.

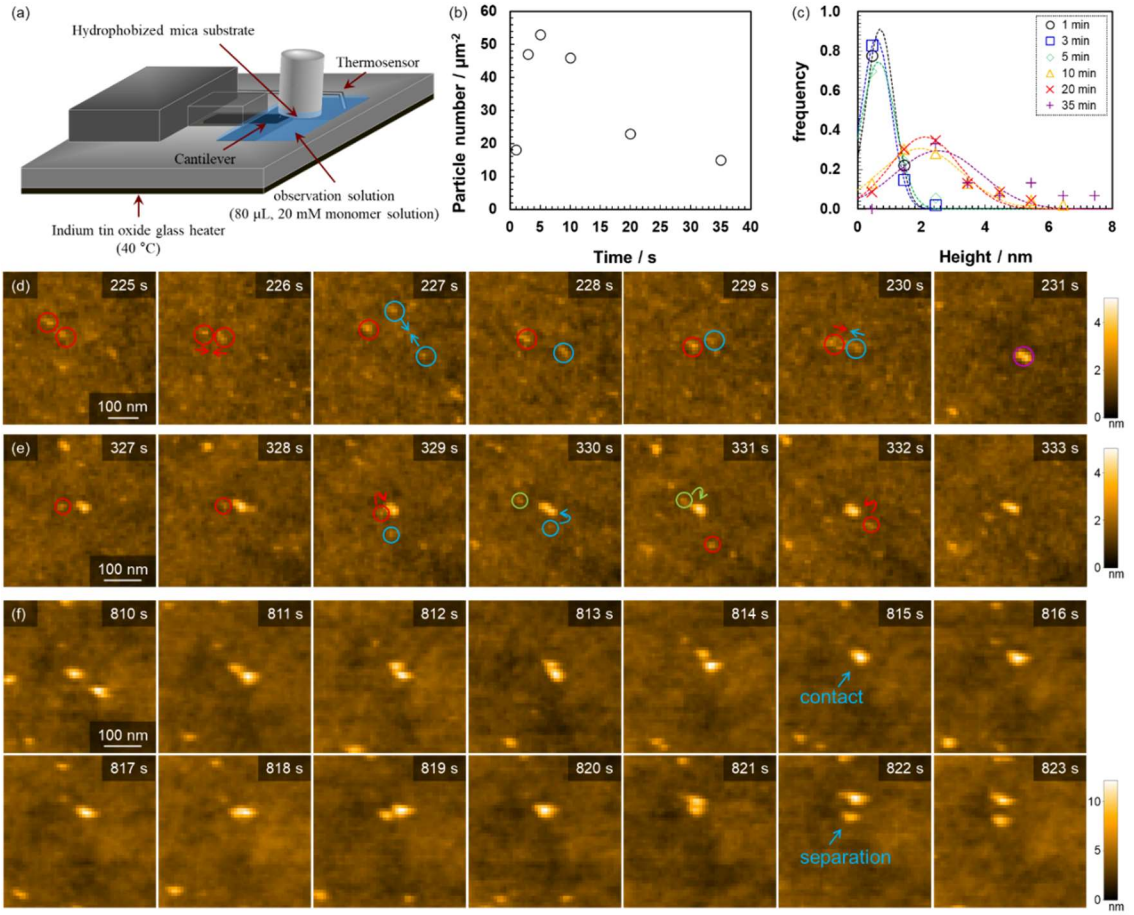

Figure 4.11. (a) Schematic illustration of the polymerization system. (b) Number of particles in the range of 1 μm^2 as a function of the polymerization time. (c) Histogram of the height of the particles as the polymerization proceeded. The dashed lines show the results of Gaussian fitting. (d-f) Direct visualization of precipitation polymerization behaviors: (d) Multistep aggregation of precursor particles (height: ~1 nm), (e) adsorption of precursor particles onto a larger particle, and (f) a repulsive interaction.

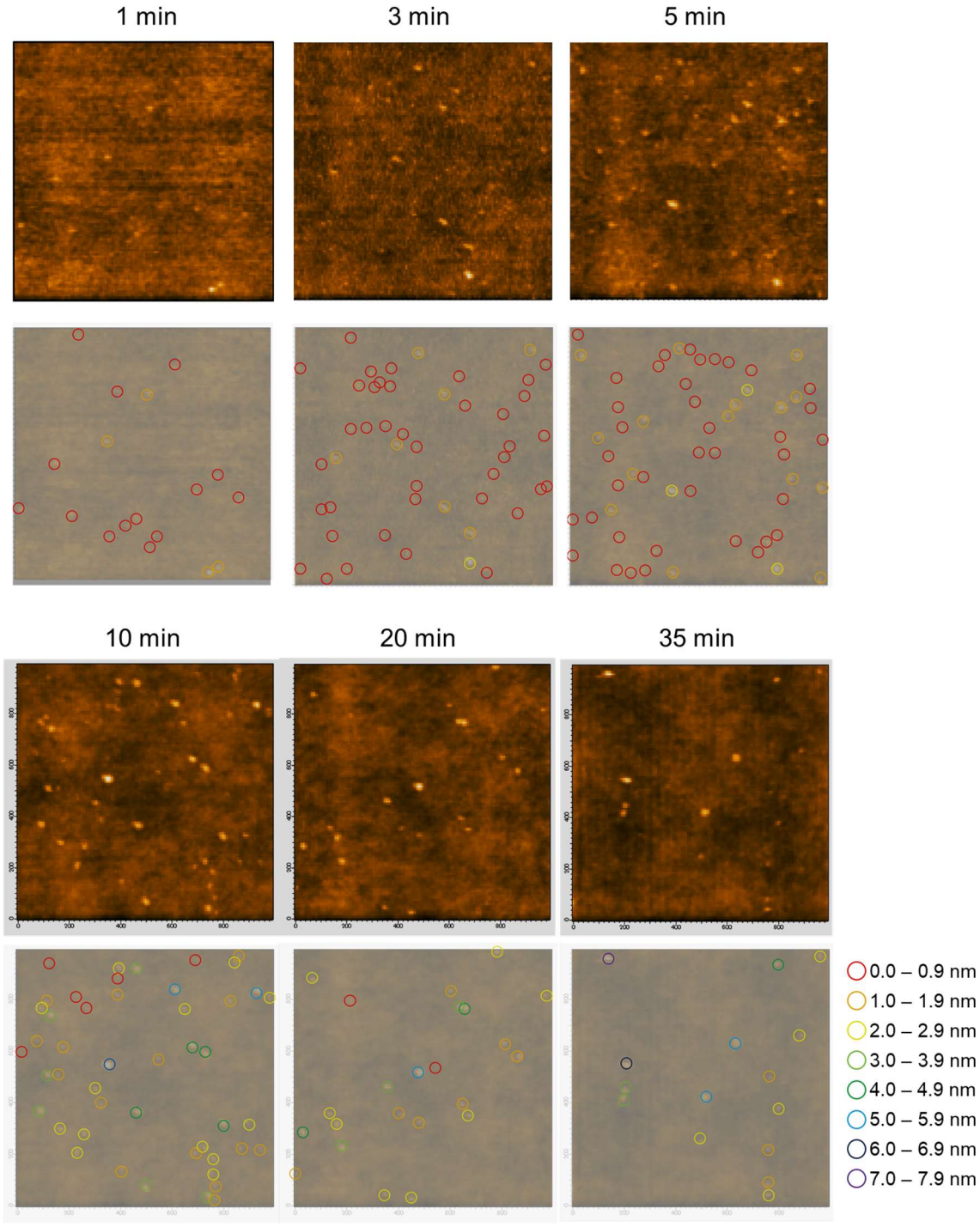

Figure 4.12. Results of the direct visualization of precipitation polymerization via TC-HS-AFM: Height images (top panels) and height analysis (bottom panels) for each polymerization time.

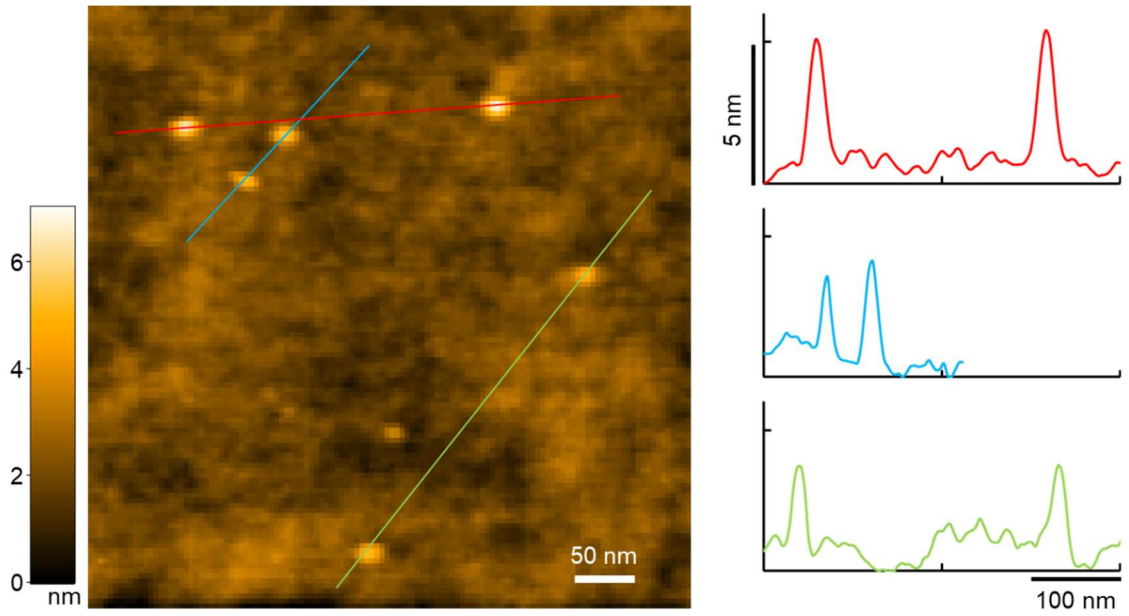

Figure 4.13. Height image and cross-sectional profiles corresponding to the respective lines in the height images of the microgels at 25 °C. The microgels maintained their spherical shape below the volume transition temperature (~32 °C), indicating that microgels were well cross-linked.

4.4. Conclusion

The changes in the thermoresponsiveness and nanostructure of developing p(NIPAm-*co*-BIS) microgels during precipitation polymerization were evaluated by TC-HS-AFM and DLS measurements. Careful evaluation of the microgels prepared by conventional precipitation polymerization at different polymerization times revealed that at polymerization times of 10 min or less, the microgels exhibited low swelling properties and thermoresponsiveness and that non-thermoresponsive spherical domains existed in the microgels just after formation due to the incorporation of a high concentration of cross-linkers. The lower swelling properties and thermoresponsiveness of the microgels formed in the early stages of the polymerization were largely overcome by using feeding precipitation polymerization, which allows for constant consumption of the cross-linker BIS by tuning the polymerization mechanism, even though the presence of non-thermoresponsive domains could not be completely eliminated. Thus, the aggregation/adsorption process in precipitation polymerization must be responsible for the formation of the non-thermoresponsive nanoarchitecture. Furthermore, the formation of microgels during precipitation polymerization was visualized directly in real time. These direct observations clarified that the multistep aggregation of precursor particles occurred only in the early stages of polymerization, while larger particles did not aggregate with one another due to their surface charges, which originated from the initiator fragments. The findings in this study are expected to further the understanding of the polymerization mechanism of uniformly sized microgels and the design of functionalized microgels, such as tough microgels cross-linked with rotaxanes.

4.5. Reference

1. R. Pelton, Temperature-Sensitive Aqueous Microgels. *Adv. Colloid Interface Sci.* **2000**, *85*, 1–33.
2. R. H. Pelton, P. Chibante, Preparation of aqueous latices with *N*-isopropylacrylamide. *Colloids Surf.* **1986**, *20*, 247–256.
3. S. Nayak, L. A. Lyon, Soft Nanotechnology with Soft Nanoparticles. *Angew. Chem. Int. Ed.* **2005**, *44*, 7686–7708.
4. A. Pich, W. Richtering, Chemical Design of Responsive Microgels; Springer-Verlag: Berlin, Heidelberg, **2010**; 1−37.
5. T. J. Merkel, S. W. Jones, K. P. Herlihy, F. R. Kersey, A. R. Shields, M. Napier, J. C. Luft, H. Wu, W. C. Zamboni, A. Z. Wang, J. E. Bear, J. M. DeSimone, Using Mechanobiological Mimicry of Red Blood Cells to Extend Circulation Times of Hydrogel Microparticles. *Proc. Nat. Acad. Sci. U.S.A.* **2011**, *108*, 586–591.
6. I. Capek, On Inverse Miniemulsion Polymerization of Conventional Water-Soluble Monomers. *Colloid Interface Sci.* **2010**, *156*, 35–61.
7. B. Wedel, Y. Hertle, O. Wrede, J. Bookhold, T. Hellweg, Smart Homopolymer Microgels: Influence of the Monomer Structure on the Particle Properties. *Polymers* **2016**, *8*, 162.
8. T. Cai, M. Marquez, Z. Hu, Monodisperse Thermoresponsive Microgels of Poly(ethylene glycol) Analogue-Based Biopolymers. *Langmuir* **2007**, *23*, 8663–8666.
9. T. Kureha, D. Suzuki, Nanocomposite Microgels for the Selective Separation of Halogen Compounds from Aqueous Solution. *Langmuir* **2018**, *34*, 837–846.
10. J. Maldonado-Valderrama, T. del Castillo-Santaella, I. Adroher-Benitez, A. Moncho-Jorda, A. Martin-Molina, Thermoresponsive Microgels at the Air–Water Interface: The Impact of the Swelling State on Interfacial Conformation. *Soft Matter* **2017**, *13*, 230−238.
11. F. A. L. Janssen, M. Kather, A. Ksiazkiewicz, A. Pich, A. Mitsos, Synthesis of Poly(*N*-vinylcaprolactam)-Based Microgels by Precipitation Polymerization: Pseudo-Bulk Model for Particle Growth and Size Distribution. *ACS Omega* **2019**, *4*, 13795–13807.
12. X. Wu, R. H. Pelton, A. E. Hamielec, D. R. Woods, W. McPhee, W. The Kinetics of Poly(*N*-isopropylacrylamide) Microgel Latex Formation. *Colloid Polym. Sci.* **1994**, *272*, 467–477.
13. T. Hoare, R. Pelton, Characterizing Charge and Crosslinker Distributions in Polyelectrolyte Microgels. *Curr. Opin. Colloid Interface Sci.* **2008**, *13*, 413−428.
14. T. Watanabe, Y. Nishizawa, H. Minato, C. Song, K. Murata, D. Suzuki, Hydrophobic Monomers Recognize Microenvironments in Hydrogel Microspheres during Free-Radical-Seeded Emulsion Polymerization. *Angew. Chem. Int. Ed.* **2020**, *23*, 8849–8853.
15. I. Varga, T. Gilanyi, R. Meszaros, G. Filipcsei, M. Zrinyi, Effect of Cross-Link Density on the Internal Structure of Poly(*N*-isopropylacrylamide) Microgels. *J. Phys. Chem. B* **2001**, *105*, 9071–9076.

16. A. Fernandez-Barbero, A. Fernandez-Nieves, I. Grillo, E. Lopez-Cabarcos, Structural modifications in the swelling of inhomogeneous microgels by light and neutron scattering. *Phys. Rev. E* **2002**, *66*, 051803.
17. B. R. Saunders, On the Structure of Poly(*N*-isopropylacrylamide) Microgel. *Langmuir* **2004**, *20*, 3925–3932.
18. M. Stieger, W. Richtering, J. S. Pedersen, P. Lindner, Small-Angle Neutron Scattering Study of Structural Changes in Temperature Sensitive Microgel Colloids. *J. Chem. Phys.* **2004**, *120*, 6197–6206.
19. A. Mourran, Y. Wu, R. A. Gumerov, A. A. Rudov, I. I. Potemkin, A. Pich, M. Moeller, When Colloidal Particles Become Polymer Coils. *Langmuir* **2016**, *32*, 723–730.
20. G. M. Conley, S. Nojd, M. Braibanti, P. Schurtenberger, F. Scheffold, Superresolution Microscopy of the Volume Phase Transition of pNIPAM Microgels. *Colloids Surf. A* **2016**, *499*, 18–23.
21. B. R. Saunders, N. Laajam, E. Daly, S. Teow, X. Hu, R. Stepto, Microgels: From responsive polymer colloids to biomaterials. *Adv. Coll. Int. Sci.* **2009**, *147*, 251–262.
22. A. A. Karanastasis, Y. Zhang, G. S. Kenath, M. D. Lessard, J. Bewersdorf, C. K. Ullal, 3D mapping of nanoscale crosslink heterogeneities in microgels. *Mater. Horiz.* **2018**, *5*, 1130–1136.
23. Y. Nishizawa, S. Matsui, K. Urayama, T. Kureha, M. Shibayama, T. Uchihashi, D. Suzuki, Non-Thermoresponsive Decanano-sized Domains in Thermoresponsive Hydrogel Microspheres Revealed by Temperature-Controlled High-Speed Atomic Force Microscopy. *Angew. Chem. Int. Ed.* **2019**, *58*, 8809–8813.
24. O. L. J. Virtanen, W. Richtering, Kinetics and Particle Size Control in Non-Stirred Precipitation Polymerization of *N*-isopropylacrylamide. *Colloid Polym. Sci.* **2014**, *292*, 1743–1756.
25. M. de Kanter, J. Meyer-Kirschner, J. Viell, A. Mitsos, M. Kather, A. Pich, C. Janzen, Enabling the Measurement of Particle Sizes in Stirred Colloidal Suspensions by Embedding Dynamic Light Scattering into an Automated Probe Head. *Measurement* **2016**, *80*, 92–98.
26. A. Rauh, T. Honold, M. Karg, Seeded Precipitation Polymerization for the Synthesis of Gold-Hydrogel Core-Shell Particles: The Role of Surface Functionalization and Seed Concentration. *Colloid Polym. Sci.* **2016***, 294,* 37–47.
27. O. L. J. Virtanen, M. Kather, J. Meyer-Kirschner, A. Melle, A. Radulescu, J. Viell, A. Mitsos, A. Pich, W. Richtering, Richtering, W. Direct Monitoring of Microgel Formation during Precipitation Polymerization of *N*-Isopropylacrylamide Using in Situ SANS. *ACS Omega* **2019**, *4*, 3690–3699.
28. N. Gnan, L. Rovigatti, M. Bergman, E. Zaccarelli, In Silico Synthesis of Microgel Particles. *Macromolecules* **2017**, *50*, 8777−8786.
29. V. Y. Rudyak, E. Y. Kozhunova, A. V. Chertovich, Towards the Realistic Computer Model of Precipitation Polymerization Microgels. *Sci. Rep.* **2019**, *9*, 13052.
30. T. Ando, T. Uchihashi, S. Scheuring, Filming Biomolecular Processes by High-Speed Atomic

Force Microscopy. *Chem. Rev.* **2014**, *114*, 3120–3188.

31. S. Matsui, Y. Nishizawa, T. Uchihashi, D. Suzuki, Monitoring Thermoresponsive Morphological Changes in Individual Hydrogel Microspheres. *ACS Omega* **2018**, *3*, 10836–10842.
32. L. H. Alvarez, S. Eisold, R. A. Gumerov, M. Strauch, A. A. Rudov, P. Lenssen, D. Merhof, I. I. Potemkin, U. Simon, D. Woell, Deformation of Microgels at Solid−Liquid Interfaces Visualized in Three-Dimension. *Nano Lett.* **2019**, *19*, 8862–8867.
33. T. Sakai, T. Matsunaga, Y. Yamamoto, C. Ito, R. Yoshida, S. Suzuki, N. Sasaki, M. Shibayama, U.-i. Chung, Design and Fabrication of a High-Strength Hydrogel with Ideally Homogeneous Network Structure from Tetrahedron-Like Macromonomers. *Macromolecules* **2008**, *41*, 5379–5384.
34. A. Bin Imran, K. Esaki, H. Gotoh, T. Seki, K. Ito, Y. Sakai, Y. Takeoka, Extremely Stretchable Thermosensitive Hydrogels by Introducing Slide-Ring Polyrotaxane Cross-Linkers and Ionic Groups into the Polymer Network. *Nat. Commun.* **2014**, *5*, 5124.
35. R. Acciaro, T. Gilanyi, I. Varga, Preparation of Monodisperse Poly(*N*-isopropylacrylamide) Microgel Particles with Homogenous Cross-Link Density Distribution. *Langmuir* **2011**, *27*, 7917–7925.
36. C. D. Jones, L. A. Lyon, Shell-Restricted Swelling and Core Compression in Poly(*N*-isopropylacrylamide) Core-Shell Microgels. *Macromolecules* **2003**, *36*, 1988–1993.
37. M. Shibayama, T. Norisuye, Gel Formation Analyses by Dynamic Light Scattering. *Bull. Chem. Soc. Jpn.* **2002**, *75*, 641–659.
38. J. N. Israelachvili, *Intermolecular and Surface Forces*, 3rd ed.; Academic Press: Cambridge, MA, **2011**.
39. T. Kureha, D. Aoki, S. Hiroshige, K. Iijima, D. Aoki, T. Takata, D. Suzuki, Decoupled Thermo- and pH-Responsive Hydrogel Microspheres Cross-Linked by Rotaxane Networks. *Angew. Chem. Int. Ed.* **2017***, 56,* 15393–15396.

5. Summary and outlook

In this thesis, the nanostructure and thermoresponsiveness of microgels were revealed using conventional microscopy, scattering techniques, and HS-AFM. The microgels synthesized by precipitation polymerization exhibited non-thermoresponsive spherical domains, as well as the widely accepted core–shell structure. These inhomogeneous nanostructures were also formed in microgels synthesized by precipitation polymerization with different sizes, cross-linking densities, and chemical compositions. In addition, scattering techniques and HS-AFM observation clarified that the feeding method and the reactivity ratio between the main monomer and cross-linker affected the core-shell structure. Moreover, the mechanism of precipitation polymerization was carefully evaluated in order to understand the formation of the inhomogeneous nanoarchitectures in the microgels. Precipitation polymerization proceeded via multistep aggregation, adsorption, and repulsive interactions, and these processes impacted the formation of non-thermoresponsive spherical domains. Indeed, microgels prepared by inverse miniemulsion polymerization did not exhibit core–shell and non-thermoresponsive nanostructures.

Recently, the evaluation of dynamic behavior using advanced measurement techniques has attracted attention, but in order to understand the observed phenomena, it is important to combine various evaluation methods that provide complementary data. The next challenge in this field is to clarify how the dynamic behavior affects the physicochemical properties of microgels. The established evaluation techniques will clarify the structure of many types of functionalized microgels, and the findings in this thesis will aid in the understanding of the relationship between the structure, physicochemical properties, and functions of microgels.

6. Publication / Presentation

List of Publications

1. Yuichiro Nishizawa, Shusuke Matsui, Kenji Urayama, Takuma Kureha, Mitsuhiro Shibayama, Takayuki Uchihashi, Daisuke Suzuki:
"Non-Thermoresponsive Decanano-sized Domains in Thermoresponsive Hydrogel Microspheres Revealed by Temperature-Controlled High-Speed Atomic Force Microscopy"
Angewandte Chemie International Edition, 58, 8809-8813 (2019).

2. Yuichiro Nishizawa, Haruka Minato, Takumi Inui, Takayuki Uchihashi, Daisuke Suzuki:
"Nanostructures, Thermoresponsiveness, and Assembly Mechanism of Hydrogel Microspheres during Aqueous Free-Radical Precipitation Polymerization"
Langmuir, 37, 151-159 (2021).

3. Yuichiro Nishizawa, Haruka Minato, Takumi Inui, Ikuma Saito, Takuma Kureha, Mitsuhiro Shibayama, Takayuki Uchihashi, Daisuke Suzuki:
"Nanostructure and thermoresponsiveness of poly(*N*-isopropyl methacrylamide)-based hydrogel microspheres prepared via aqueous free radical precipitation polymerization"
RSC Advances, 11, 13130-13137 (2021).

Other Publications

1. Takuma Kureha, Yuichiro Nishizawa, Daisuke Suzuki:
"Controlled Separation and Release of Organoiodine Compounds using Poly(2-methoxyethyl acrylate)-analogue Microspheres",
ACS Omega, 2, 7686-7694 (2017).

2. Shusuke Matsui, Yuichiro Nishizawa, Takayuki Uchihashi, Daisuke Suzuki:
"Monitoring Thermo-responsive Morphological Changes in Individual Hydrogel Microspheres"
ACS Omega, 3, 10836-10842 (2018).

3. Takumi Watanabe, Yuichiro Nishizawa, Haruka Minato, Chihong Song, Kazuyoshi Murata, Daisuke Suzuki:
"Hydrophobic monomers recognize microenvironments in hydrogel microspheres during free radical seeded emulsion polymerization"
Angewandte Chemie International Edition, 59, 8849-8853 (2020).

4. Haruka Minato, Yuichiro Nishizawa, Takayuki Uchihashi, Daisuke Suzuki:
"Thermo-responsive structural changes of single poly(*N*-isopropyl acrylamide) hydrogel microspheres under densely packed conditions on a solid substrate"
Polymer Journal, 52, 1137-1141 (2020).

5. Seina Hiroshige, Haruka Minato, Yuichiro Nishizawa, Yuma Sasaki, Takuma Kureha, Mitsuhiro Shibayama, Kazuya Uenishi, Toshikazu Takata, Daisuke Suzuki
"Temperature-dependent Relationship between the Structure and Mechanical Strength of Volatile Organic Compound-free Latex Films Prepared from Poly(butyl acrylate-co-methyl methacrylate) Microspheres"
Polymer Journal, 53, 345-353 (2021).

6. Yuma Sasaki, Seina Hiroshige, Masaya Takizawa, Yuichiro Nishizawa, Takayuki Uchihashi, Haruka Minato, Daisuke Suzuki:
"Non-close-packed arrangement of soft elastomer microspheres on solid substrates"
RSC Advances, 11, 14562-14567 (2021).

7. Yuichiro Nishizawa, Kenshiro Honda, Matthias Karg, Daisuke Suzuki:
"Controlling the shell structure of hard core/hydrogel shell microspheres"
Colloid and Polymer Science, accepted (2021).

Books

1. 鈴木大介、西澤佑一朗:
「第 3 章 第 1 節 第 4 項 ミクロゲル」
現代界面コロイド化学の基礎 第 4 版、丸善出版、129-131 (2018).

2. 西澤佑一朗、呉羽拓真、松井秀介、渡邊拓巳、鈴木大介:
「第 3 章 第 8 節 刺激応答性ハイドロゲル微粒子の機能化」
刺激応答性高分子ハンドブック、エヌ・ティー・エス、pp239-244 (2018).

Reviews

1. Yuichiro Nishizawa, Kenshiro Honda, Daisuke Suzuki:
"Recent Development in the Visualization of Microgels"
Chemistry Letters, 50, 1226-1235 (2021).

2. 西澤佑一朗
「単一ハイドロゲル微粒子が示す温度応答挙動のリアルタイム解析」
Colloid & Interface Communication, Vol. 46, No.2, pp39-41(2021).
Interface(7), 若手注目研究

Oral Presentations (International conference)

1. ○Yuichiro Nishizawa, Shusuke Matsui, Kenji Urayama, Takuma Kureha, Mitsuhiro Sibayama, Takayuki Uchihashi, Daisuke Suzuki:
"Evaluation of Thermoresponsive Structural Changes in Hydrogel Microspheres by High-Speed Atomic Force Microscopy"
ACS Fall 2019 National Meeting (San Diego, USA) August 28 (2019) Oral (COLL 665)

2. ○Yuichiro Nishizawa, Takayuki Uchihashi, Daisuke Suzuki:
"Structural Analysis of Thermoresponsive Microgels by Temperature-Controllable High-Speed AFM"
2020 Virtual Symposium on Microgels (Online meeting) September 30th (2020) Oral (Session 1)

3. ○Yuichiro Nishizawa, Haruka Minato, Takumi Inui, Takayuki Uchihashi, Daisuke Suzuki:
"Investigation for formation process of hydrogel microspheres during precipitation polymerization"
ACS Spring 2021 National Meeting (Online meeting) April 13 (2021) Oral (POLY 3555068)

4. ○Yuichiro Nishizawa, Haruka Minato, Takumi Inui, Takayuki Uchihashi, Daisuke Suzuki:
"Formation mechanism of hydrogel microspheres during precipitation polymerization"
ACS Fall 2021 (Online meeting) August 27 (2021) Oral (POLY 3595794)

Oral Presentations (National conference)

1. ○西澤佑一朗、松井秀介、渡辺大輝、内橋貴之、鈴木大介:
「界面活性剤添加時のハイドロゲル微粒子の膨潤ダイナミクス」
第 67 回高分子討論会、北海道大学、北海道、9 月 13 日(2018)、口頭(2S03)

2. ○西澤佑一朗、松井秀介、渡辺大輝、内橋貴之、鈴木大介:
「界面活性剤と相互作用するハイドロゲル微粒子の動的な膨潤挙動評価」
第 69 回コロイドおよび界面化学討論会、筑波大学、茨城、9 月 20 日(2018)、口頭(3G09)

3. ○西澤佑一朗、松井秀介、渡辺大輝、内橋貴之、鈴木大介:
「ハイドロゲル微粒子の刺激応答速度の検討」
第 20 回高分子ミクロスフェア討論会、岡山大学、岡山、11 月 15 日(2018)、口頭(2-07A)

4. ○西澤佑一朗、松井秀介、内橋貴之、鈴木大介:
「刺激応答性ハイドロゲル微粒子のナノ構造評価」
第 68 回高分子学会年次大会、大阪府立国際会議場、大阪、5 月 29 日(2019)、口頭(1D10)

5. ○西澤佑一朗、松井秀介、浦山健治、呉羽拓真、柴山充弘、内橋貴之、鈴木大介:
「ハイドロゲル微粒子の精密構造解析」
第 68 回高分子討論会、福井大学、福井、9 月 25 日(2019)、口頭(1F18)

6. ○西澤佑一朗、松井秀介、浦山健治、呉羽拓真、柴山充弘、内橋貴之、鈴木大介:
「ハイドロゲル微粒子のナノ構造制御に向けた検討」
第 29 回 日本 MRS 年次大会、横浜情報文化センター、神奈川、11 月 29 日(2019)、
口頭(L-O27-009)

7. ○西澤佑一朗、松井秀介、浦山健治、呉羽拓真、柴山充弘、内橋貴之、鈴木大介:
「高速原子間力顕微鏡と散乱法を駆使した温度応答性ゲル微粒子のナノ構造評価と制御」
第 31 回高分子ゲル研究討論会、産業技術総合研究所、東京、1 月 16 日(2020)、口頭(14)

8. ○Yuichiro Nishizawa, Shusuke Matsui, Kenji Urayama, Takuma Kureha, Mitsuhiro Shibayama, Takayuki Uchihashi, Daisuke Suzuki:
"Structural Analysis of Hydrogel Microspheres by Light Scattering and High-Speed AFM"
第 69 回高分子学会年次大会、福岡国際会議場、福岡、5 月 27 日(2020)、口頭 (1K17)

9. ○西澤佑一朗、齋藤生真、呉羽拓真、柴山充弘、内橋貴之、鈴木大介:
「ハイドロゲル微粒子の構造制御と精密構造解析」
第 69 回高分子学会年次大会、福岡国際会議場、福岡、5 月 28 日(2020)、口頭 (2D03)

10. ○西澤佑一朗、齋藤生真、呉羽拓真、鈴木大介:
「高分子微粒子の構造が分子分離機能に与える影響」
第 69 回高分子学会年次大会、福岡国際会議場、福岡、5 月 29 日(2020)、口頭 (3H17)

11. ○西澤佑一朗、松井秀介、浦山健治、呉羽拓真、柴山充弘、内橋貴之、鈴木大介:
「単一ハイドロゲル微粒子が有する温度応答挙動のリアルタイム解析」
第 71 回コロイドおよび界面化学討論会、オンライン開催、9 月 14-16 日(2020)、口頭(B-31)

12. ○西澤佑一朗、松井秀介、浦山健治、呉羽拓真、柴山充弘、内橋貴之、鈴木大介:
「高速原子間力顕微鏡を活用したハイドロゲル微粒子の温度応答性評価」
第 69 回高分子討論会、オンライン開催、9 月 16 日(2020)、口頭(1I14)

13. ○西澤佑一朗、松井秀介、浦山健治、呉羽拓真、柴山充弘、内橋貴之、鈴木大介:
「ナノスケール可視化技術を活用した単一ハイドロゲル微粒子の構造解析」
第 10 回 CSJ 化学フェスタ、オンライン開催、10 月 20 日(2020)、口頭(J2-11)

14. ○西澤佑一朗、内橋 貴之、鈴木大介:
「温度応答性ゲル微粒子のナノスケール構造解析」
2020 年度東海高分子研究会学生発表会、オンライン開催、11 月 7 日(2020)、口頭(2-18)

15. ○西澤佑一朗、湊遥香、乾拓海、内橋貴之、鈴木大介:
「沈殿重合時におけるハイドロゲル微粒子のナノ構造・温度応答特性の時間発展評価」
第 30 回日本 MRS 年次大会、オンライン開催、12 月 9 日(2020)、口頭(M-O9-012)

16. ○西澤佑一朗、湊遥香、乾拓海、内橋 貴之、鈴木大介:
「重合時におけるハイドロゲル微粒子の形態発展解析」
第 32 回高分子ゲル研究討論会、オンライン開催、1 月 21 日(2021)、口頭(8)

17. ○西澤佑一朗、乾拓海、内橋貴之、鈴木大介:
「多様な手法により評価したゲル微粒子の温度応答性挙動」
第 70 回高分子学会年次大会、オンライン開催、5 月 27 日(2021)、口頭(2C08)

18. ○西澤佑一朗、内橋貴之、鈴木大介:
「刺激応答性ハイドロゲル微粒子のナノ構造解析と制御」
第 70 回高分子討論会、オンライン開催、9 月 6 日(2021)、口頭(1O10)

19. ○西澤佑一朗、内橋貴之、鈴木大介:
「温度応答性ゲル微粒子のナノ構造に化学種が与える影響」
第 72 回コロイドおよび界面化学討論会、オンライン開催、9 月 16 日(2021)、口頭(2D08)

Awards

1. 第 69 回コロイドおよび界面化学討論会　ポスター賞（2018 年）
2. 第 68 回高分子討論会　優秀ポスター賞（2019 年）
3. 第 31 回高分子ゲル研究討論会　最優秀ポスター賞（2020 年）
4. 第 71 回コロイドおよび界面化学討論会　オンライン優秀講演賞（2020 年）
5. 第 10 回 CSJ 化学フェスタ 2020　CSJ 化学フェスタ博士オーラル賞（2020 年）
6. 第 72 回コロイドおよび界面化学討論会　若手口頭講演賞（2021 年）

7. Acknowledgements

First of all, I would like to express my sincerest gratitude and appreciation to my supervisor Prof. Dr. Daisuke Suzuki (Shinshu University) for all kind help and support. His guidance allowed me not only learned the abilities of a researcher and joy of exploring science, but also grew significantly as a human being. I will cherish his teachings in my future career and life.

I would like to thank Prof. Dr. Takayuki Uchihashi (Nagoya University.) and Prof. Dr. Mitsuhiro Shibayama (Cross) for their kind discussions and advice regarding HS-AFM and Scattering measurement, respectively.

I greatly thank Emeritus Prof. Dr. Haruma Kawaguchi (Keio Univ.), Prof. Dr. Kenji Urayama (Kyoto Institute of Technology Univ.), Prof. Dr. Michinari Kohri (Chiba Univ.), Prof. Dr. Masahiro Suzuki (Shinshu Univ.), Prof. Dr. Yoshitake Akiyama (Shinshu Univ.) Prof. Dr. Tomoki Nishimura (Shinshu Univ.), Prof. Dr. Takuma Kureha (Hirosaki Univ.), Dr. Shusuke Matsui, Dr Haruka Minato, Dr. Takumi Watanabe, Dr Seina Hiroshige for useful discussions about colloid and polymer science, especially microgels.

My study was financially supported by fellowship from the Japan Society for Promotion of Science (JSPS; 20J1272700) and a Sasagawa Scientific Research Grant from the Japanese Science Society (2019-3013). I am thankful for all the supports.

I would like to thank Suzuki lab. Members. Inspired by the daily discussions with them, I was able to continue my research positively and develop my research. I sincerely wish for their continued success in all their future.

Finally, I would like to express my gratitude to my family, Tadahiko, Sumiko and Nana. Thank you for all support and warm encouragements.

Yuichiro Nishizawa
西澤　佑一朗